3-2006

Characterizing the Impact of Precision Time and Range Measurements from Two-Way Time Transfer Systems on Network Differential GPS Position Solutions

Kendra L. B. Cook

CHARACTERIZING THE IMPACT OF PRECISION TIME AND RANGE MEASUREMENTS FROM TWO-WAY TIME TRANSFER SYSTEMS ON NETWORK DIFFERENTIAL GPS POSITION SOLUTIONS

THESIS

Kendra L. B. Cook, 2D LT, USAF

AFIT/GA/ENG/06-02

DEPARTMENT OF THE AIR FORCE
AIR UNIVERSITY

AIR FORCE INSTITUTE OF TECHNOLOGY

Wright-Patterson Air Force Base, Ohio

The views expressed in this thesis are those of the author and do not reflect the official policy or position of the United States Air Force, Department of Defense, or the U.S. Government.

AFIT/GA/ENG/06-02

CHARACTERIZING THE IMPACT OF PRECISION TIME AND RANGE MEASUREMENTS FROM TWO-WAY TIME TRANSFER SYSTEMS ON NETWORK DIFFERENTIAL GPS POSITION SOLUTIONS

THESIS

Presented to the Faculty

Department of Aeronautics and Astronautics

Graduate School of Engineering and Management

Air Force Institute of Technology

Air University

Air Education and Training Command

In Partial Fulfillment of the Requirements for the

Degree of Master of Science in Astronautical Engineering

Kendra L. B. Cook, B.S.A.E.

2D LT, USAF

March 2006

AFIT/GA/ENG/06-02

CHARACTERIZING THE IMPACT OF PRECISION TIME AND RANGE MEASUREMENTS FROM TWO-WAY TIME TRANSFER SYSTEMS ON NETWORK DIFFERENTIAL GPS POSITION SOLUTIONS

Kendra L. B. Cook, B.S.A.E.

2D LT, USAF

Approved:

//signed//	
Dr. John F. Raquet (Chairman)	date
//signed//	
Dr. Kerry D. Hicks, Lt Col, USAF (Member)	date
//signed//	
Dr. Nathan A. Titus, Lt Col, USAF (Member)	date
//signed//	
Dr. Richard R. Beckman, Capt, USAF (Member)	date

Abstract

Precise positioning plays an important role for both military and civilian users, from cell phones and OnStar to precision munitions and swarms of UAVs. Many applications require precise relative positioning of a network of vehicles (such as aircraft, tanks, troops, etc). Currently, the primary means for performing precise positioning is by using the Global Positioning System (GPS), and although GPS has become commonplace in today's society, there are still limitations affecting the system. Recent advances in dynamic Two-Way Time Transfer (TWTT) have potentially provided a means to improve precise relative positioning accuracy over differential GPS (DGPS)-only approaches. TWTT is a technique in which signals are simultaneously exchanged between users. This research investigates the impact of using Two-Way Time Transfer (TWTT) time measurements to augment differential GPS systems to improve the relative positioning solutions of vehicle networks. Incorporating the TWTT time measurement into the DGPS solution improves the 3-D relative positioning accuracy by up to 44% with pseudorange measurements and 35% with carrier-phase measurements.

Normally, the TWTT measurements are used in a manner that cancels out the impact of the vehicle position in order to obtain a precise relative time measurement. The research also implements an innovative approach to using TWTT measurements to actually obtain a precise measurement of the vehicle position in addition to the time measurement. The results show that 3-D relative positioning solutions can be improved by up to 48% when using pseudorange measurements augmented with TWTT time and range measurements, and up to 40% when using carrier-phase measurements augmented with TWTT time and range measurements.

For my brother

Acknowledgments

Above all, I want to thank Jesus Christ, my Lord and Savior, for all of the blessings He's given me, especially my family and friends. It is because of Him that this was possible. "I can do everything through Him who gives me strength" (Philippians 4:13). I would like to thank my thesis advisor, John Raquet, for his wisdom and insight that guided this research. I would like to extend my sincerest appreciation to Rich Beckman for his enthusiasm for teaching and his expertise in the field of Two-Way Time Transfer. Because of their dedication, I was able to mold this research into something I can be proud of.

I would like to express my heartfelt gratitude to my husband, whose unfailing love and support enabled me to put the required time and effort into this research. He helped me to keep life in perspective and he truly is a blessing. I would like to thank my parents and sister for their unwavering love and encouragement that they've given me my entire life. It is because of them that I am the person I am today. I would also like to thank my yellow lab, Montana, for eating my thumb drive earlier rather than later in my research and teaching me the important lesson of constantly backing up my work.

I would like to recognize all of my professors who have invested their lives in their students, including me. Finally, I would like to thank my committee members for taking the time and putting the effort into offering me valuable comments and suggestions for further developing my thesis. Their feedback was greatly appreciated.

Kendra L. B. Cook.

Table of Contents

List of Figures

List of Tables

CHARACTERIZING THE IMPACT OF PRECISION TIME AND RANGE MEASUREMENTS FROM TWO-WAY TIME TRANSFER SYSTEMS ON NETWORK DIFFERENTIAL GPS POSITION SOLUTIONS

I. Introduction

1.1 Overview

The challenge of determining precise position and time measurements is one that is important in many facets of life for both civilian and military users. Standard cell phones are being equipped with a Global Positioning System (GPS) receiver so that users who dial '911' can be located quickly in the event of an emergency. Vehicles are now sporting OnStar systems that can pinpoint the vehicle's location and quickly contact help on the user's behalf [44]. Farmers are now using GPS to perform 'precision farming', a method of farming that allows the farmers to precisely and accurately farm their land without missing areas or overlapping others [46]. The requirements for determining precise positioning are even more critical in military applications. Precision bombing can use GPS-guided munitions to precisely target the enemy while aiming to reduce collateral damage. Knowledge of precise positioning is required for identifying both friendly and enemy troops when trying to out maneuver the enemy. In addition to knowing the precise *absolute* position of a receiver, often times it is necessary to determine the position of a receiver relative to another receiver whose absolute position is precisely known. This is known as relative positioning and is illustrated in Figure 1.1.1.

With the advent of the unmanned aerial vehicle (UAV), the military is seeking to send out 'swarms' of UAVs to blanket an area and provide cooperative sensing – a

scenario in which precise relative positioning is imperative [45]. These are only a few examples of situations that require a precise positioning measurement. In these situations, if precise positioning is not achieved, civilians in an emergency situation may wait longer than necessary for help, bombs may not hit their target exactly increasing the number of civilian casualties, and UAVs in a swarm may collide with one another. Currently, the primary means for performing precise absolute and relative positioning is by using the Global Positioning System.

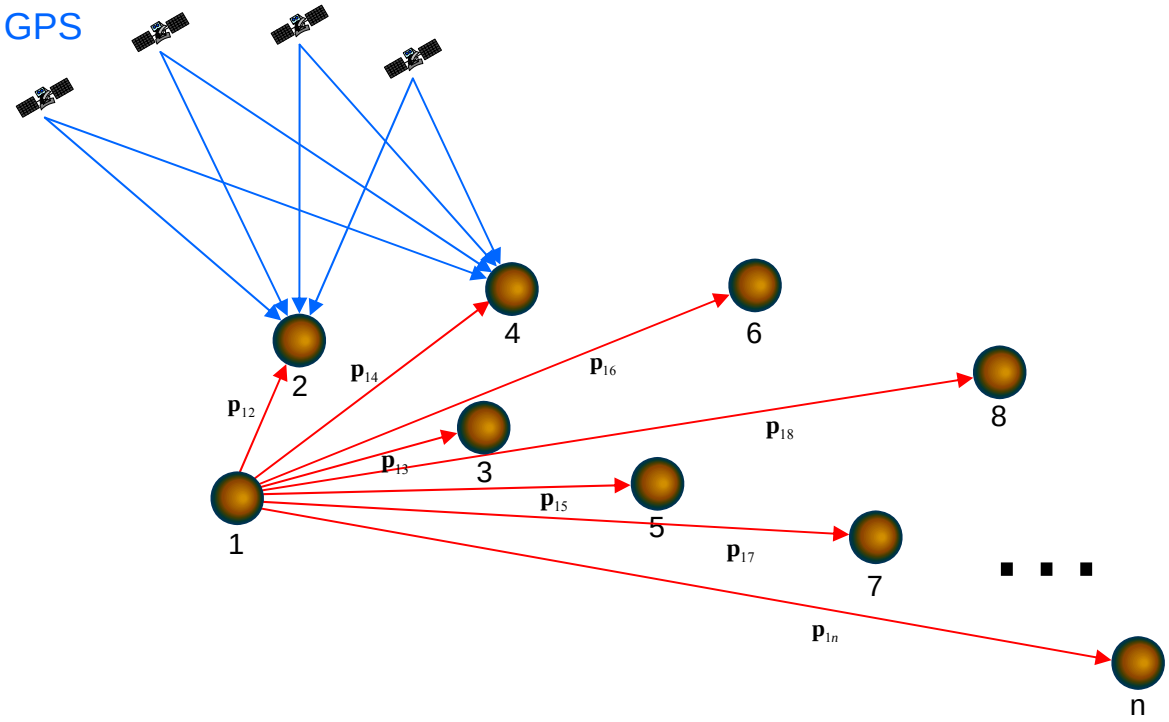

Figure 1.1.1 Illustration of Relative Positioning Using GPS [37]

The Global Positioning System (GPS) was originally created by the Department of Defense (DoD) to give a distinct advantage over adversaries in knowing precise

position, velocity, and time. It has become an integral part of both military and civilian lives since its initial operational capability was declared on 8 December 1993 [25]. GPS applications range from vehicle navigation to international banking operations to construction to outdoor recreational activities. GPS measurements can also be used to determine relative positioning of vehicles, such as aircraft, tanks, troops, etc. Although GPS has become commonplace in today's society, there are still limitations affecting the system.

GPS measurements are bound by inherent local clock errors that are a common error source to all GPS measurements. This error does not average out when using an estimation filter because it is a common bias present in the GPS observables. It is often necessary to estimate the relative clock errors between the vehicles as 'nuisance parameters.' Another option is to double-difference the solution in order to remove the need to calculate differential clock errors but at the cost of degraded measurement geometry. The clock errors and differential GPS are discussed further in detail in Section 2.2.5. Recent advances in dynamic Two-Way Time Transfer have potentially provided an approach to compensate for the limitations of GPS due to these clock errors.

Two-Way Time Transfer (TWTT) is a technique (that can be conducted with static or dynamic receivers) in which signals are simultaneously exchanged between users via a communications satellite. If the paths between the receiver clocks are reciprocal (or very nearly so), as would be the case with static receivers, the propagation delays cancel and the difference between the clocks can be precisely measured [9]. The first static TWTT tests were run in 1962 by the United States and the United Kingdom

[1]. Since then, many experiments and tests have been conducted, producing continually improved results. The first successful dynamic TWTT test was conducted by the Air Force Research Lab (AFRL) at Wright Patterson Air Force Base in 2002 [3]. Two-Way Time Transfer is potentially one of the most accurate ways to compare clocks, and dynamic TWTT offers a method of determining clock errors for moving platforms independent of the Global Positioning System. GPS accuracy remains limited by clock errors, and recent advances in the dynamic TWTT technique provide a method of supporting dynamic GPS users by determining those clock errors. It is therefore logical to integrate the two methods in order to potentially obtain a more accurate solution.

1.2 Problem Statement

The main objective of this research is to evaluate the impact on network differential positioning accuracy of adding Two-Way Time Transfer (TWTT) time measurements to standard differential GPS observables. By helping to constrain the relative clock errors, TWTT measurements can improve the relative positioning accuracy. Another research objective is to determine the advantage of using TWTT range measurements in addition to the TWTT time measurements.

This thesis proposes a new method of using TWTT measurements. Normally, raw TWTT measurements are used in a manner that cancels out the impact of the vehicle position, in order to obtain a precise relative time measurement. Typically, the raw TWTT measurements are differenced, canceling the delays and leaving only the clock terms – these are referred to as TWTT time measurements. These same raw TWTT

measurements can be applied in a different way to actually obtain a precise measurement of the vehicle position. By adding the raw TWTT measurements as opposed to differencing them, the clock terms cancel leaving the sum of the delays. These delays can then be used as an additional measurement when using a filter to solve for a positioning solution – these are referred to as TWTT range measurements. Another benefit of using TWTT range measurements is that it potentially reduces by two the number of GPS measurements required to get a position. Using the TWTT time and range measurements eliminates the time variable and provides another range measurement to the system; therefore, only two GPS measurements are required (instead of the standard four) in addition to the TWTT measurements in order to obtain a positioning solution. This is explained in more detail in Section 2.4. This innovative approach shows the ability to enable high-precision relative positioning of a vehicle network using systems that are intended for other purposes, such as communications systems.

This research includes five trade studies that quantify the benefits of using TWTT in addition to GPS over solely using GPS. The first trade study is performed to confirm that the results obtained are valid regardless of which day's ephemeris is used. The second trade study seeks to determine if the overall solution can be improved by varying the number of receivers used. The separation distance is varied in the third trade study to determine what, if any, effect is has on the overall solution. The location of the TWTT satellite is varied in the fourth trade study to try to optimize the 3-D positioning solution.

Finally, the satellite cutoff elevation is varied in the fifth trade study to determine potential benefits of using TWTT-augmented GPS measurements.

1.3 Methodology

A simulation was created using MATLAB® to perform trade studies exploring the potential benefits of using TWTT measurements in addition to differential GPS in order to obtain a more precise relative positioning solution. Figure 1.3.1 shows a block diagram of the simulation, which includes the parameters, truth model, generated measurements, estimation filter, and performance analysis.

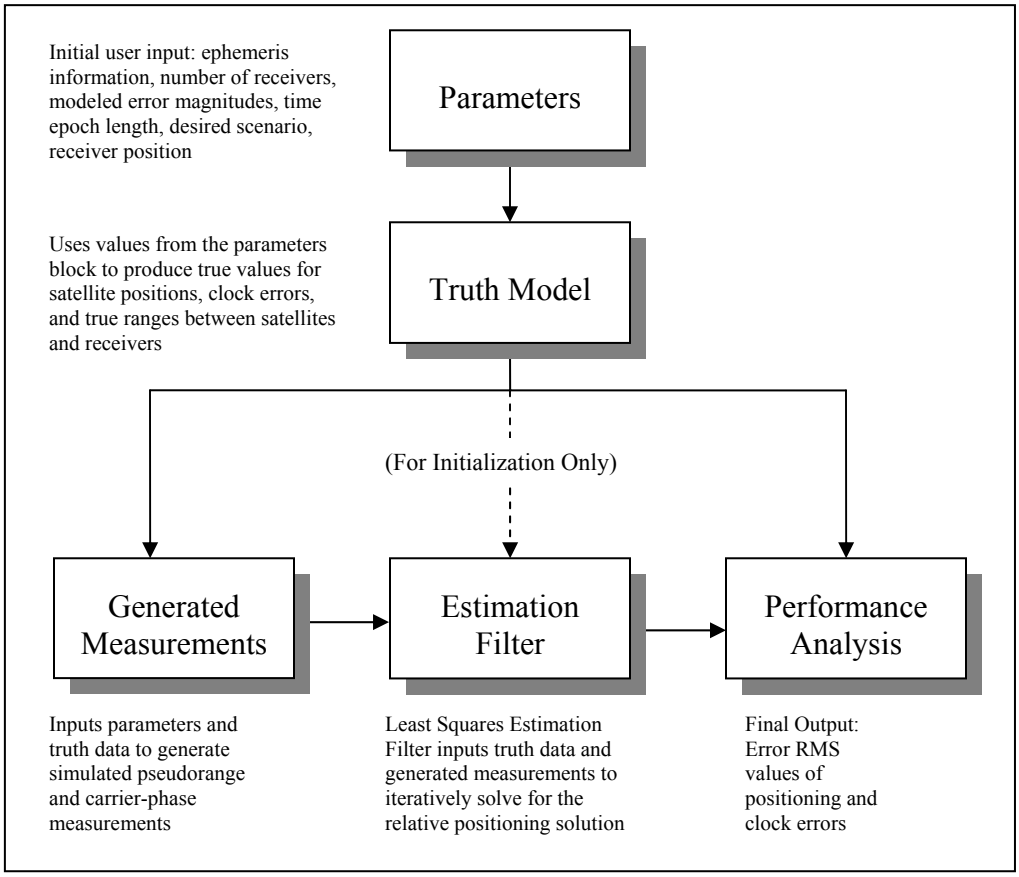

Figure 1.3.1 Simulation Block Diagram

The user inputs the desired parameters into the 'parameters' function. Those parameters are then used to obtain the 'true' values for the satellite positions and satellite clock errors using the precise ephemeris and the true ranges between the satellites and receivers in the truth model. The 'generated measurements' block takes the truth data from the truth model and creates simulated measurements. GPS-satellite position and clock errors are obtained using the broadcast ephemeris, which is less exact than the precise ephemeris that was used to obtain those values in the truth model. This function also generates the pseudorange and carrier-phase measurements. The pseudorange measurements are generated by adding pseudorange noise and clock bias to the true ranges obtained in the truth model. The carrier-phase measurements are generated by adding the carrier-phase noise and clock bias to the true ranges and multiplying everything by the speed of light divided by the frequency of the GPS L1 signal. The TWTT time and range measurements are calculated in the generated measurements block as well. The Least-Squares Estimation Filter takes the true data and the generated data and performs an iterative process to determine the accuracy of the relative positioning solution at any given time. This data is fed into the performance analysis block where the delta positioning and clock errors are determined as are the mean errors and the root-mean-square of the errors.

A more detailed description of each of the simulation's block functions can be found in Chapter 3.

1.4 Thesis Overview

Chapter Two describes the background of the fundamental topics related to the research. This includes a background of GPS, TWTT, and the least squares estimation filter. Within the topic of GPS the equations governing pseudorange and carrier-phase measurements are explained and the concept of differential GPS is discussed. The Earth-Centered Earth-Fixed (ECEF) reference frame, which was the reference frame used, is described. Within the topic of TWTT the history and theory for both static TWTT and dynamic TWTT are discussed. The equations governing TWTT performance are given and explained. Typical errors for both GPS and TWTT measurements are also discussed. Chapter Three describes a relative positioning simulation environment in which an arbitrary number of vehicles are positioned using a combination of simulated GPS code and carrier-phase measurements with and without additional TWTT measurements. By using a simulation, trade studies were conducted to identify the key factors that influenced system performance. The five trade studies include comparison of results between two different days' ephemeris, varying the number of receivers used, varying the separation distance between the receivers, varying the location of the TWTT satellite, and varying the satellite elevation cutoff. Chapter Four discusses the results obtained for each trade study and provides a detailed analysis of the results. Finally, Chapter Five presents conclusions and recommendations for further research in this area.

II. Background

2.1 Introduction

This chapter presents the background of the fundamental topics of this research. First, a brief overview of the pertinent GPS segments will be given. The equations describing pseudorange measurements and carrier-phase measurements will be introduced and explained. The reference frame used will also be discussed. Next, the history and theory of static and dynamic TWTT will be covered. Typical errors will be addressed and finally, the method of using a non-linear least squares estimator will be discussed in detail.

2.2 GPS Overview

The following sections briefly discuss the history and theory of GPS and give details on the GPS pseudorange and carrier-phase measurements. Differential GPS is explained in Section 2.2.5.

2.2.1 GPS History

In 1519, Magellan set out on a quest to circumnavigate the globe equipped with "sea charts, a terrestrial globe, wooden and metal theodolites, wooden and wood-and-bronze quadrants, compasses, magnetic needles, hour glasses and timepieces, and a log to be towed astern" [28]. With these instruments and great skill, he was able to estimate the ship's speed, direction, and latitude, but not longitude. It was another 250 years before John Harrison invented a chronometer that allowed for longitude determination [30].

More than 200 years after Harrison's invention, amazingly accurate estimates of position, velocity, and time are obtainable with the use of the Global Positioning System.

The initial prototype satellites, called Block I Satellites, were launched between 1978 and 1985. Block II and Block IIA satellites, the production model satellites, were then launched to create the currently operational GPS constellation. Beginning in 1997, the next generation of GPS satellites called the Block IIR satellites were launched to sustain and upgrade the capabilities of the constellation [35]. The current GPS constellation consists of a mix of Block II, IIA, IIR and IIR-M satellites. Since its conception, GPS has become a vital part of the lives of military and civilian users alike.

2.2.2 GPS Theory

GPS is comprised of three separate segments: the Operational Control Segment (OCS), the space segment, and the user segment. The OCS is made up of the Master Control Station (MCS), monitor stations, and ground antennas. Figure 2.2.1 illustrates the three major GPS segments.

The nominal GPS constellation consists of 24 satellites. The satellites are located on six equally spaced orbital planes (four satellites per plane with room for a fifth satellite in each plane) that are all inclined at 55 degrees from the equator. Figure 2.2.2 shows the GPS constellation.

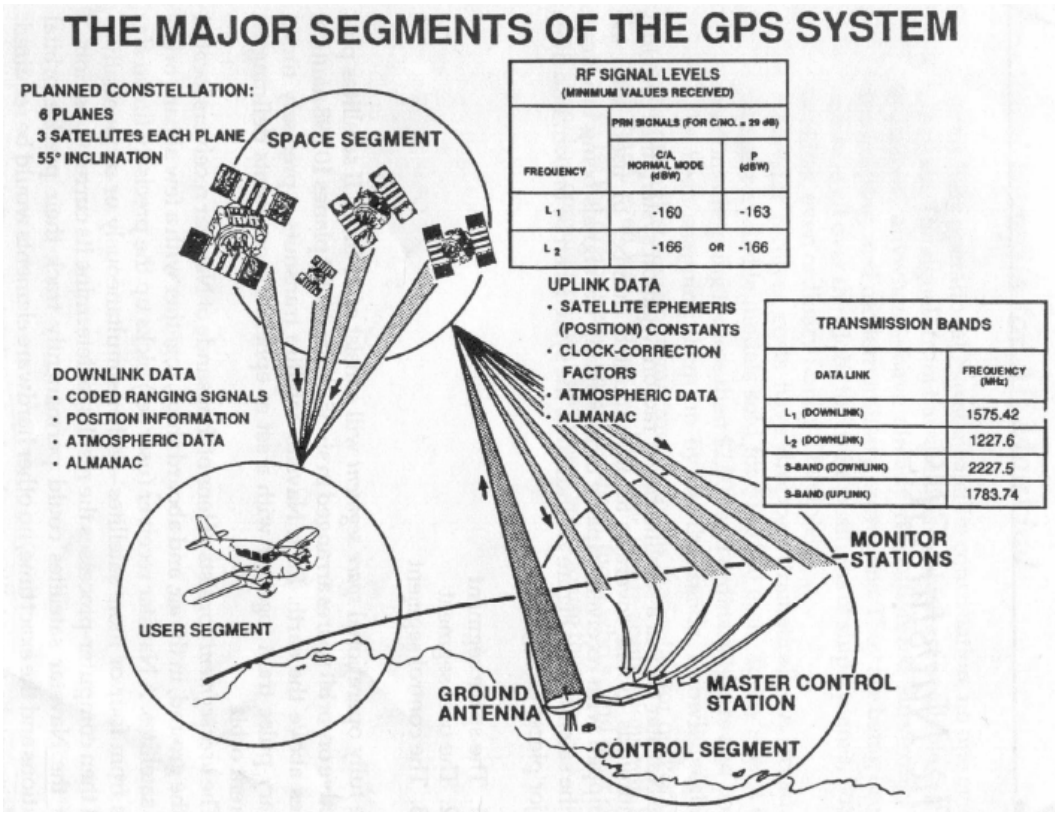

Figure 2.2.1 The Major Segments of the GPS System [31]

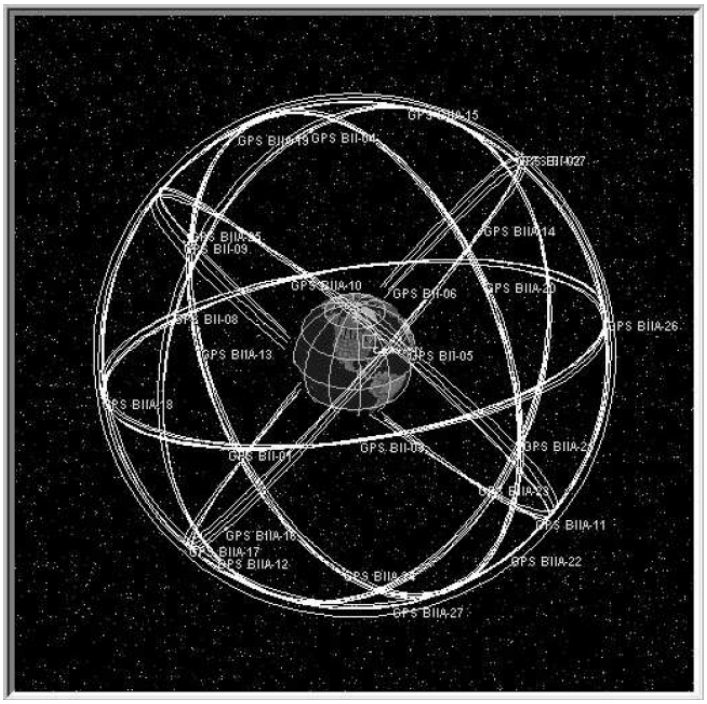

Figure 2.2.2 GPS Satellite Constellation [32]

The satellite ephemeris is a compiled set of state vectors for a given satellite predicted over time [24]. The ephemeris values are computed by the OCS using a Kalman filter to propagate the satellites' positions and velocities to future time epochs. Each satellite's ephemeris describes the satellite's orbit in terms of Keplerian orbital elements. Keplerian orbital elements, also known as classical orbital elements, form the baseline for the GPS ephemeris parameters. The ephemeris parameters are described in detail in the U.S. Air Force document ICD-200c [33]. This document also provides details on computing satellite positions and velocities in the Earth-Centered Earth-Fixed (ECEF) frame [28].

The GPS satellites broadcast a navigational message to the global users of GPS. Each GPS satellite generates a navigational message on two L-band frequencies, denoted L1 (1575.42 MHz) and L2 (1227.60 MHz). The message is unique to each satellite and includes the orbital parameters of the satellites predicted by the MCS.

A typical GPS receiver must have certain components to receive the GPS signals including [34]:

-- an omni-directional antenna to receive the encoded navigational message broadcast by the GPS satellites

-- a filter/amplifier to filter out interfering signals and amplify the GPS signal

-- a delay lock loop receiver / demodulator to provide estimates of the pseudorange, carrier-phase, and navigation data for each satellite

-- a navigation data processor to calculate the position of each satellite based on the navigation data

-- a Kalman filter to estimate the user position and velocity state vector

-- a reference oscillator to provide time and frequency reference for the receiver

A more detailed description of a typical GPS receiver can be found in [34].

2.2.3 Pseudorange Measurements

The MATLAB® simulation created for this research is primarily focused on the impact of adding the TWTT technique to the pseudorange measurements. The generation of an operational GPS pseudorange measurement is described in detail in [24] and [28] and is summarized in this section.

Two pseudorandom noise code- (PRN)-codes, the Coarse-Acquisition (C/A) code and the Precision (P(Y)) code, are modulated onto the L1 and L1/L2 bands respectively. These PRN-codes are unique to each GPS satellite. A basic measurement made by a GPS receiver is the apparent transmit time of the signal from a satellite to the receiver. To determine this signal transmit time, the receiver can compare an internal copy of the PRN signal with the one received from the GPS satellite. The user can then determine the pseudorange between the receiver and the GPS satellite by calculating the time shift required to align the internal PRN signal with the observed signal. Multiplying this phase time shift by the speed of light provides the value of the pseudorange.

Ideally, one would like to measure the true range to the satellite, but instead the pseudorange is used. The term 'pseudorange' is derived from a time difference between the satellite and the receiver, so the effects of the satellite and receiver clock errors are also part of the pseudorange measurement. Since the clock errors are multiplied by the

speed of light, small clock errors can result in large pseudorange errors. A pseudorange measurement (ρ) can be expressed as:

$$\rho = \sqrt{(x^{sat} - x_{rec})^2 + (y^{sat} - y_{rec})^2 + (z^{sat} - z_{rec})^2} + \delta t_{rec} - \delta t^{sat} + \upsilon_{PR} \qquad (2.2.1)$$

where

x^{sat}, y^{sat}, z^{sat} = true ECEF position of the satellite
x_{rec}, y_{rec}, z_{rec} = true ECEF position of the receiver
δt_{rec} = receiver clock bias (units of meters)[1]
δt^{sat} = satellite clock bias (units of meters)
υ_{PR} = pseudorange error expressed in meters

Figure 2.2.3 illustrates the concept of the pseudorange measurement. As shown, at least four GPS satellites are needed to estimate the user position and the receiver clock error (x, y, z, and δt). In Figure 2.2.4, $b = -\delta t_{rec} + \delta t^{sat} - \upsilon_{PR}$.

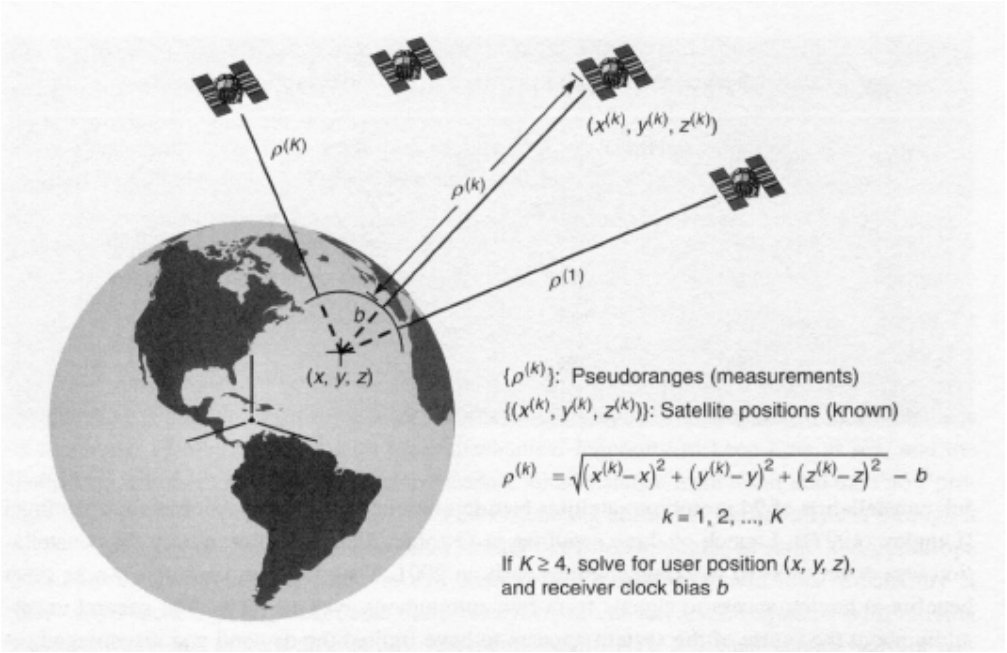

Figure 2.2.3 Illustration of Pseudorange Measurements [28]

[1] Both the receiver and satellite clock bias are multiplied by the speed of light to obtain units of meters.

2.2.4 Carrier-Phase Measurements

The research performed was also concerned with the resulting impact of combining TWTT measurement and carrier-phase GPS measurements. The technique of using carrier-phase GPS measurements uses both the L1 and L2 carrier frequencies instead of the codes transmitted by the GPS satellites. The carrier-phase measurement is the difference between the phases of the receiver-generated carrier signal and the carrier received from a satellite at the instant of the measurement [28]. The phase of the received signal at any point in time can be related to the phase at the satellite and the time of transmission in terms of the transit time of the signal. The carrier phase measurement is consequently indirect and is an ambiguous measurement of the signal transit time. Using this measurement requires correcting for cycle slips that introduce integer ambiguities, which are equal to multiples of the carrier period (635 ps in L1) [28].

In the field of time transfer, the carrier-phase measurement is primarily used for frequency transfer. According to the Time and Frequency Division of the National Institute of Standards and Technology (NIST), results show that the method of using carrier-phase measurements is capable of providing frequency comparisons with a fractional uncertainty of about 2 x 10^{-15} using one day of averaging [27].

The basic carrier-phase measurement, which is in units of cycles, is written as:

$$\phi=\frac{1}{\lambda}\left(\sqrt{(x^{sat}-x_{rec})^2+(y^{sat}-y_{rec})^2+(z^{sat}-z_{rec})^2}+\delta t_{rec}-\delta t^{sat}+\upsilon_{PM}\right)+N \qquad (2.2.2)$$

where

λ = speed of light / f_{L1} = 0.1903 meters/cycle
x^{sat}, y^{sat}, z^{sat} = true ECEF position of the satellite
x_{rec}, y_{rec}, z_{rec} = true ECEF position of the receiver
δt_{rec} = receiver clock bias (units of meters)[2]
δt^{sat} = satellite clock bias (units of meters)
υ_{PM} = phase measurement error expressed in meters
N = integer ambiguity

The trade off is that the code tracking provides essentially unambiguous pseudoranges which are coarse measurements when compared to the carrier phase measurements. The carrier-phase measurements are extremely precise, but are impeded with integer ambiguities that need to be resolved.

2.2.5 Differential GPS

Differential GPS (DGPS) takes advantage of the correlation of errors between receivers [37]. Many error sources are identical (or very similar) for receivers that are relatively close to one another. If one receiver is located at a known point, then the GPS error corrections can be calculated. These corrections can then be applied to multiple receivers in the local area resulting in significantly improved performance. DGPS accuracy is anywhere from 6m down to 1cm depending on which method is used [37]. Table 2.2.1 summarizes the accuracies for different methods of DGPS and non-DGPS.

[2] Both the receiver and satellite clock bias are multiplied by the speed of light to obtain units of meters.

Table 2.2.1 Typical GPS Accuracy [37]

	Mode	Approximate Horizontal Accuracy (RMS)
Stand-Alone	Civilian receiver, SA on (historical)	100 m
Stand-Alone	Civilian receiver, SA on (current)	10 m
Stand-Alone	Military receiver (dual frequency)	6 m
Differential	Code differential	1-5 m
Differential	Carrier-smoothed code differential	0.1-1 m
Differential	Precise carrier-phase (kinematic)	1-2 cm
Differential	Precise carrier-phase (static)	0-2 mm

Differential GPS yields results that are *relative* between two receivers; it doesn't provide *absolute* positioning solutions. One receiver is typically the receiver whose exact location is known, i.e. the reference receiver. The positions of the other receivers are determined relative to the location of the reference receiver. Receivers that are fairly close to each other (within a few hundred km), will have virtually the same errors since the signals that reach them from the satellites will have traveled through virtually the same segment of atmosphere. The idea behind DGPS is that differential corrections are given for each measurement at the reference receiver, and these corrections are then applied to the mobile receiver measurements [38]. If the location of the reference receiver is very accurately known, then it can use its known position to calculate the timing errors. It figures out what the travel time of the GPS signals should be, and compares it with what they actually are. The difference is an error correction factor [38]. This correction factor can then be used by the other receivers to correct their measurements. Using DGPS, many of the errors can be eliminated from the system, including the satellite and receiver clock errors [37].

Two types of differencing methods are commonly used: single-differencing and double-differencing, as shown in Figure 2.2.4. Typically, the single-differencing method is typically used with code differential (pseudoranges) and double-differencing is commonly used with carrier-phase differential. Single-differencing differences the measurements between one satellite and two receivers, in which case the satellite clock error is canceled, the tropospheric and ionospheric errors are reduced and the multipath and noise are amplified by a factor of the square root of two [37]. Double-differencing is differencing two single-differenced measurements. With double-differencing, the satellite clock error and receiver clock error are canceled, the tropospheric and ionospheric errors are reduced and the multipath and noise are amplified by a factor of two [37]. Therefore, double-differencing the GPS measurements offers a way to remove the satellite and receiver clock errors, but at the cost of degraded measurement geometry. When dealing with double-differenced measurements, often the measurements do not reflect what is actually happening in the system due to geometry limitations. This is explained in further detail in [28].

As shown in Figure 2.2.4, consider two satellites ('a' and 'b') and two receivers ('1' and '2'). The phase measurements between receiver one and satellites 'a' and 'b' are φ_1^a and φ_1^b, respectively. Similarly, the phase measurements between receiver two and satellites 'a' and 'b' are φ_2^a and φ_2^b, respectively. The equation for a single-differenced phase measurement is shown in equation (2.2.3). This equation shows that single-differencing takes the difference of the phase measurements between receiver '1' and satellite 'a' and receiver '2' and satellite 'a'. The equation for double-differenced

measurements is shown in the following equation (2.2.4). It is the difference of the single-differenced measurements between receivers '1' and '2' and satellites 'a' and 'b'. GPS pseudorange and carrier-phase measurements are typically expressed using the Earth-Centered Earth-Fixed reference frame that is described in the next section.

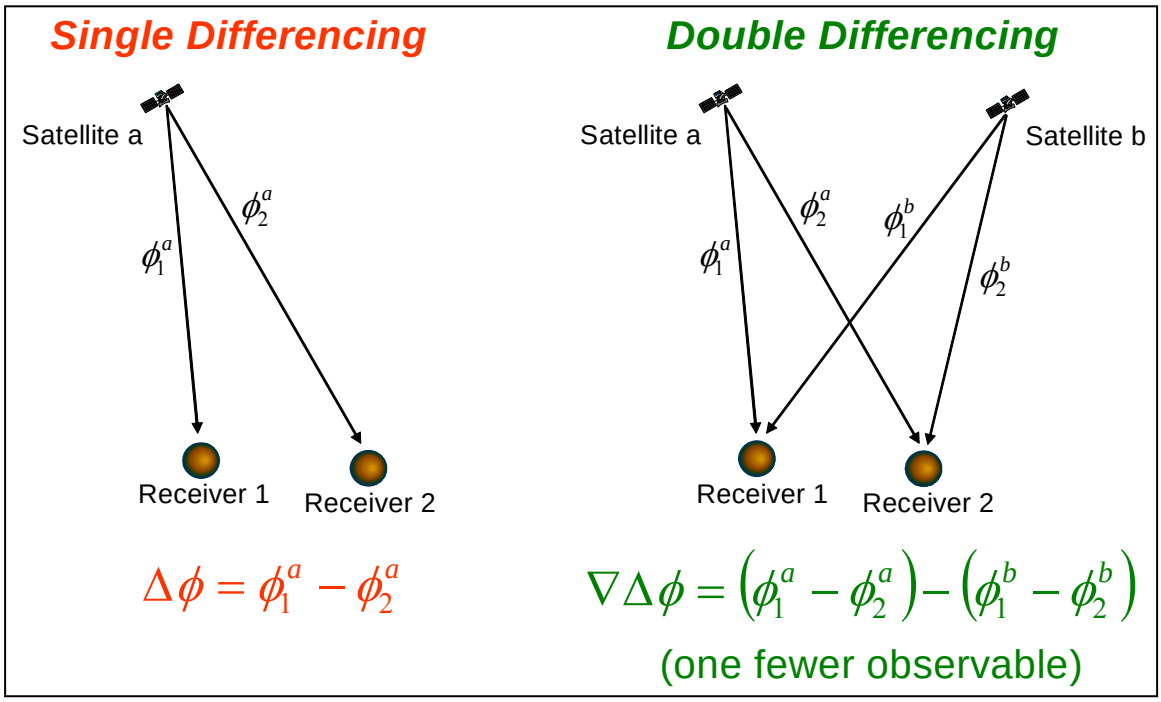

Figure 2.2.4 Differential GPS [37]

$$\Delta\phi_{12}^{a} = \phi_1^a - \phi_2^a \tag{2.2.3}$$

$$\nabla\Delta\phi_{12}^{ab} = \Delta\phi_{12}^{a} - \Delta\phi_{12}^{b} \tag{2.2.4}$$

2.3 ECEF Reference Frame

The Earth-Centered Earth-Fixed (ECEF) reference frame is a Cartesian (orthogonal) reference frame. It is always aligned with a particular meridian, typically the Prime Meridian at Greenwich, and therefore rotates with the Earth. It is not considered an inertial reference frame due to this rotation. The x-axis of the ECEF frame points towards a chosen meridian in the equatorial plane. The y-axis points 90˚ from the x-axis in the direction of Earth's rotation. The z-axis is then determined using the right-hand rule. Figure 2.3.1 shows the ECEF reference frame.

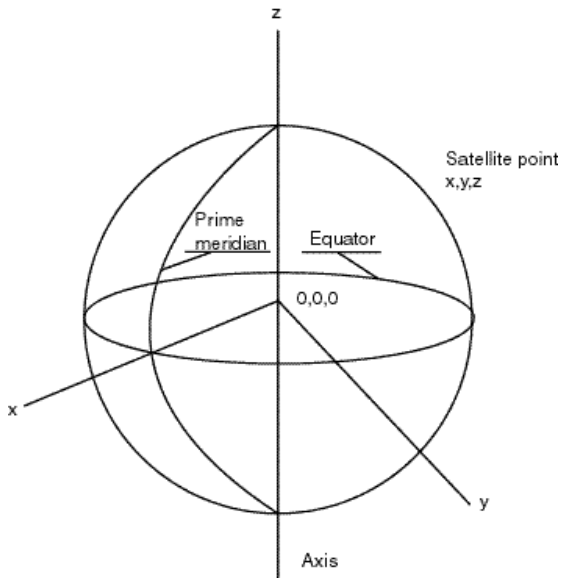

Figure 2.3.1 ECEF Reference Frame [36]

In this simulation, the x-axis points away from the Earth where the equator and the Prime meridian intersect, which is the ECEF frame commonly used by GPS. Using this reference frame is very useful for Earth-based satellite tracking operations because it is easy to calculate distances and vectors between two points and is usually

computationally straightforward. Therefore, it was the obvious reference frame choice for this simulation. The main disadvantage to using this reference frame is that it is not geographically intuitive. The measurements obtained using the method of Two-Way Time Transfer (TWTT) can also be expressed in the ECEF frame. TWTT is described in detail in the next section.

2.4 Two-Way Time Transfer Overview

Two-Way Time Transfer (TWTT) is a technique in which signals are simultaneously exchanged between users to measure their relative clock offsets. If the paths between the clocks are reciprocal (or very nearly so), which is the case for static TWTT systems, the delays cancel and the difference between the clocks is half of the difference in time interval counter readings [9]. TWTT is potentially one of the most accurate ways to compare clocks. There are two forms of the TWTT method: static and dynamic. The static TWTT (S-TWTT) method uses two or more receivers whose x,y,z positions are fixed in the ECEF frame over the measurement interval. Recent advancements in TWTT have enabled the exploitation of dynamic TWTT (D-TWTT) in which one or more receivers is moving. Both of these forms are described in detail in the sections that follow.

2.4.1 Static TWTT

The technique of synchronizing clocks using the two-way satellite time transfer method is not new. The first satellite-based, two-way time transfer took place between the United States and the United Kingdom in 1962 using the Telstar satellite, an early

telecommunication satellite [1]. During the period of 1962-1965, experiments were run using the Telstar II and Relay satellites and included participation by Japan [2]. These experiments utilized large fixed Earth stations, pulses as the signals, and frequency division multiple access. Results during this period were accurate to the order of 0.1 to 20 microseconds (μs). These results illustrated the potential of the method for immense improvements in time coordination on a global basis.

Between 1967 and 1975, several clock synchronization experiments were supported by the Application Technology Satellites (ATS) series operated by the National Aeronautics and Space Administration (NASA). The majority of these experiments were run in laboratories in the U.S. and Japan [4]-[8]. Some of these experiments for the first time obtained a better use of the space segment by involving small on-site earth stations and pseudo-noise sequences. These experiments also allowed the use of code division multiple access (CDMA), helped identify the Sagnac effect as a significant effect to the TWTT technique and overall led to a 5 μs accuracy. The Sagnac effect is an error due to the rotation of the Earth, and is described in detail in Section 2.5.4. Many improvements were made during this period but only with experimental satellites as commercial contributions were not fully suitable or affordable for time transfer [9].

Around 1975, the use of the DoD's Defense Satellite Communication System (DSCS) was implemented as an alternate to the experimental satellites for two-way time transfer. Using the DSCS along with large earth stations and CDMA led to a 0.2 μs operational system that satisfied specific military requirements [10].

Experiments continued between 1976 and 1979 using experimental satellites [17]-[21]. The Communications Technology Satellite (CTS), also known as Hermes by the Canadians, was a high-powered communication satellite operated by the United States. It offered the first look at long term comparisons of time scales in Canada and the U.S [17]. The European satellite, *Symphonie*, provided time scale comparisons across the Atlantic Ocean, within Europe, and between India and Europe [18]-[20]. However, it was generally limited when compared to the CTS.

From 1978 to 1980 an Italian experimental satellite, *SIRIO*, was able to achieve accuracies of a few nanoseconds (ns) [22]. It accomplished this by integrating the satellite motion over periods of a few seconds. In 1983, precision of 1 ns was routinely accomplished by commercially available modems. In 1989 clocks at NIST in Boulder, CO and the U.S. Naval Observatory (USNO) in Washington, D.C. were able to maintain measurement precision of 0.5 ns or better at all times [9].

After more than forty years of improving the two-way time transfer technique, successful results are continuously obtained that include 20 ps time synchronization over fiber and sub-nanosecond time synchronization over satellite communications channels [3].

There are a variety of methods for TWTT. TWTT is most commonly used with static clocks in which a geostationary communications satellite is used as a relay between them. The clocks are then effectively connected using a transmitter and antenna, an uplink to the satellite, a path through the satellite, a downlink (potentially at a different

frequency from the uplink), and an antenna and receiver [9]. This setup can be seen in Figure 2.4.1.

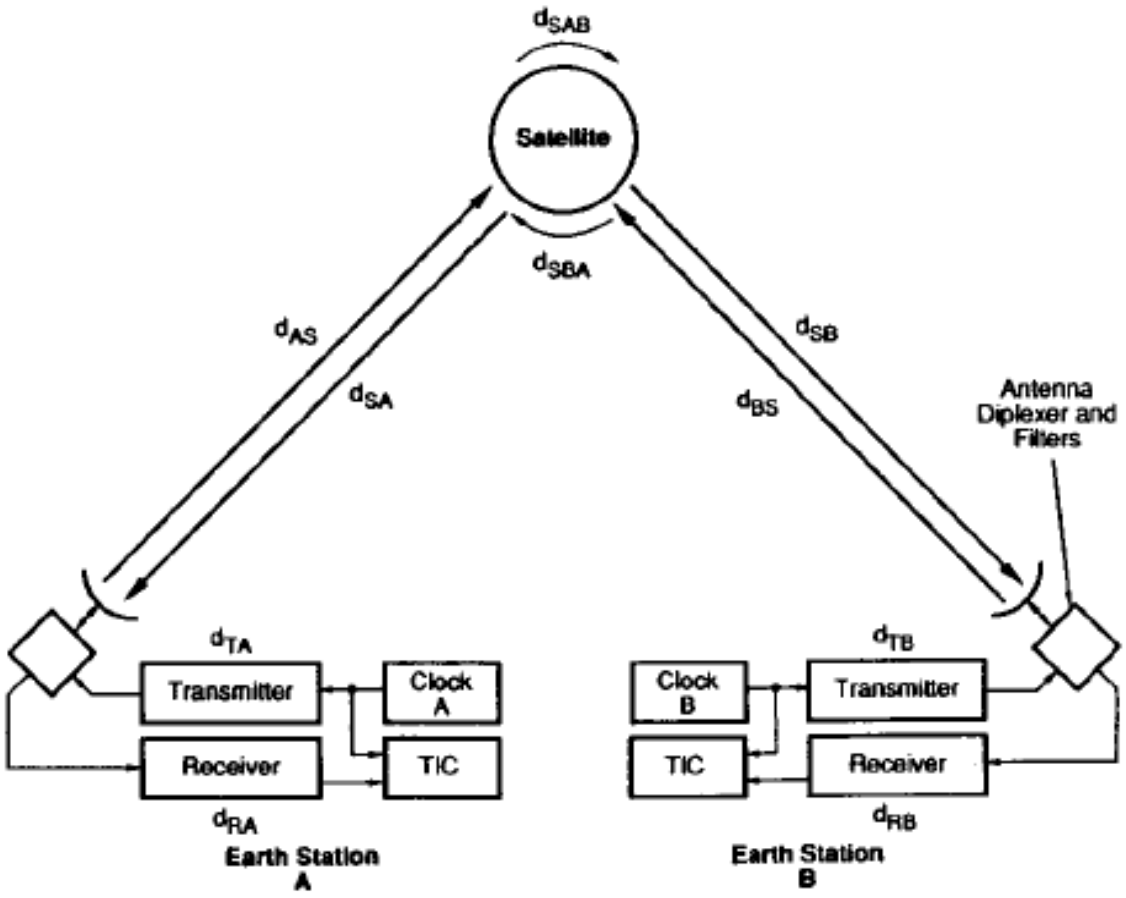

Figure 2.4.1 Static Two-Way Time Transfer Using a Satellite [9]

In Figure 2.4.1,

d_{AS} = delay between receiver A and the satellite during time of transmission
d_{SA} = delay between the satellite and receiver A during time of transmission
d_{BS} = delay between receiver B and the satellite during time of transmission
d_{SB} = delay between the satellite and receiver B during time of transmission
d_{TA} and d_{TB} = delay in transmitter A and B respectively
d_{RA} and d_{RB} = delay in receiver A and B respectively
d_{SAB} and d_{SBA} = delays in the satellite when the signal is going from receiver A to B and B to A respectively
TIC = Time Interval Counter

The basic time interval measurements are made with Time Interval Counters (TICs) at each site. The TICs are started by a pulse from the local clock and stopped by the received pulse from the second station's clock. At the same time as the local clock pulse is starting the TIC it is also being transmitted to the other station. The same process goes on at both stations. Typically a one pulse per second (PPS) signal is used. This time interval data is recorded at both sites and then the data files are exchanged and differenced. Generally there is ample bandwidth in the communications link that the data can be transferred at the same time that the timing pulses are being transmitted. Thus, the two-way technique can effectively be used in real time [9].

The time interval information that is recorded at each station contains the clock differences as well as the delays as shown in the following equations. The variables are the same as were defined for Figure 2.4.1, with additional Sagnac delay terms seen at each station, S_{AB} and S_{BA}.

$$TIC(A) = A - B + d_{TB} + d_{BS} + d_{SBA} + d_{SA} + d_{RA} + S_{AB} \quad (2.4.1)$$

$$TIC(B) = B - A + d_{TA} + d_{AS} + d_{SAB} + d_{SB} + d_{RB} + S_{BA} \quad (2.4.2)$$

Where TIC(A) and TIC(B) are the time interval counter readings, A and B are the clock times of the respective ground stations. The time difference between clocks A and B can be determined by differencing equations (2.4.1) and (2.4.2) for individual, simultaneous TIC readings. The result of the time difference is shown in Table 2.4.1.

Table 2.4.1. Time Difference (ΔT) Using TWTT

A-B = [TIC(A)-TIC(B)]/2	TIC readings
$+ (d_{TA}-d_{RA})/2 - (d_{TB}-d_{RB})/2$	Earth Station Equipment Delay
$+ (d_{AS}-d_{SA})/2 – (d_{BS}-d_{SB})/2$	Propagation Delay
$+ (d_{SAB}-d_{SBA})/2$	Satellite Delay
$- 2\omega Ar/c^2$	Sagnac Effect

In the case S-TWTT, $d_{SA} \approx d_{AS}$ and $d_{SB} \approx d_{BS}$ over the measurement interval. Let $\Delta Sagnac = S_{AB}-S_{BA}$. For the static case, ΔSagnac is a constant. The delay in the Earth station equipment is the same when transmitting and receiving and consequently gets subtracted out when differencing the measurements. The satellite delay is also the same when relaying information from clock A to clock B as it is when relaying from clock B to clock A; for that reason it cancels as well when the measurements are differenced. Therefore, the time difference measurement ΔT reduces to:

$$\Delta T = A - B = \frac{1}{2}[TIC(A) - TIC(B) + \Delta Sagnac] \qquad (2.4.3)$$

Using a geostationary satellite for two-way time transfer can be a practical technique for comparing and synchronizing clocks. This method offers high levels of precision and accuracy at reasonable costs because (1) the use of a transfer or calibration earth station that provides the required measure of earth station delays, (2) the Sagnac effects may be accurately calculated with relatively imprecise information on the locations of the satellite and receiver clocks, and (3) satellite and propagation path delays cancel to a large extent due to a high degree of path reciprocity [9]. Recent work has been done to increase the potential of using TWTT by studying the effects of dynamic TWTT, as will be described next.

2.4.2 Dynamic TWTT

Dynamic TWTT involves obtaining the same raw TWTT measurements described in the previous section for static TWTT, now between two nodes where one (or both) may be moving. This research is based upon recent advancements in dynamic TWTT (D-TWTT) [3]. As stated previously, the first successful tests using dynamic TWTT were not completed until 2002 [3] in which geostationary communications satellites were used as a relay between two clocks that are on moving vehicles separated by large distances. Results from these tests maintain accuracy on the order of 2-5 nanoseconds (ns) for D-TWTT using line-of-sight measurements. Motion-related errors that are not present in the S-TWTT are introduced in the D-TWTT system due to the moving receivers. Figure 2.4.2 illustrates the dynamic TWTT configuration, which is identical to the static case in Figure 2.4.1 except one of the nodes is now moving over the measurement interval. The addition of receiver motion changes the value of the two-way clock difference [43].

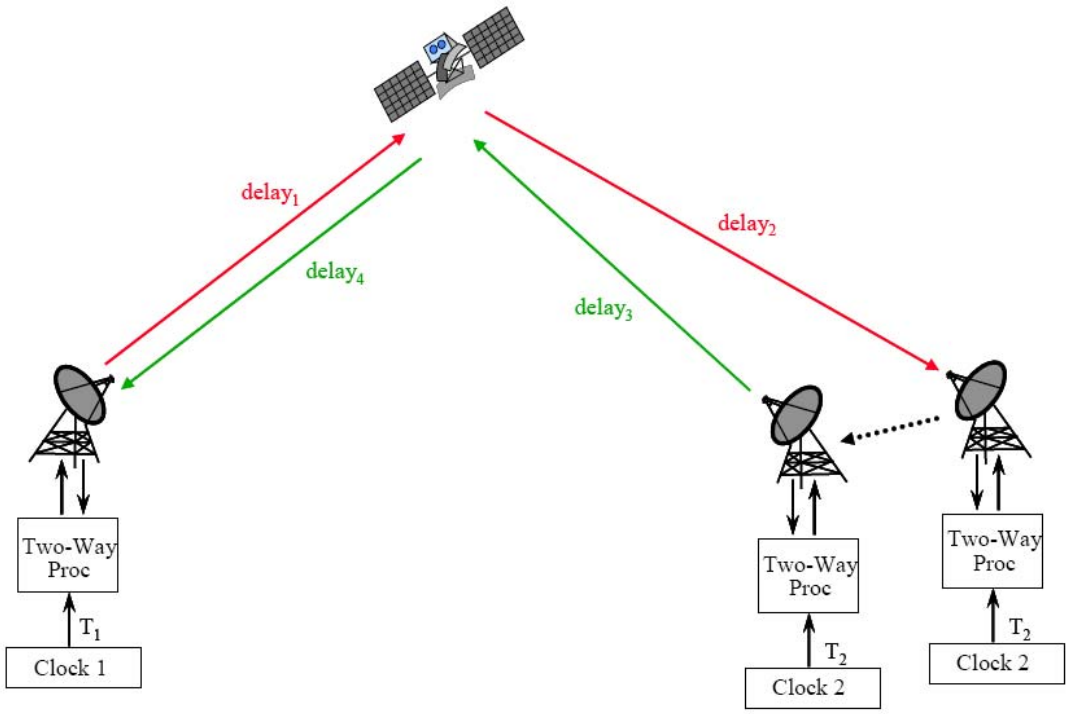

Figure 2.4.2 Dynamic Two-Way Time Transfer Using a Satellite [43]

For the dynamic case, the cancellations assumed in the static case are not entirely valid. For the D-TWTT example shown in Figure 2.4.2, $delay_1 \approx delay_4$, but $delay_2 \neq delay_3$ over the measurement interval. These correspond to $d_{AS} \approx d_{SA}$ and $d_{SB} \neq d_{BS}$ in the S-TWTT notation. This is because over the time interval between transmitting a signal and receiving the signal from clock 1, the platform containing clock 2 has moved and the radial delay to and from the satellite has changed. Additionally, the Sagnac term for the moving platform becomes time varying, based on the change in location of the platform as well as the path traveled over the measurement interval [43].

The time differenced measurement in the dynamic case can be written as:

$$\Delta T = A - B = \frac{1}{2}[TIC(A) - TIC(B) + \Delta prop\_delay + \Delta Sagnac] \quad (2.4.4)$$

Where Δprop_delay is the change in the propagation delay over the measurement interval. The Δprop_delay is a time-varying value that depends on the relative platform motion as well as how the velocity vector is projected onto the line of sight vector to the satellite over the measurement interval. In the S-TWTT case, the ΔSagnac term is a constant, but in the D-TWTT case it is a time-varying value that depends on the absolute position of the two platforms on the earth and the velocity vector projected onto the equatorial plane [43].

This section discussed the history and theory of GPS as well as the differences between static TWTT and dynamic TWTT. Section 2.5 covers in more detail the typical errors observed when performing these methods.

2.5 Typical Errors

The following is a list of the typical errors seen when using GPS and/or TWTT. Sources of errors include equipment delays, propagation delays, satellite delays, Sagnac delay, and motion-related errors.

2.5.1 Equipment Delays

Transmit and receive delays within the same piece of earth station equipment cancel when differencing measurements including these terms. However, there is no reason for transmit and receive delays of different earth station equipment to cancel perfectly since they are caused by physically different pieces of equipment. This is one of the main sources of inaccuracy in the TWTT technique and is present in GPS as well.

2.5.2 Propagation Delays

When the uplink and downlink frequencies are the same, the paths followed by the uplink and downlink are essentially the same for static receivers. Therefore, nearly all of the propagation delays cancel out due to symmetry. It is possible for the uplink frequency to be different than the downlink frequency, in which case the propagation delay will not be exactly the same. In dynamic systems, the paths followed by the uplink and downlink are not exactly symmetric and therefore produce a delay. These delays are present in both dynamic GPS and dynamic TWTT measurements and must be accounted for.

2.5.3 Satellite Delays

The satellite time delay term represents the delays in the signal due to the satellite, d_{SAB} and d_{SBA}. These usually cancel nearly perfectly since in most cases the same satellite transponder is used for both directions. In other cases different transponders are used and then the cancellation is not exact. These delays are important to model and account for when performing TWTT. The performance of TWTT using a satellite as a relay between two clocks to accurately determine clock differences is bound by how accurately satellite delays can be estimated. When considering GPS measurements, the satellite delays are included in the broadcast ephemeris as known biases that are then removable.

2.5.4 Sagnac Delay

The Sagnac delay is due to a rotating system and finite signal velocity [9]. It corrects for the fact that the system is not in a fixed inertial reference frame. The value of

the Sagnac delay is $2\omega Ar/c^2$ for stations on the Earth's surface, where ω is the angular velocity of the earth, c is the speed of light, and Ar is the area defined by the projections onto the equatorial plane by the line segments connecting the satellite and the earth's center to the two earth stations as illustrated in Figure 2.5.1.

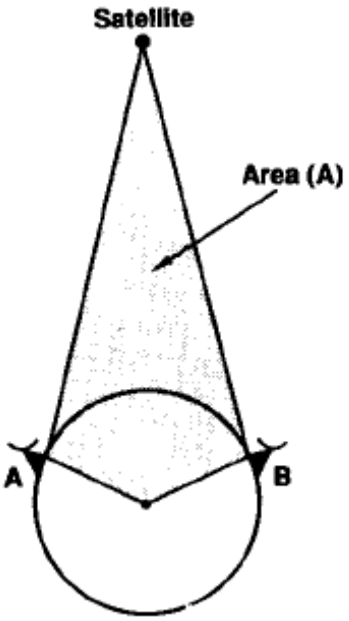

Figure 2.5.1 Area in the Sagnac Equation [9]

Figure 2.5.2 demonstrates the concept of the Sagnac delay. It shows earth stations A and B, and the satellite at an instant in time (1) when the pulses are sent to the satellite. The earth rotates causing the earth station A to be at location (3) when the signal from earth station B arrives. The earth's rotation and the finite velocity of the signal have combined to increase the path length from B to A. Likewise, the signal from A to B experiences a corresponding decrease in path length.

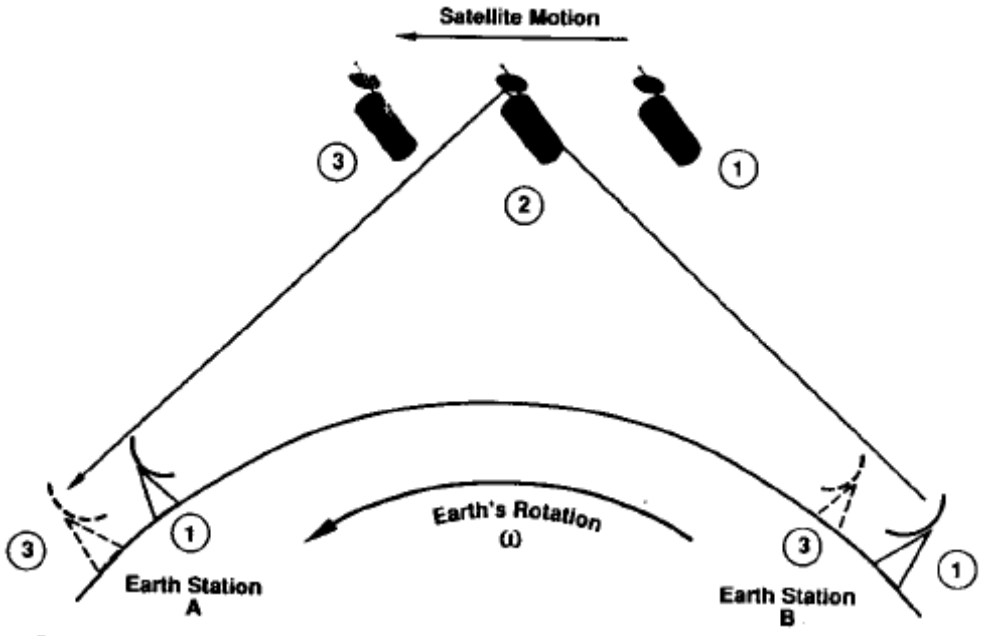

Figure 2.5.2 Demonstration of the Sagnac Delay i.e.: Earth's Rotation Introduces Non-reciprocity [9]

In the static TWTT case, the Sagnac error is effectively a propagation delay. The effect of the Sagnac error acts on the physical clock, altering its performance from its static state. The Sagnac error is not generally corrected in the TWTT measurements but compensated for by the user of the two-way data [43].

However, in dynamic TWTT, the Sagnac is non-constant and non-reciprocal. In the D-TWTT case, the Sagnac error is a function of the motion of a platform (not just the rotation of the earth) and, if not corrected, will cause the TWTT calculation to be compromised [43]. It is a measurement effect that is a direct result of the two-way measurement that is being made using a moving platform.

2.5.5 Motion-Related Errors

As mentioned in Chapter One, modeling dynamic TWTT includes simulating motion of the vehicles that will introduce additional relativistic and non-relativistic errors [9]. These errors include errors in the receiver velocity, the velocity propagation, the exact TWTT satellite location, and the relativistic effects on clocks.

The velocity error for the dynamic TWTT scenario is similar to the Sagnac error in the static case, except now the error includes a moving platform, not just the Earth's rotation. An error in velocity also directly affects the propagation delay errors as well as the clock errors. Theoretically, satellites in a geostationary orbit remain in the exact same location relative to the Earth's reference frame. In reality, however, a geostationary satellite's location actually varies slightly while it maintains the same view of the earth.

Finally, relativity induces clock errors. The higher in altitude a clock is located, the faster it will go due to a reduced force of gravity. This error affects both GPS and TWTT measurements. In both cases, the satellite clocks have gravitational and motional frequency shifts that are so large that without carefully accounting for them, the systems would not work [40]. The results of this error source can be seen in Figure 2.5.3. If the motion-related errors are known or can be closely approximated, these terms can be calculated and removed.

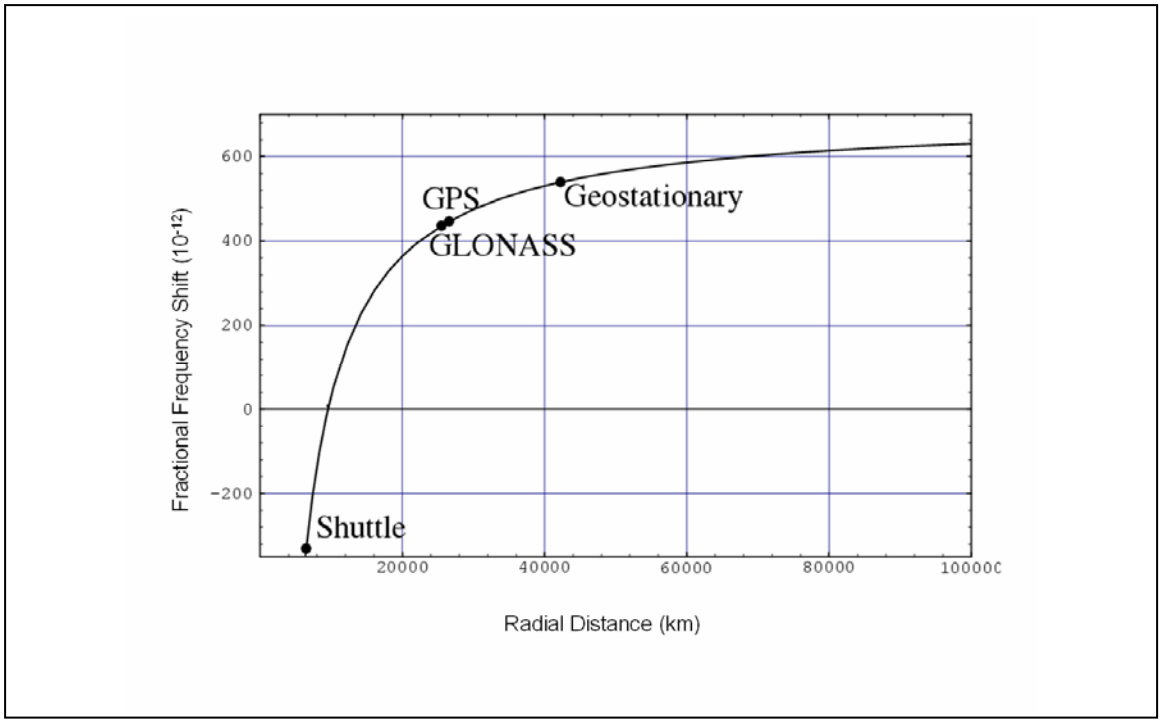

Figure 2.5.3 Net Fractional Frequency Shift of a Clock in a Circular Orbit [39]

This section described the typical errors seen in GPS measurements and also in static TWTT and dynamic TWTT measurements. Next, the least squares estimation filter will be described as it is typically the filter used when propagating states containing to GPS measurements.

2.6 Least Squares Estimation Filter

When dealing with GPS, the desired states to be estimated are the 3-D receiver position and clock errors. These states are not continuously being updated in an iterative manner as with a Kalman filter. Instead, they are estimated independently on an epoch-by-epoch basis.

For this research, all measurements for a given time epoch or range of time epochs are available before the estimation process begins, and the states are then processed in one group, or in a "batch" [23]. One objective of a least squares estimator is to find one solution among all of the possible solutions that will minimize the mean square difference between the actual observations and the generated observations derived by the filter [24]. The process of minimizing the sum of the squares of the observation residuals (actual - generated) is known as the method of least squares.

The state vector X is a set of variables that describe everything that is desired to be known about a system. It often includes all of the information needed to determine how the system changes over time, however in this research this is not the case. Knowing an estimate alone is not adequate; the accuracy of that estimate must also be known. The covariance matrix $P_{\delta x}$ reflects how well the state is known.

Each measurement update gives information about the state values. For example, for a GPS system it might give updates of the position or clock biases. State values are adjusted to reflect the updated measurement. The covariance matrix is adjusted to reflect how well the state is known with the updated measurement. The measurement can only be as precise as the magnitude of the measurement noise. The effect of a measurement on the state and covariance is determined by a tradeoff between the measurement noise (how good the measurement is) and the covariance matrix (how well the state is known at this point) [41].

The vector of measurements, also known as the observation relation, is expressed in terms of the state values and is written as:

$$z_i(t_i) = G(x(t_i), t_i) \tag{2.6.1}$$

where

z_i is the observation relation at time t_i

$G(x(t_i),t_i)$ is a function that describes what it is thought that the measurement should be based on the current state

i is the index, from 1 to N, of the number of observations in the batch

The relationship between the measurements and states is given by the observation matrix, H. H contains the partial derivatives of the observations with respect to the state vector components. Again, i is the index, from 1 to N, of the number of observations in the batch.

$$H_i = \frac{\partial G(x(t_i), t_i)}{\partial X} \tag{2.6.2}$$

The resulting H will be an m x n matrix where m is the number of measurements and n is the number of states. Each row of the observation matrix corresponds to one measurement. Each term in the row is the partial derivative of the measurement equation with respect to the corresponding state variable.

Next, the measurement error covariance matrix Q is determined. The matrix Q is a diagonal matrix whose diagonal values are the error variances of the estimated states, and the off-diagonal terms are cross-covariances describing the correlations of the errors between the states. It is typically based on expected error statistics, which are based on knowledge of the problem. The residual vector is the 'actual' minus the 'expected' measurement values, and is shown in equation (2.6.3).

$$\vec{r}_i = z_i - G(x(t_i), t_i) \tag{2.6.3}$$

where

$\vec{r}_i$ is the measurement residual vector

z_i is the observation vector

$G(x(t_i),t_i)$ is a function that describes what it is thought that the measurement should be based on the current state

Finally, correction to the state vector, $\delta x(t_i)$, and its error covariance, $P_{\delta x}$, can now be computed.

$$P_{\delta x} = (H_i^T Q^{-1} H_i)^{-1} \tag{2.6.4}$$

$$\delta x(t_i) = (H_i^T Q^{-1} H_i)^{-1} H_i^T Q^{-1} \vec{r} \tag{2.6.5}$$

Equation (2.6.5) can be used to turn the current state into an updated estimate of the state:

$$\vec{x}(t_i) = \vec{x}(t_i) + \delta x(t_i) \tag{2.6.6}$$

When two successive values of δx both lie well within the one-sigma error ellipsoid, the result has converged. If the process has not converged, the estimation process must begin again. If it has converged, it can be said that $\vec{x}(t_i)$ is an estimate of the true state whose covariance is $P_x = P_{\delta x}$. The process of the non-linear least squares estimator that was used is summarized in the flow chart in Figure 2.6.1.

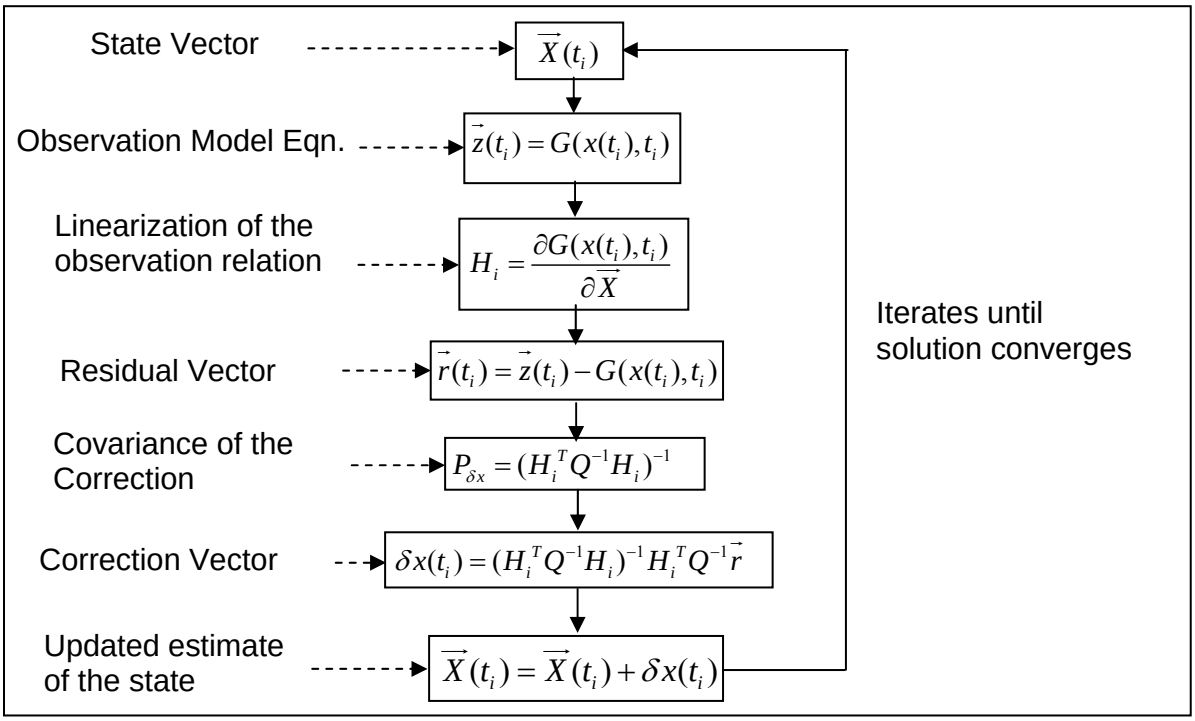

Figure 2.6.1 Non-Linear Least Squares Estimator Flow Chart

2.7 Summary

This chapter presented the pertinent background information on the fundamental concepts of the research. An overview of the GPS and TWTT algorithms was given as well as an overview of the typical errors seen in GPS and TWTT measurements. Finally, an introduction to least-squares batch filtering was given. Chapter 3 will discuss the methodology of the research and how it utilized the concepts described in Chapter 2.

III. Methodology

3.1 Introduction

This chapter describes in detail the methodology, algorithms, and assumptions used to successfully accomplish the research objectives identified in Chapter One. This research is based on a MATLAB®-based simulation, described below. Chapter One gave a general overview of the simulation and a block diagram of the simulation was presented in Figure 1.3.1. The simulation is comprised of five major sub-components. Each of these sub-components of the simulation including the user-input parameters, the process of determining the 'true data', the clock model used in the simulation, and the method of generating simulated measurements, the process of the least-squares filter, and the performance analysis will be described in detail in the following sections. The overall approach is to use a batch least-squares algorithm to estimate position and clock error for each receiver in the network. This is done independently at each measurement epoch, as will be explained. Finally, the random number seed concept and use will be explained.

3.2 Parameters

The simulation for this research starts with a parameters block whose purpose is to get the user's desired input for certain variables. It gathers user defined values for variables such as:

1) The number of receivers to use – this simulation was created to support multiple applications and, depending on the application, the user may wish to use a variable number of receivers.
2) The time history of receiver position – depending on the desired application, the simulation allows for variable receiver positions. It can support both static and dynamic receivers and allows the user to input position vectors in Longitude/Latitude/Altitude for each receiver over the entire time interval. For the baseline results, a 6-receiver network was used where the receivers are separated by 1 km. They are positioned 1 km above sea-level at the point where the Equator and the Prime Meridian intersect. This location was chosen for simplicity of analysis, however, the receiver network location can be specified to be located anywhere.

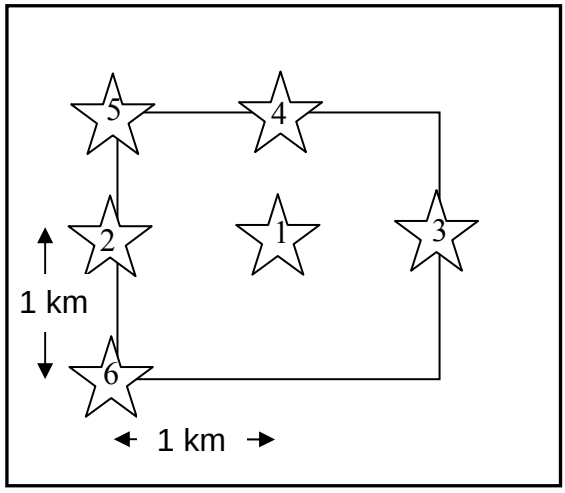

Figure 3.2.1 Baseline Receiver Configuration

3) A broadcast ephemeris file as well as the corresponding precise ephemeris file for the date desired – as will be shown by the first trade study in Section 4.4, this simulation is valid for any day of the year. The user can determine which day's records are preferred and input the corresponding file names for the broadcast and precise ephemeris.

4) The type of observables to use – the user can decide to use single and/or double differenced pseudoranges and phase measurements, and whether or not to include the TWTT measurements. Any combination may be specified for complete versatility.

5) Modeled Error Magnitudes – as technology improves, the noise values for certain measurements may decrease. This simulation allows the user to specify the standard deviation of the noise and error values for pseudorange noise, phase measurement noise, position error, clock noise, TWTT satellite position error, and the TWTT noise.

Table 3.2.1 Modeled Error Magnitudes

Error	**Standard Deviation (m)**
Pseudorange	1
Carrier Phase	0.01 (0.053 cycles)
TWTT Satellite Position	5
Initial Receiver Position	10
Clock Bias	3
TT(A)	3
TT(B)	0.3
TT(C)	0.03
TT(D)	0.003

6) Epoch length – as will be discussed in more detail in Section 3.7, the length of the time epoch has an effect on statically similar results when using the random number generator in MATLAB®.

Within this block the user-specified receiver positions are converted from Longitude/Latitude/Altitude into time-dependent vectors in the Earth-Centered Earth-Fixed (ECEF) coordinates. This reference frame was described in detail in Section 2.3. The parameters block takes the variables described above and re-distributes them globally to the remaining sub-components of the simulation. The parameters block is shown in Figure 3.2.2. The next function called in the simulation is the truth model, which is described in Section 3.3.

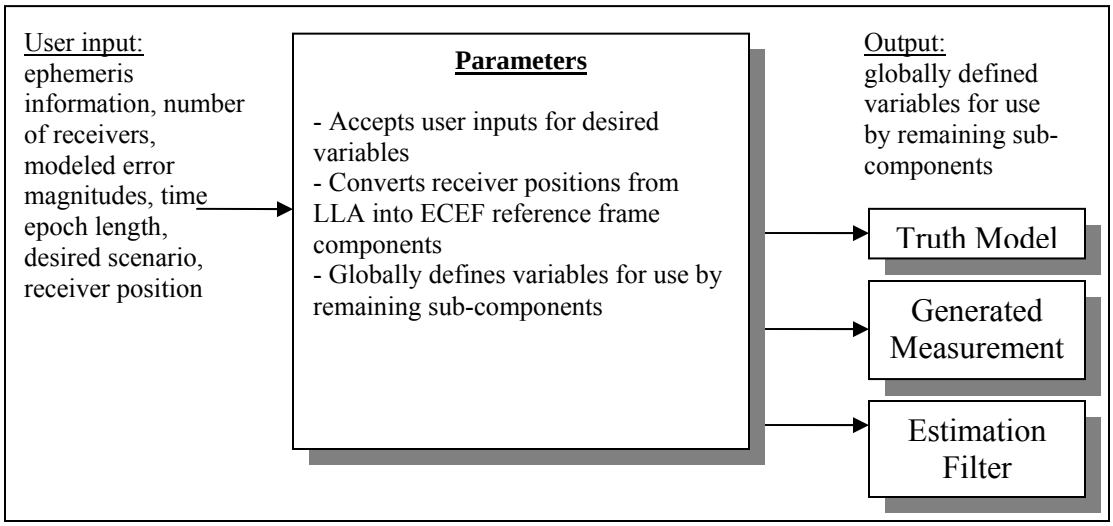

Figure 3.2.2 Block Diagram of Parameters Function

3.3 Truth Model

The truth model takes inputs from the parameters specified by the user. The receiver locations specified by the user are assumed to be the "true" locations at each time epoch. Using the precise ephemeris, the precise satellite positions and their corresponding clock errors can be determined, and these are assumed to be the "true" position and clock error for each satellite. A block diagram of the truth model is shown in 3.3.1.

Satellite visibility is based on satellite location relative to the receivers. A minimum satellite elevation cutoff is specified by the user (one trade study looks at varying this cutoff to determine effects on the solution) which also dictates whether or not the satellite is visible. If a satellite is valid in the ephemeris and is above the elevation cutoff at a certain epoch, it is deemed 'visible' to the receivers.

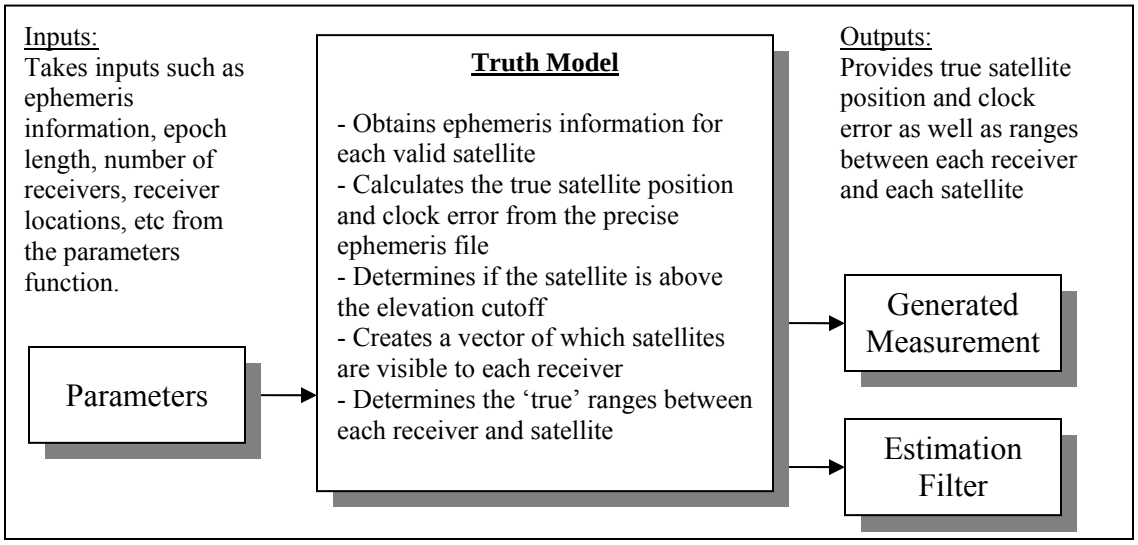

Figure 3.3.1 Block Diagram of the Truth Model

The number of visible satellites for each receiver and the pseudo-random noise (PRN) identifiers of those satellites are determined and stored for future reference. The true ranges between each receiver and the satellites that are visible to that receiver are simply:

$$R_{true}(t) = X^{sat}(t) - X_{rec}(t) \tag{3.3.1}$$

where

R_{true} = true range between the satellite and receiver
X^{sat} = true ECEF satellite position (x,y,z)
X_{rec} = true ECEF receiver position (x,y,z)
t = time epoch

The communications satellite used for the two-way transfer is typically in geosynchronous orbit above the receivers. The user can input the location of the satellite and that is considered the 'true' position. For this research the two-way reference

satellite was specified to be directly above where the equator and Greenwich Meridian intersect at geosynchronous orbit (35,786 km above the earth's surface).

The true range between the communications satellite and the receivers can be calculated using equation (3.3.1).

3.4 Clock Model

When using the Least Squares Estimator to propagate the state values forward in time, it is necessary to properly simulate the real performance of the Rubidium atomic clocks used by the GPS satellites in order to provide realistic inputs to the simulation. Rb clock q values were used for each GPS clock because of the singularity that the Cs clock q_3 value created when propagating the clock states with the 3-state model. The performance of the positioning system is bound by the clock errors so a realistic clock model is desired. Satellite clock synchronization is achieved by estimating the time offset, drift, and drift rate of each satellite clock relative to GPS time and transmitting the clock parameters of the estimated model in the satellite's navigation message [1]. Therefore, the true GPS clock performance has to be measured and approximated for use in the least squares filter.

In this research, however, since the estimation filter is iterating on an epoch-by-epoch basis and does not propagate the state forward, the clock errors do not need to be explicitly modeled in this manner. The clock model explained in this section will become important in the next generation of the simulation, when the simulation will be used to propagate the state forward in time.

The performance of atomic clocks can be simulated using a 3-state polynomial process driven by white noise. The discrete process model and its covariance can be written as [12]:

$$\Phi(\tau) = \begin{bmatrix} 1 & \tau & \frac{1}{2}\tau^2 \\ 0 & 1 & \tau \\ 0 & 0 & 1 \end{bmatrix} \tag{3.4.1}$$

$$\begin{bmatrix} x_1(t_{k+1}) \\ x_2(t_{k+1}) \\ x_3(t_{k+1}) \end{bmatrix} = \begin{bmatrix} 1 & \tau & \frac{1}{2}\tau^2 \\ 0 & 1 & \tau \\ 0 & 0 & 1 \end{bmatrix} \begin{bmatrix} x_1(t_k) \\ x_2(t_k) \\ x_3(t_k) \end{bmatrix} + \begin{bmatrix} w_1(k) \\ w_2(k) \\ w_3(k) \end{bmatrix} \tag{3.4.2}$$

$$Q_k(\tau) = E\left[w(k)w(k)^T \right] = \begin{bmatrix} q_1\tau + \frac{1}{3}q_2\tau^3 + \frac{1}{20}q_3\tau^5 & \frac{1}{2}q_2\tau^2 + \frac{1}{8}q_3\tau^4 & \frac{1}{6}q_3\tau^3 \\ \frac{1}{2}q_2\tau^2 + \frac{1}{8}q_3\tau^4 & q_2\tau + \frac{1}{3}q_3\tau^3 & \frac{1}{2}q_3\tau^2 \\ \frac{1}{6}q_3\tau^3 & \frac{1}{2}q_3\tau^2 & q_3\tau \end{bmatrix} \tag{3.4.3}$$

where

$x_1(t_k)$ and $x_1(t_{k+1})$ = the clock bias error at times t_k and t_{k+1}

$x_2(t_k)$ and $x_2(t_{k+1})$ = the clock drift error at times t_k and t_{k+1}

$x_3(t_k)$ and $x_3(t_{k+1})$ = the clock drift rate error at times t_k and t_{k+1}

$\tau = t_{k+1} - t_k$ = the time interval

$w_1(k)$, $w_2(k)$, and $w_3(k)$ = independent white noises

q_1, q_2, and q_3 = the continuous process noise power spectral densities representing the bias, drift, and drift rate respectively

$\Phi(\tau)$ is the state transition matrix that propagates the current clock bias, drift, and drift rate errors forward in time from t_k to t_{k+1}

Q_k is the discrete-time process noise covariance matrix

Due to their stochastic nature, the clocks cannot be modeled deterministically. By modeling the performances of the random walk noise values (w_1, w_2, and w_3), the

characteristic Allan Variance curves of the atomic frequency standards can be matched [14]. Figure 3.4.1 is an example of a 3-state random clock process. Drawing a best fit curve through the simulated clock error, it is apparent that the performance of a 3-state atomic clock is quadratic in nature. The statistics of the random walk noise values are determined by the values of the variance elements (q_n) of Q_k in equation (3.4.3) [14,15].

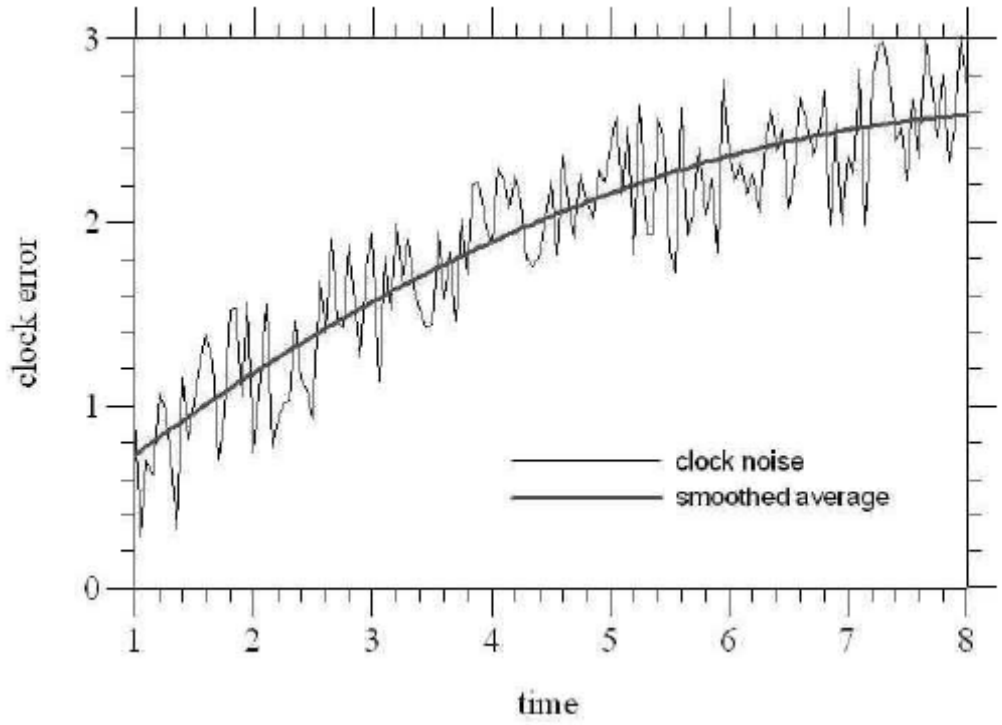

Figure 3.4.1 Comparison of Simulated Clock Error
and a Quadratic Fit (used in batch filters) [14]

The GPS satellites depend on either Cesium (Cs) or Rubidium (Rb) clocks to provide a stable output frequency. This research used research performed in the Clock Improvement Initiative [16] to choose q values for equation (3.4.3). Table 3.4.1 shows the resulting q values for the Cs and Rb clocks following the conclusion of the Clock Improvement Initiative [16].

Table 3.4.1 Process Noise Values for GPS Rb and Cs Clocks [16]

	Rubidium Clock	Cesium Clock
q1 (bias)	1.11 x 10-22 s2/s	4.44 x 10-22 s2/s
q2 (drift)	2.22 x 10-32 s2/s	3.33 x 10-32 s2/s
q3 (drift rate)	6.66 x 10-45 s2/s	0 s2/s

The initial clock bias and drift parameters were collected from [11] for each satellite in order to calculate each GPS satellite clock's 3-state random process. The initial drift rate was assigned a value of zero. The bias, drift, and drift rate initial values were propagated each time step using equation (3.4.2). In order to calculate the random walk noise (w_1, w_2, and w_3) of each GPS clock for each time step, equation (3.4.3) was multiplied by a MATLAB® normalized random number generator. This allowed the amount of random walk for each clock at each time step to be randomly scaled by a specified amount. Rb clock q values were chosen for each GPS clock due to the singularity that the Cs clock q_3 value created when propagating the clock states with the 3-state model being implemented [13].

Each receiver was given a random initial bias and drift. The drift rate (time derivative of drift) was assumed to start at zero for each receiver. The receiver clock biases, drifts, and drift rates were simulated to be similar to the satellite values and were propagated using the satellite clock propagation procedure described above. These biases, drifts, and drift rates were used in the 'generated measurements' sub-component of the simulation, which is described in detail in the next section.

3.5 Generated Measurements

The generated measurements sub-component creates a simulation of the desired measurements based on the true measurement values obtained from the truth model and the modeled errors specified by the user in the parameters function. A block diagram of the 'generated measurements' sub-component is shown in Figure 3.5.1.

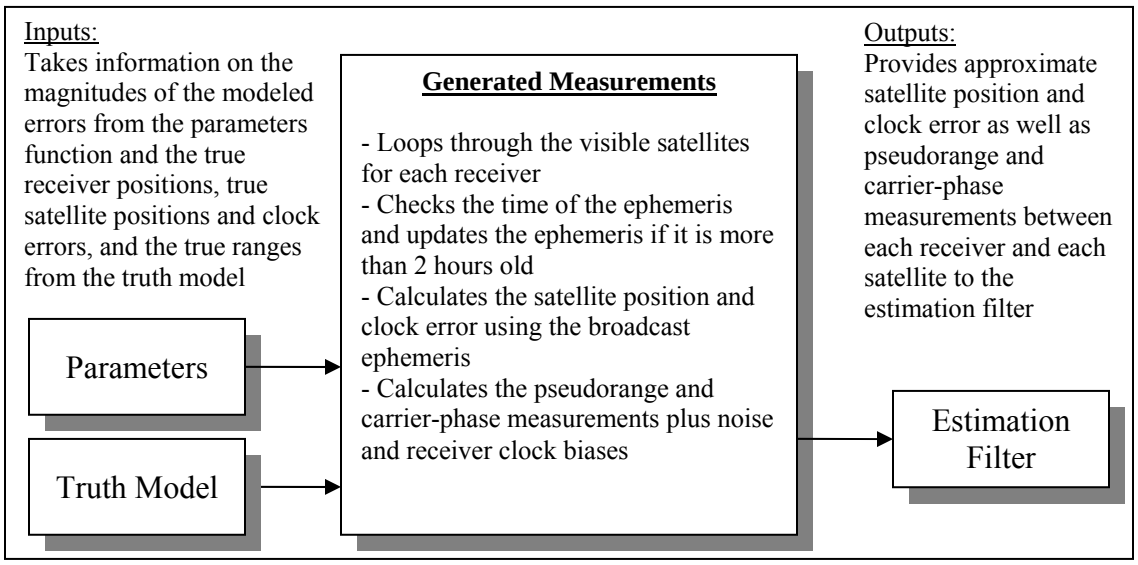

Figure 3.5.1 Block Diagram of the Generated Measurements Function

Using the broadcast ephemeris, an approximate position and clock error can be determined for each satellite. The satellite position obtained using the broadcast ephemeris is used along with the true receiver position plus the position error specified by the user in order to approximate the range between receivers and satellites.

As defined in Chapter 2, the pseudorange values are the normalized true range measurements plus the pseudorange noise specified by the user, the satellite clock bias, and the receiver clock bias. It is rewritten below for easy reference.

$$\rho = \sqrt{(x^{sat} - x_{rec})^2 + (y^{sat} - y_{rec})^2 + (z^{sat} - z_{rec})^2} + \delta t_{rec} - \delta t^{sat} + \upsilon_{PR} \qquad (2.2.1)$$

where

x^{sat}, y^{sat}, z^{sat} = true ECEF position of the satellite
x_{rec}, y_{rec}, z_{rec} = true ECEF position of the receiver
δt_{rec} = receiver clock bias (units of meters)[3]
δt^{sat} = satellite clock bias (units of meters)
υ_{PR} = pseudorange error expressed in meters

The carrier-phase measurement is simply the pseudorange equation (with the carrier phase measurement error replacing the pseudorange error) multiplied by 1/lambda, where lambda is the speed of light divided by the frequency of the GPS L1 signal, 1575.42MHz. It is rewritten below for quick reference. It is assumed in this research that the integer ambiguity is deterministic and resolvable and, therefore, N = 0. This assumption was made for simplicity in the simulation.

$$\phi = \frac{1}{\lambda}\left(\sqrt{(x^{sat} - x_{rec})^2 + (y^{sat} - y_{rec})^2 + (z^{sat} - z_{rec})^2} + \delta t_{rec} - \delta t^{sat} + \upsilon_{PM}\right) + N \qquad (2.2.2)$$

where

υ_{PM} = phase measurement error expressed in meters

The time difference between the reference receiver clock and the remaining receiver clocks was calculated using the two-way time transfer technique. The Sagnac error and the motion related errors were not included since they are deterministic and can be removed. They could be included, modeled, and then removed, in which case they would have no impact on the results of the simulation. The only time the deterministic

[3] Both the receiver and satellite clock bias are multiplied by the speed of light to obtain units of meters.

effects need to be modeled in the simulation is when real data is being input in real time. This simulation assumes the propagation delays cancel as they would in the S-TWTT scenario for simplicity. Assuming the motion effects are properly accounted for, the TWTT time measurement (ΔT) can be described as:

$$\begin{aligned}\Delta T &= \frac{1}{2}\big(TIC(1) - TIC(n)\big) \\ &= \frac{1}{2}\Big[\delta t_1 - (\delta t_n + d_n + d_1) - \big(\delta t_n - (\delta t_1 + d_1 + d_n)\big)\Big] \\ &= \frac{1}{2}\big[2\delta t_1 - 2\delta t_n\big] \\ &= \delta t_1 - \delta t_n + \upsilon_{TWTT}\end{aligned} \tag{3.5.2}$$

where

δt_1, δt_n are the clock errors at receivers 1 and n respectively
υ_{TWTT} is the TWTT error

Another observable can be obtained from the TWTT measurements that can be used to decrease positioning error as well. The sum of the delays in the TWTT are obtained by adding equations (2.4.1) and (2.4.2). The clock errors of the ground stations δt_1 and δt_n cancel when summing the delays and all that remains is the sum of the propagation delays d_1 and d_n plus the TWTT error. For this simulation, the uplink and downlink distances between each receiver and the TWTT satellite are assumed to be equal for simplicity. With this assumption, the four propagation delays shown in equations (2.4.1) and (2.4.2) can be represented as two (where $d_{AS} = d_{SA} = d_1$ and $d_{BS} = d_{SB} = d_n$). These delays represent distances between the receivers and the TWTT satellite, and they are used as an additional range-like observable in the estimation algorithm.

$$\Sigma D = -\frac{1}{2}\left(TIC(1) + TIC(n)\right)$$
$$= -\frac{1}{2}\left[\delta t_1 - (\delta t_n + d_n + d_1) + \delta t_n - (\delta t_n + d_n + d_1)\right] \quad (3.5.3)$$
$$= -\frac{1}{2}[-2d_1 - 2d_n] = d_1 + d_n + \upsilon_{TWTT}$$

This method provides an additional ranging measurement so when it is included in the simulation the positioning errors are further reduced. This is the first known proposal that these measurements be used as additional ranging measurements.

These generated measurements are fed into the estimation filter along with the parameters data and data from the truth model. The estimation filter is described in detail in the following section.

3.6 Least Squares Estimation Filter

The least squares estimation filter sub-component of the simulation takes inputs from the parameters function, the truth model and the generated measurements sub-component. The block-diagram of the filter is shown in figure 3.6.1. With these inputs the filter performs an iterative process to determine the best state estimate as will be described in detail below. It outputs the solution to the relative positioning problem to the performance analysis sub-component, which then processes the data as will be described in the following section.

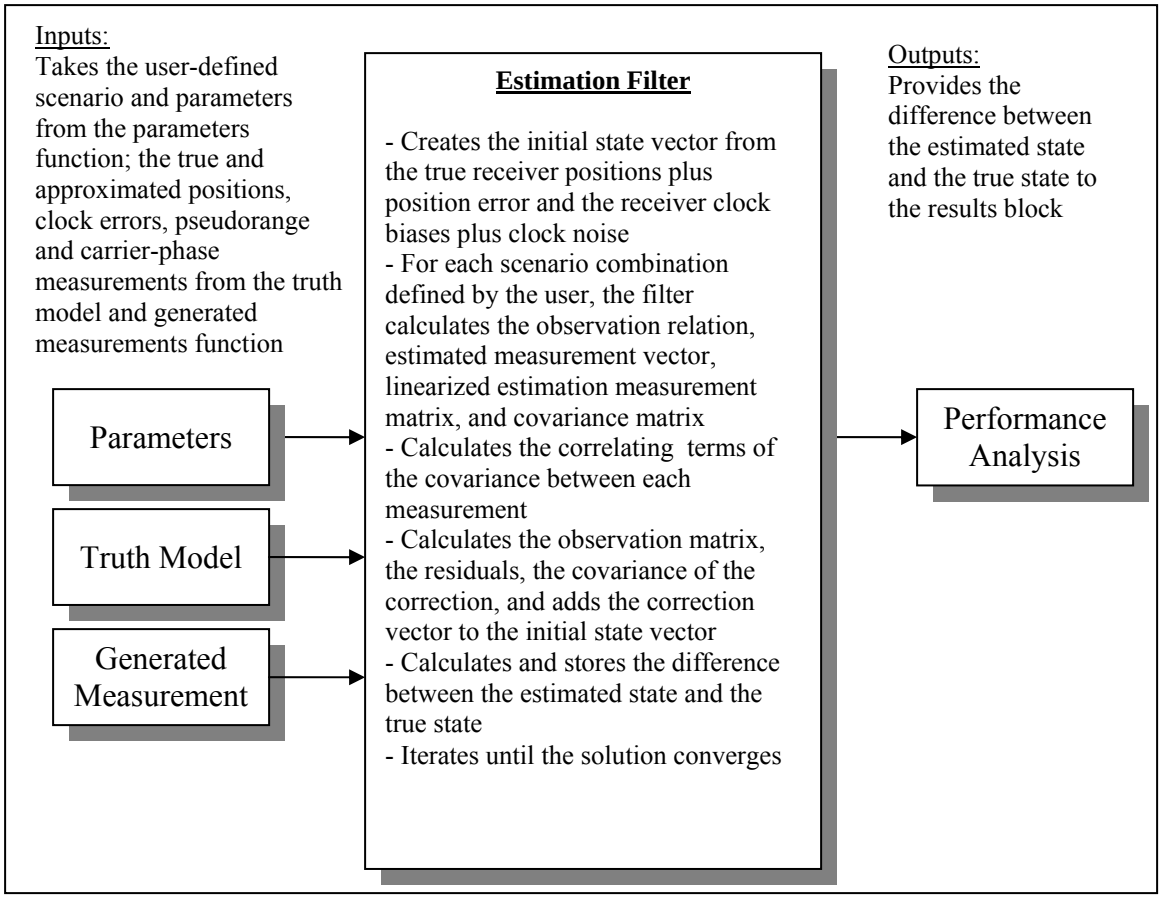

Figure 3.6.1 Block Diagram of the Estimation Filter

The state vector X for the least squares estimation filter is comprised of the 3-D receiver positions and their clock errors. The state vector is initialized with receiver positions plus a 10 meter, 1-σ initialization error, and the receiver clock bias plus a 3 meter, 1-σ initialization error. (Note that clock errors are expressed in units of meters).

$$X = \begin{bmatrix} x_1 \\ y_1 \\ z_1 \\ \delta t_1 \\ \vdots \\ x_n \\ y_n \\ z_n \\ \delta t_n \end{bmatrix} \tag{3.6.1}$$

where

x_1,y_1,z_1 = ECEF positions of receiver 1
δt_1 = clock bias for receiver 1
x_n,y_n,z_n = ECEF positions of receiver n
δt_n = clock bias for receiver n

This state vector gets updated with each iteration of the least squares filter.

For each of the possible scenarios defined by the user (i.e., single and/or double differenced pseudoranges and phase measurements) the actual data or observation relation – the relation between the observations, z, the estimated measurement vector, G, the linearized estimated measurement matrix, H, and the measurement error covariance matrix, Q, are formed. If the user specifies not to use one of the scenarios, all of these matrices are empty for that scenario. At the end of the least squares filter, each of the 'total' z, G, H, and Q matrices are formed by combining all of the individual scenario matrices. For example:

$$z = \begin{bmatrix} \begin{bmatrix} z_{dd\rho} \end{bmatrix} \\ \begin{bmatrix} z_{sd\rho} \end{bmatrix} \\ \begin{bmatrix} z_{dd\phi} \end{bmatrix} \\ \begin{bmatrix} z_{sd\phi} \end{bmatrix} \\ \begin{bmatrix} z_{rec1} \end{bmatrix} \\ \begin{bmatrix} z_{TT} \end{bmatrix} \end{bmatrix} \tag{3.6.2}$$

where

$z_{dd\rho}$ is the z-vector for the double-differenced pseudoranges
$z_{sd\rho}$ is the z-vector for the single-differenced pseudoranges
$z_{dd\varphi}$ is the z-vector for the double-differenced carrier-phase measurements
$z_{sd\varphi}$ is the z-vector for the single-differenced carrier-phase measurements
z_{rec1} is the z-vector for receiver 1 pseudoranges
z_{TT_time} is the z-vector for the TWTT time measurements
z_{TT_range} is the z-vector for the TWTT range measurements

The total observation relation z, as shown in equation (3.6.2), is a column vector composed of the double differenced pseudoranges, single differenced pseudoranges, double differenced phase measurements, single difference phase measurements, two-way time transfer time and range measurements, and the receiver 1 pseudorange measurements[4] (if all are desired). The values used in the observation vector are the simulated pseudorange and phase measurements, and the simulated TWTT time and range measurements described in Equations (2.2.1), (2.2.2), (3.5.2), and (3.5.3), which are based on the true satellite and receiver position and clock errors.

The estimated measurement vector G is a column vector whose values are the pseudoranges, phase measurements, and clock biases written in terms of the x,y,z and δt

[4] Note that the values for the reference receiver must be included to avoid singularities due to the fact that the measurements are differences but the final desired output are receiver positions and their corresponding clock errors.

components for both the satellite and receiver. The estimated measurement vector uses the estimated positions and clock errors. For example, if only the single differenced pseudorange measurements between two receivers were desired, the G-matrix would look like equation (3.6.3).

$$G = \begin{bmatrix} [G_{sd\rho}] \\ [G_{rec1}] \end{bmatrix} = \begin{bmatrix} \begin{bmatrix} \sqrt{(x^1 - x_1)^2 + (y^1 - y_1)^2 + (z^1 - z_1)^2} - \sqrt{(x^1 - x_2)^2 + (y^1 - y_2)^2 + (z^1 - z_2)^2} + \delta t_1 - \delta t_2 \\ \vdots \\ \sqrt{(x^1 - x_1)^2 + (y^1 - y_1)^2 + (z^1 - z_1)^2} - \sqrt{(x^i - x_2)^2 + (y^i - y_2)^2 + (z^i - z_2)^2} + \delta t_1 - \delta t_2 \end{bmatrix} \\ \begin{bmatrix} \sqrt{(x^1 - x_1)^2 + (y^1 - y_1)^2 + (z^1 - z_1)^2} + \delta t_1 \\ \vdots \\ \sqrt{(x^j - x_1)^2 + (y^j - y_1)^2 + (z^j - z_1)^2} + \delta t_1 \end{bmatrix} \end{bmatrix} \quad (3.6.3)$$

where

x,y,z^1 = calculated ECEF position (from broadcast ephemeris) of the first common visible satellite between receivers 1 and 2

$x,y,z_{1,2}$ = nominal ECEF position for receivers 1 and 2 (from state vector)

x,y,z^i = calculated ECEF position of the i^{th} common visible satellite between receivers 1 and 2

x,y,z^j = calculated ECEF position of the j^{th} satellite visible to receiver 1

$\delta t_{1,2}$ = nominal clock bias for receivers 1 and 2 (from state vector)

Residuals are calculated by differencing the observation relation and the estimated measurement vector:

$$\vec{r}_i = z_i - G(x(t_i), t_i) \quad (3.6.4)$$

The linearized observation matrix is calculated by taking the partial derivatives of each component of the estimated measurement vector G with respect to each component of the state vector X.

$$H = \begin{bmatrix} \partial G_1 / \partial X_1 & \cdots & \partial G_1 / \partial X_n \\ \vdots & \ddots & \\ \partial G_n / \partial X_1 & & \partial G_n / \partial X_n \end{bmatrix} \tag{3.6.5}$$

When only differential GPS measurements are used, the absolute position of the reference receiver (receiver 1) is determined from the pseudorange measurements between the GPS satellites and the receiver. All of the measurements are purely differential in nature, yielding the positions of the remaining receivers relative to the reference receiver. Any absolute position error in the network does not have an effect on the relative positions between the receivers. However, when the TWTT ranging measurements are used, they provide absolute ranging measurements as well. Each TWTT ranging measurement is an absolute ranging measurement between the TWTT satellite and the receivers involved in the TWTT measurement. In this case, an error in the position of the TWTT satellite results in a change in the absolute position of the entire network. This absolute position of the network may be in disagreement with the absolute position of the reference receiver obtained from the GPS measurements. If a disagreement occurs, the TWTT ranging measurements actually induce errors in the differential GPS solution. To account for this, the effect of the error in the position of the TWTT satellite must be modeled to make the TWTT ranging measurements essentially differential in nature (not absolute). The measurement model of the TWTT ranging measurements must be updated to include a bias that is common to all TWTT ranging measurements. The measurement model is updated by simply including a correlating

term in the last column of the linearized observation matrix indicating that ranging errors between the TWTT satellite and the receiver locations are correlated. Once the linearized observation matrix is computed, the measurement error covariance matrix is determined.

The measurement error covariance matrix Q is a block diagonal matrix composed of the covariance matrices for each group of measurements in the z-matrix. If the measurements contained in z are independent, Q is a diagonal matrix whose diagonal values are the standard deviations of the measurements squared:

$$Q = \begin{pmatrix} \sigma_1^2 & 0 & 0 & 0 \\ 0 & \sigma_2^2 & 0 & 0 \\ 0 & 0 & \ddots & 0 \\ 0 & 0 & 0 & \sigma_N^2 \end{pmatrix} \tag{3.6.6}$$

Where there are N scalar measurements of this kind in the z-matrix. Then:

$$Q_{total} = \begin{pmatrix} Q_1 & 0 & 0 & 0 \\ 0 & Q_2 & 0 & 0 \\ 0 & 0 & \ddots & 0 \\ 0 & 0 & 0 & Q_N \end{pmatrix} \tag{3.6.7}$$

The covariance of the correction (P) is:

$$\mathrm{P} = (H_i^T Q^{-1} H_i)^{-1} \tag{3.6.8}$$

The matrix ($H^TQ^{-1}H$) must be invertible for an estimate to exist. This requirement is also known as the observability condition.

Then the state correction vector at each epoch is:

$$\delta x(t_i) = (H_i^T Q^{-1} H_i)^{-1} H_i^T Q^{-1} \vec{r} \tag{3.6.9}$$

This correction vector is added to the state vector and the updated state vector is compared to the previous state vector.

$$\vec{x}(t_i) = \vec{x}(t_i) + \delta x(t_i) \tag{3.6.10}$$

The least squares estimation filter continues to iterate at each epoch until two successive values of δx both lie well within the one-sigma error ellipsoid indicating the result has converged. Once the delta x converges, the estimation filter outputs the estimate of the state vector to the performance analysis block.

3.7 Performance Analysis

The performance analysis function of the simulation takes the difference in the estimated state and the true state from the estimation filter as an input. Figure 3.7.1 illustrates the block diagram of the performance analysis sub-component of the simulation.

The performance analysis block inputs the estimated state from the estimation filter and determines the difference from the true state (obtained from the truth model), as shown in Equation 3.7.1.

$$\overrightarrow{X}_{diff} = \overrightarrow{X} - \overrightarrow{X}_{true} \tag{3.7.1}$$

where X is the estimated state from the estimation filter and X_{true} is the true state obtained from the truth model. It then computes the delta position and clock errors as shown in Equation (3.7.2).

$$\delta\overrightarrow{X}_{1,n} = \overrightarrow{X}_{diff,1} - \overrightarrow{X}_{diff,n} \tag{3.7.2}$$

where

$X_{diff,1}$ is the difference between the estimated state and the true state for receiver 1
$X_{diff,n}$ is the difference between the estimated state and the true state for receiver n

The mean position errors and clock errors for each receiver pair is calculated as shown in Equation (3.7.3).

$$\overline{\delta\overrightarrow{X}_{1,n}} = \frac{\sum_{i=1}^{480} \delta\overrightarrow{X}_{1,n}}{480} \tag{3.7.3}$$

where

$\delta X_{1,n}$ is the delta position and clock errors between receivers 1 and n
480 is the number of epochs used in the simulation

The Root-Mean-Square (RMS) of the delta position error (in each axis as well as in 3-D) and the delta clock error for each receiver with respect to the reference receiver is then calculated:

$$RMS(\delta\overrightarrow{X}_{1,n}) = \sqrt{\frac{\sum_{i=1}^{480} \delta\overrightarrow{X}_{1,n}^{\,2}}{480}} \tag{3.7.4}$$

Finally, the combined position error RMS over the total number of receivers (N) is calculated:

$$RMS(\delta\vec{X}) = \sqrt{\frac{RMS(\delta\vec{X}_{1,n})^2}{N}} = \sqrt{\frac{\left(\sqrt{\frac{\sum_{i=1}^{480}\delta\vec{X}_{1,n}^{\,2}}{480}}\right)^2}{N}} \tag{3.7.5}$$

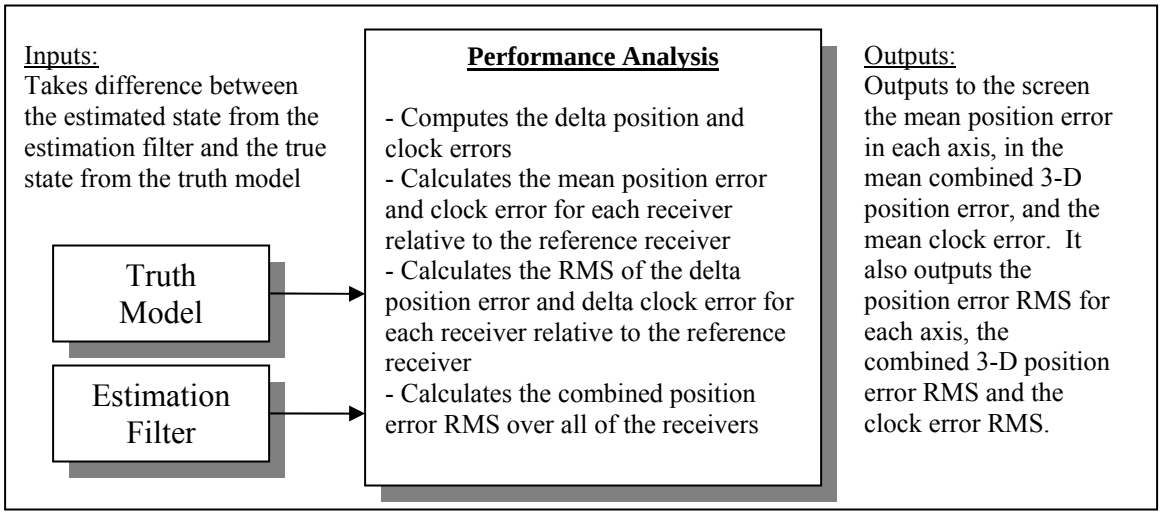

Figure 3.7.1 Block Diagram of the Performance Analysis Function

The five major sub-components of the simulation have been described in detail. As mentioned, the standard deviations of different errors were multiplied by a random number generator in the simulation. The random number generator and the concept of the random number seed are explained in the next section.

3.8 Random Number Seed

MATLAB® has the ability to generate normally distributed random numbers. The simulation takes the magnitudes of the modeled errors and multiplies them by this function in order to simulate white-Gaussian noise and random walks in the clock biases. The random number generator produces the random numbers based on its 'seed' –

effectively a marker in the random numbers so the generator knows where its starting. This seed can be specified so that all of the random numbers generated are called in the same order. Initially, in order to provide an "apples-to-apples" comparison between different observables and obtain repeatable results, the random number seed was reset to the same value at the start of each simulation run. This ensured that any differences observed were due to changes in the noise levels as opposed to different random numbers being generated.

3.9 Summary

This chapter conceptually and mathematically described the fundamental concepts of the research simulation. The simulation was broken down into the five main sub-components and each was described in detail. Any assumptions and approximations that were made were stated. Finally, the random number generator and the random number seed concept and use were explained. Chapter 4 will present the results and analysis of the research.

IV. Results and Analysis

4.1 Introduction

This chapter provides the results of the simulation and an in-depth analysis of the results. First, the baseline results of the thesis will be described in detail. Next, results of each of the trade studies performed will be discussed and analyzed. The trade studies performed include (1) comparison of results between two different days' ephemeris, (2) varying the number of receivers used, (3) varying the separation distance between the receivers, (4) varying the location of the TWTT satellite, and (5) varying the satellite elevation cutoff.

4.2 Baseline Results

The baseline results discussed in this section are the primary results of the research. When investigating the overall impact of integrating TWTT measurements and GPS measurements, these are the results that were obtained. First, a background on the simulation configuration will be explained followed by the numerical results. The primary goal of this research is to improve the *relative* positioning solutions, so only the relative positioning results are presented.

In the simulation, data over one 24-hour period was sampled every three minutes to yield 480 time epochs. Data was collected at each epoch and averaged over the total collection time. Table 3.2.1 is rewritten below for convenience and presents the modeled error magnitudes used in the simulation.

Table 3.2.1 Modeled Error Magnitudes

Error	**Standard Deviation (m)**
Pseudorange	1
Carrier Phase	0.01 (0.053 cycles)
TWTT Satellite Position	5
Initial Receiver Position	10
Clock Bias	3
TT(A)	3 m
TT(B)	0.3 m
TT(C)	0.03 m
TT(D)	0.003 m

All simulations described in this section used non-differenced pseudorange measurements to estimate the position of receiver 1, in addition to various differenced measurements (which were simulation dependent). This was necessary to make all of the states observable, because all of the other measurements are difference measurements, which have no absolute positioning information.

The baseline simulation consists of six receivers separated by approximately 1 km, in the configuration shown in Figure 3.2.1 redrawn below for convenience. As stated in Chapter 2, the receiver network is located at the point where the equator and the Prime Meridian intersect. This location was chosen for ease of analysis. Each receiver was assumed to be at equal altitudes of 1 km (to simulate the possible altitude of UAVs), and ephemeris data was from 10 January 2002 used.

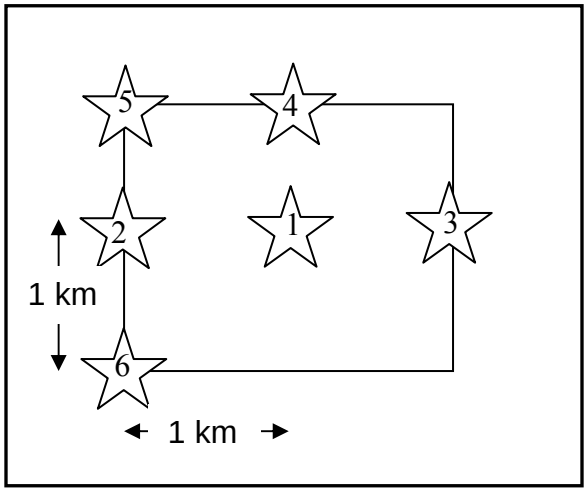

Figure 3.2.1 Baseline Receiver Configuration

Table 4.2.1 shows the results for a scenario where single-differenced pseudorange measurements were used. (No phase or time transfer measurements were used). Each of the values shown is a root-mean-square (RMS) value across all of the 480 time epochs in the simulation. For example, the root-mean-square is taken of the relative positioning error in the x-direction at each time epoch, yielding 480 values. The δx_{RMS} value shown in the table for each receiver pair is the root-mean-square of those 480 RMS values of the relative positioning error in the x-direction between receivers 1 and n. Similarly, the δy_{RMS} and δz_{RMS} are the root-mean-squares of the relative positioning error in the y-direction and z-direction respectively between receivers 1 and n. The 3-D Positioning_{RMS} is the root-mean square of the 3-dimensional positioning error between receivers 1 and n. Finally, the clock_{RMS} is the root-mean-square of the clock errors between receivers 1 and n. The combined RMS values shown in the last row of the table are the root-mean-squares of the 5 receiver pairs. These effectively represent three-tiers of RMS values. First, the RMS is taken of each receiver pair at each epoch. Then, the RMS is taken of

those 480 values for each receiver pair. Finally, the RMS is taken of the five values of the different receiver pairs.

Table 4.2.1 Results for Single-Differenced Pseudorange Scenario

Receiver Pair	δx_{RMS} (m)	δy_{RMS} (m)	δz_{RMS} (m)	3-D $Position_{RMS}$ (m)	$Clock_{RMS}$ (m)
1-2	2.469	1.022	0.837	1.617	1.433
1-3	2.348	0.993	0.816	1.546	1.340
1-4	2.433	1.016	0.817	1.594	1.444
1-5	2.468	1.064	0.815	1.622	1.417
1-6	2.366	1.013	0.812	1.558	1.364
Combined	2.417	1.022	0.820	1.587	1.400

The baseline results consist of a total of nine simulations. The only difference between simulations is the set of observables used. The results given in Table 4.2.2 are the combined RMS values for each of the different simulations. Note the last row of Table 4.2.1 is the first row of values in Table 4.2.2, the simulation where only single-differenced pseudoranges were used. The observables used, shown in the first column are interpreted as follows:

$\Delta\rho$: single-differenced pseudorange measurements
TT: two-way time transfer measurements with standard deviation indicated by letter: A = 3m, B = 0.3m, C = 0.03m, D = 0.003m

Table 4.2.2 Consolidated Baseline Results

Scenario (Observables Used)	δx_{RMS} (m)	δy_{RMS} (m)	δz_{RMS} (m)	3-D $Position_{RMS}$ (m)	$Clock_{RMS}$ (m)
$\Delta\rho$	2.417	1.022	0.820	1.587	1.400
$\Delta\rho$ +TT(A)	2.085	1.008	0.805	1.415	1.158
$\Delta\rho$ +TT(B)	1.025	0.977	0.787	0.935	0.290
$\Delta\rho$ +TT(C)	0.898	0.975	0.787	0.890	0.030
$\Delta\rho$ +TT(D)	0.895	0.975	0.787	0.889	0.003
$\Delta\rho$ +TT(A) + TWTT Ranging	1.969	1.005	0.804	1.358	1.096
$\Delta\rho$ +TT(B) + TWTT Ranging	0.793	0.975	0.787	0.856	0.250
$\Delta\rho$ +TT(C) + TWTT Ranging	0.708	0.971	0.785	0.829	0.030
$\Delta\rho$ +TT(D) + TWTT Ranging	0.705	0.971	0.786	0.828	0.003

Since the x-direction is in the vertical direction, it is no surprise that the RMS error in that direction is larger than in the other 2 directions—this is commonly seen with GPS-based positioning [42].

Augmenting the GPS measurements with the TWTT consistently reduces the positioning and clock errors. As shown, including the TWTT ranging measurements in the observables in addition to the TWTT time-difference measurements further reduces the positioning and clock errors. When comparing the GPS pseudorange-only case with highest accuracy TWTT case ($\Delta\rho$+ TT(D) + TWTT Ranging), the TWTT reduces the positioning error by over 70% in the x-direction alone, nearly 48% in the combined 3-D position, and reduces the clock error by over 99%. Even when using a TWTT accuracy of 3m and using the ranging measurements, the pseudorange-based positioning errors are reduced by over 10% and the clock errors are reduced by 22%. Including the TWTT

ranging measurements improves the 3-D relative positioning solution by approximately 4-9% over solely using the TWTT time-differencing measurements.

A special case that was looked at was running the scenario using carrier-phase measurements. The results are shown in Table 4.2.3

Table 4.2.3 Consolidated Results for Case Using Carrier-Phase Measurements

Scenario (Observables Used)	δx_{RMS} (m)	δy_{RMS} (m)	δz_{RMS} (m)	3-D $Position_{RMS}$ (m)	$Clock_{RMS}$ (m)
$\Delta\phi$	0.133	0.053	0.044	0.086	0.075
$\Delta\phi$+TT(A)	0.133	0.053	0.044	0.086	0.075
$\Delta\phi$+TT(B)	0.132	0.053	0.044	0.086	0.075
$\Delta\phi$+TT(C)	0.102	0.052	0.043	0.071	0.055
$\Delta\phi$+TT(D)	0.048	0.050	0.042	0.047	0.005
$\Delta\phi$+TT(A) + TWTT Ranging	0.133	0.053	0.044	0.086	0.075
$\Delta\phi$+TT(B) + TWTT Ranging	0.132	0.053	0.044	0.086	0.075
$\Delta\phi$+TT(C) + TWTT Ranging	0.091	0.051	0.042	0.065	0.049
$\Delta\phi$+TT(D) + TWTT Ranging	0.037	0.050	0.042	0.043	0.006
$\Delta\nabla\phi$	0.106	0.052	0.043	0.072	N/A[5]

where

$\Delta\phi$: single-differenced carrier-phase measurements

$\nabla\Delta\phi$: double-differenced carrier-phase measurements

TT: two-way time transfer measurements with standard deviation indicated by letter: A = 3m, B = 0.3m, C = 0.03m, D = 0.003m

[5] Note that the clock terms get subtracted out in the double difference phase measurements, so the clock errors do not affect these results.

As expected, including the TWTT measurements with 3 m accuracy does not improve the carrier-phase relative positioning solution. Including the TWTT measurement with 0.3 m level accuracy makes a slight improvement of 0.75% in the x (vertical) direction, but no improvements in the other results. Including the TWTT measurements (without ranging) with 3 cm accuracy improves the solution noticeably. The solution is improved by 23% in the x-direction, 2% in the y- and z-directions, 17% in the 3-D positioning, and 27% in the clock solution. For the scenario including TWTT measurements (without ranging), the solution is improved by 64% in the x-direction, 4% and 6% in the y- and z-directions respectively, 45% in the 3-D position and 93% in the clock error. When the TWTT ranging is used with 3 mm accuracy, the improvements in the vertical direction and the 3-D positioning increase to 72% and 50% respectively.

Due to the fact that the carrier phase measurements are more precise than the pseudorange measurements, the impact of the TWTT measurements on the solution is not as evident. However, it should be noted that in order to perform cm-level positioning with carrier-phase GPS measurements, it is generally necessary to determine the integer ambiguities of the carrier-phase measurements. This usually forces the use of the double differenced phase measurements, which remove the effects of clock error and makes the integer ambiguities easier to resolve. However, using the TWTT approach with a high level of precision would enable ambiguity resolution to be performed using *single*-differenced measurements. The point of comparison for phase-based positioning should therefore be to compare between double-differenced phase results (3-D RMS value of 0.072 m) with single-differenced phase results with TT(D) + TWTT ranging (3-D RMS

value of 0.043 m). This is effectively an improvement of 40% in already-precise carrier-phase-based positioning. The relative positioning in the x (vertical) direction is improved from the double-differenced phase results by nearly 65% when using TT(D) + TWTT ranging.

These baseline results show that there is potentially a 48% improvement in the pseudorange measurements and a 40% improvement in carrier-phase measurements when augmented with precise TWTT time and range measurements. Based on these results, five trade studies were performed in order to vary different parameters and determine if the overall 3-D positioning solution could be optimized. The following five sections discuss the five trade studies that were performed in detail.

4.3 Trade Study 1: Compare Results Using Two Different Ephemeris

This trade study was performed to show that the results obtained are valid regardless of which day's ephemeris is used, that they are not just tailored for one particular day's ephemeris. This is important, because if the results are significantly different, the baseline results are not valid and the simulation is of no use. If the results confirm that the simulation is valid for any day, then it validates the universal use of the simulation. The two dates being compared are 10 January 2002 and 5 May 1994. Table 4.2.2 in the previous section shows the consolidated baseline results for the pseudorange measurements using the ephemeris from 10 January 2002. Table 4.3.1, below, shows the consolidated results for the pseudorange and measurements using the ephemeris from 5 May 1994.

Table 4.3.1 Consolidated Baseline Results for 5 May 1994

Scenario (Observables Used)	δx_{RMS} (m)	δy_{RMS} (m)	δz_{RMS} (m)	3-D $Position_{RMS}$ (m)	$Clock_{RMS}$ (m)
$\Delta \rho$	2.426	1.078	0.834	1.607	1.426
$\Delta \rho$ +TT(A)	2.085	1.073	0.822	1.435	1.178
$\Delta \rho$ +TT(B)	1.015	1.056	0.796	0.963	0.288
$\Delta \rho$ +TT(C)	0.895	1.054	0.795	0.921	0.030
$\Delta \rho$ +TT(D)	0.893	1.054	0.795	0.920	0.003
$\Delta \rho$ +TT(A) + TWTT Ranging	1.946	1.073	0.819	1.367	1.109
$\Delta \rho$ +TT(B) + TWTT Ranging	0.763	1.054	0.796	0.881	0.248
$\Delta \rho$ +TT(C) + TWTT Ranging	0.693	1.051	0.794	0.860	0.030
$\Delta \rho$ +TT(D) + TWTT Ranging	0.693	1.051	0.794	0.859	0.003

Comparing Tables 4.2.2 and 4.3.1, one can see the individual values vary up to approximately 6%, but the general trends are the same: including the TWTT measurements improve the solution when compared to the GPS pseudorange-only scenario, and including the TWTT ranging in the TWTT measurements improves the solution when compared to the TWTT measurements with no ranging. More importantly, the percentages of improvements within each day's results are nearly identical. Table 4.3.2 shows the 3-D positioning solution for each of the days as well as the percentages of improvement over the single-differenced pseudorange scenario. As shown in the table, the percentages of improvement over the single-differenced pseudorange case are within approximately 1% between the two days, validating the performance of the simulation.

Table 4.3.2 Comparative Baseline Results Between 5 May 1994 and 10 Jan 2002

Scenario (Observables Used)	10 Jan 2002 3-D Position_{RMS} (m)	5 May 1994 3-D Position_{RMS} (m)	10 Jan 2002 Improvement Over DGPS-only	5 May 1994 Improvement Over DGPS-only
$\Delta\rho$ only	1.587	1.607	0%	0%
$\Delta\rho$ +TT(A)	1.415	1.453	10.8%	9.6%
$\Delta\rho$ +TT(B)	0.935	0.963	41.1%	40.1%
$\Delta\rho$ +TT(C)	0.890	0.921	43.9%	42.7%
$\Delta\rho$ +TT(D)	0.889	0.920	44.0%	42.8%
$\Delta\rho$ +TT(A) + TWTT Ranging	1.358	1.367	14.4%	14.9%
$\Delta\rho$ +TT(B) + TWTT Ranging	0.856	0.881	46.1%	45.2%
$\Delta\rho$ +TT(C) + TWTT Ranging	0.829	0.860	47.7%	46.5%
$\Delta\rho$ +TT(D) + TWTT Ranging	0.828	0.859	47.8%	46.7%

The results of this trade study indicate that the particular satellite constellation and day selected do not have a significant impact on the results. The second trade study looked at varying the number of receivers in the network and described in detail in the following section.

4.4 Trade Study 2: Vary the Number of Receivers

This trade study was performed to determine if the relative positioning solution has a dependence on the number of receivers used. The simulation takes as an input 'N' number of independent receivers. The positions of the receivers are determined with respect to the first (reference) receiver, but no measurements are done in-between receivers two through N (because they would be linear combinations of the

measurements between receiver 1 and each receiver). Since there are no correlating measurements between the receivers, it is expected that the overall positioning solution should not be affected by the number of receivers used. This trade study was performed in order to confirm that the receivers are in fact independent and there are no hidden correlations between them in the simulation.

The receivers were separated by 1 km in this trade study. Five scenarios were run in which the number of receivers was varied by two from 2 to 10. The five different receiver configurations are shown below.

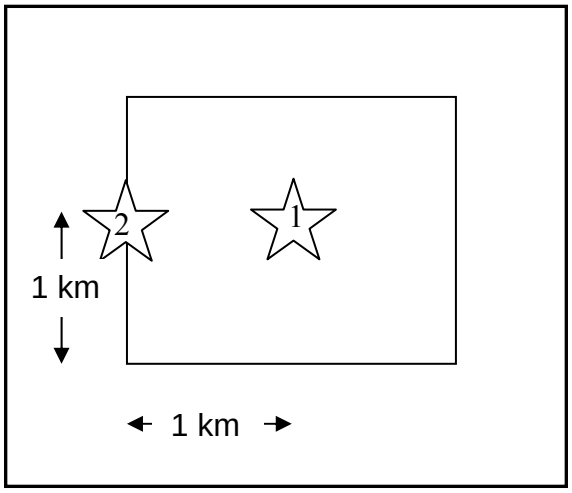

Figure 4.4.1 Two-Receiver Configuration

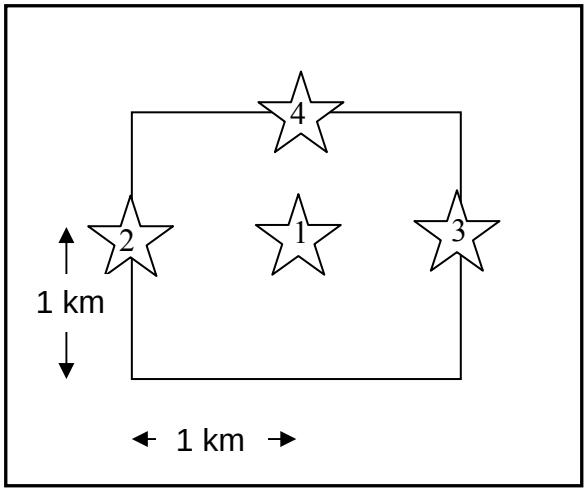

Figure 4.4.2 Four-Receiver Configuration

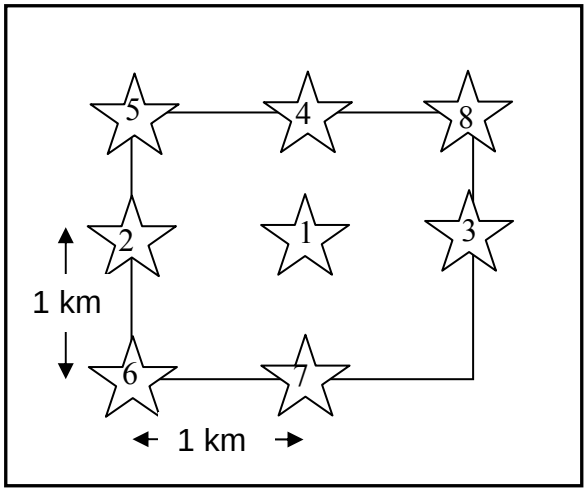

Figure 4.4.4 Eight-Receiver Configuration

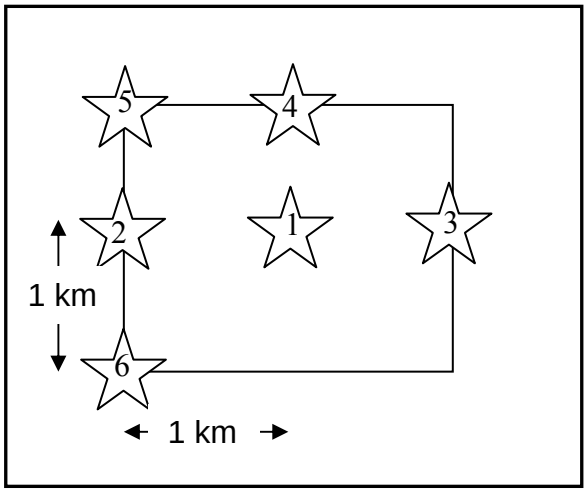

Figure 4.4.3 Six-Receiver Configuration

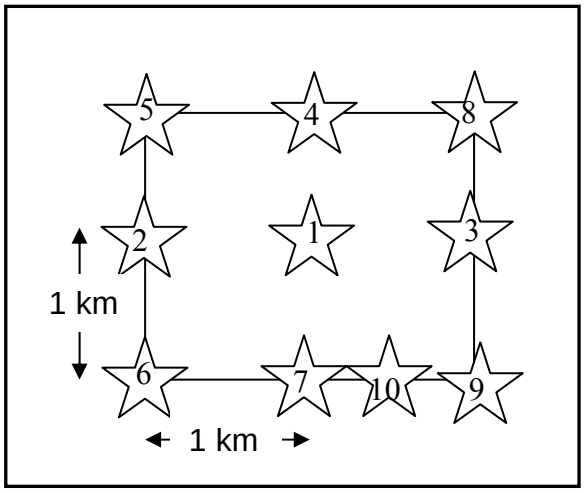

Figure 4.4.5 Ten-Receiver Configuration

Figures 4.4.6 and 4.4.7 show the combined 3-D RMS errors vs. the number of receivers and the RMS of the clock error vs. the number of receivers for the cases of not including the TWTT ranging measurements and including the TWTT ranging measurements, respectively. Figures 4.4.8 and 4.4.9 show the error RMS vs. the number of receivers in each axis for the cases of not including the TWTT ranging measurements and including the TWTT ranging measurements, respectively. As seen in Figures 4.4.8 and 4.4.9, the solution for the vertical direction (the x-direction) is significantly greater than the solutions for the y- and z-directions. The x-direction is also the direction most affected by varying the number of receivers.

Comparing Figures 4.4.6 and 4.4.7, it is seen that including the TWTT ranging measurements slightly improves the solutions over the cases where the TWTT ranging measurements are not included.

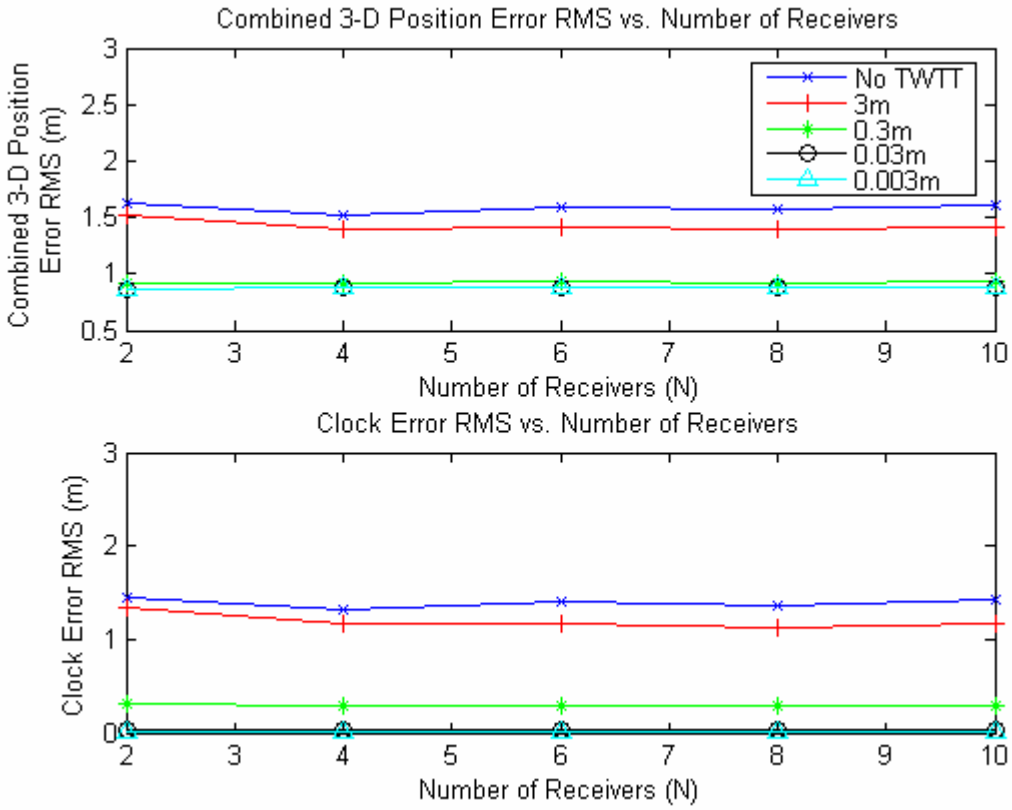

Figure 4.4.6 Combined 3-D Position Error RMS and Clock Error RMS vs. Number of Receivers (TWTT Time Measurements Only)

Whether the TWTT ranging measurements are included or not, the scenarios where there is no TWTT measurement included and the scenarios for the 3m TWTT standard deviation have the greatest variation over the number of receivers. The fluctuation that is seen between the solutions for each number of receivers is proportional to the magnitude of the standard deviation of the GPS receiver positioning accuracy and the standard deviation of TWTT error. The TWTT scenarios were run with standard deviations of the error on the order of 10 ns 1 ns 0.1 ns and 0.01 ns, which expressed as positions are 3 m, 0.3 m, 3 cm, and 3 mm. The more accurate the TWTT measurement, the less fluctuation is seen in the overall solution.

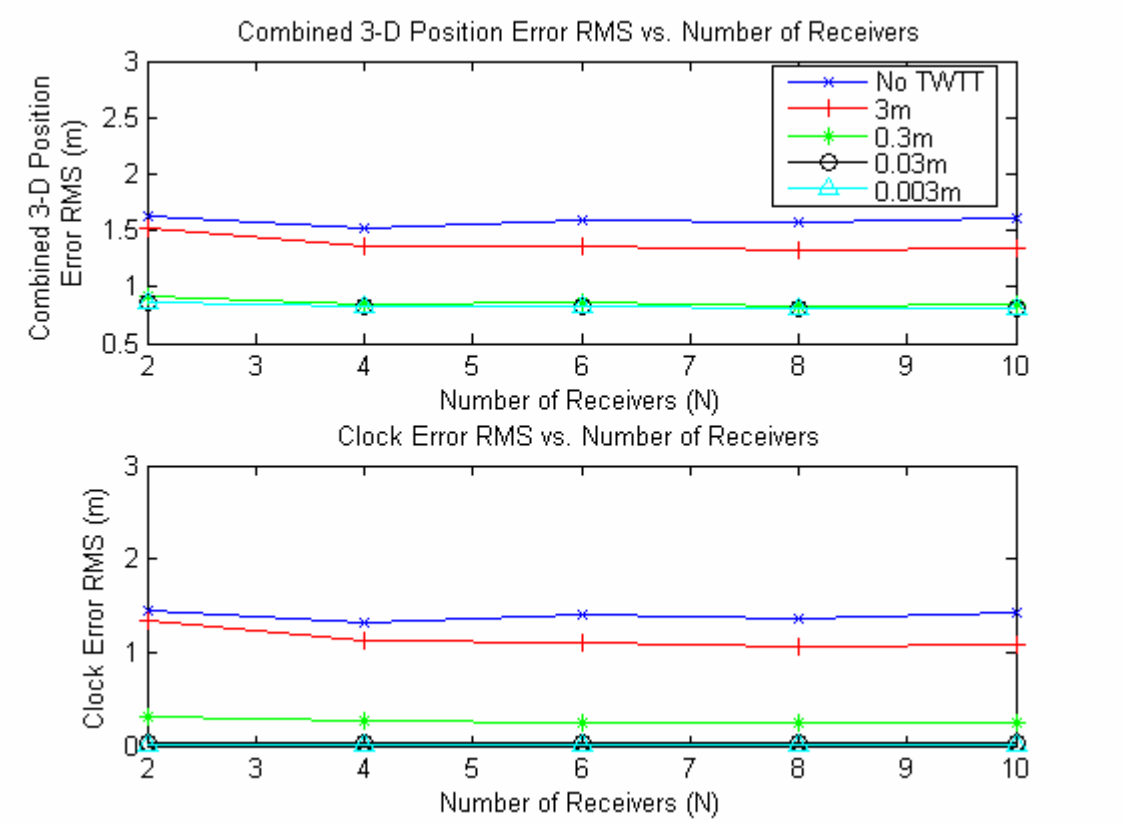

Figure 4.4.7 Combined 3-D Position Error RMS and Clock Error RMS vs. Number of Receivers (TWTT Time and Range Measurements)

The measurement noise values are generated from the MATLAB® random number generator. When the number of receivers is changed, the random number generator is called a different number of times in the simulation. This results in slight variations in the solution because the simulation is not producing the same realized noise values. This explains why there is more fluctuation in the scenarios that have larger magnitudes of errors.

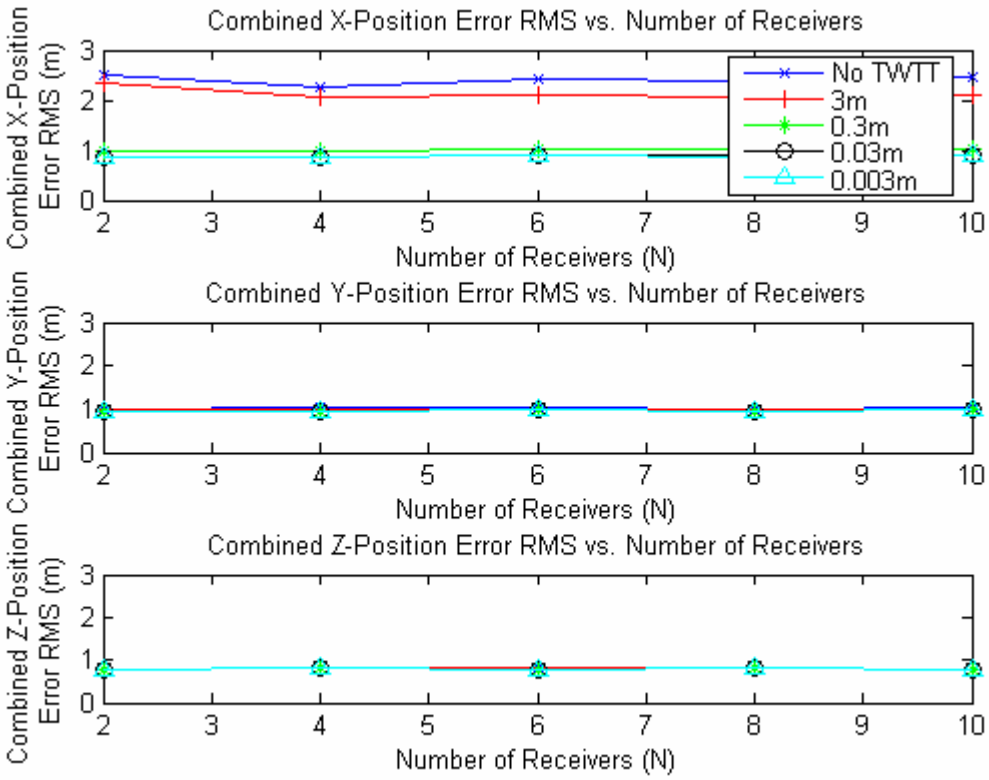

Figure 4.4.8 RMS Position Error vs. Number of Receivers in Each Axis
(TWTT Time Measurements Only)

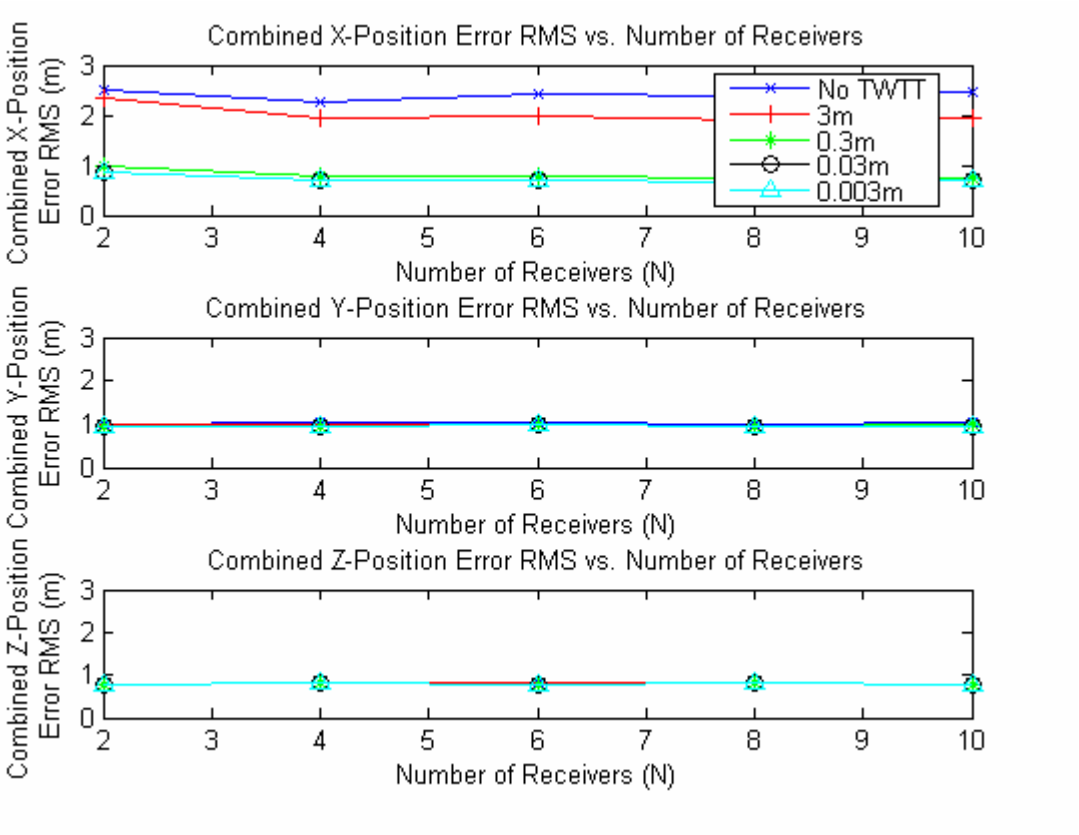

Figure 4.4.9 RMS Position Error vs. Number of Receivers in Each Axis
(TWTT Time and Range Measurements)

The results are as expected and confirm that the overall positioning solution is not significantly impacted by varying the number of independent receivers. The results also indicate that there are no hidden correlations between the receivers present in the simulation. The third trade study looked at the effects of varying the separation distance between the receivers and is described in detail in the following section.

4.5 Trade Study 3: Vary the Separation Distance Between Receivers

This trade study was performed to determine the impact of separation distance between the receivers on the relative positioning solution accuracy. It was expected that as the separation distance between the receivers is increased, the overall positioning solution will get worse. As the separation distance between the receivers increases, there are fewer similarities in the errors of the receivers. Therefore, when differencing the measurements, the errors do not cancel perfectly and the relative positioning solution will become worse.

There were six receivers used in this trade study, and the separation distance between the receivers was varied from 1km to 100 km, 500 km, 1,000 km, and 1,500 km. Figures 4.5.1 and 4.5.2 show the combined 3-D position error RMS and clock error RMS as functions of the separation distance between receivers when not including TWTT ranging measurements and including them, respectively. As shown in the figures, the GPS-only solution (no TWTT measurements) gets significantly worse than the other solutions as the separation distance increases because this scenario relies solely on the GPS satellite constellation to provide the relative positioning solution. As the receivers get separated by increased distance, the number of commonly visible GPS satellites decreases, and the receivers' geometry relative to those common satellites becomes weaker. Unlike the GPS-only case, when the TWTT measurements are included, there is almost no growth in error when increasing the separation distance from 1 to 1,500 km.

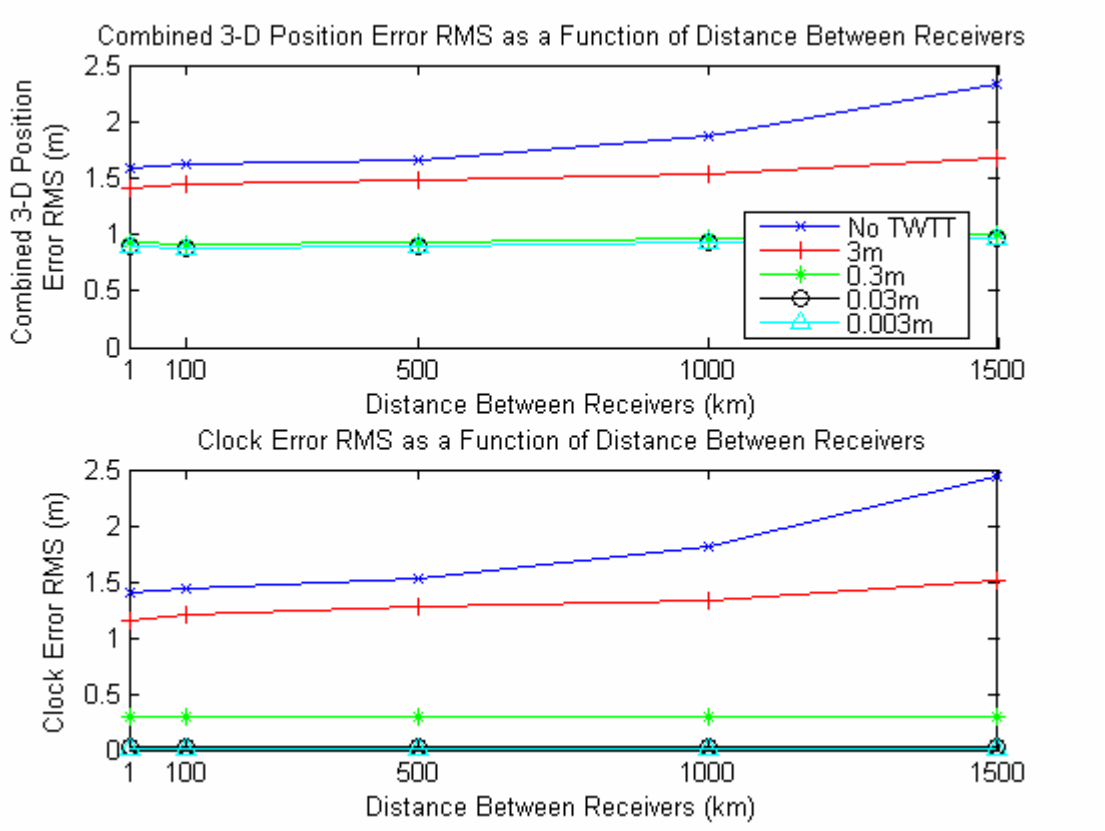

Figure 4.5.1 Combined 3-D Position Error RMS and Clock Error RMS vs. Receiver Separation (TWTT Time Measurements Only)

As one would expect and as shown in the figures in this section, the positioning solution is better for networks that are closer together than for those spread out over large distances. The results show that with large separation distances between receivers, the GPS solutions that are augmented with TWTT measurements are significantly better than the GPS-only solutions. This may be because the TWTT measurements effectively reduce by 2 the number of satellites needed to obtain a solution, so in this case where there are less commonly visible satellites, the TWTT measurements are invaluable.

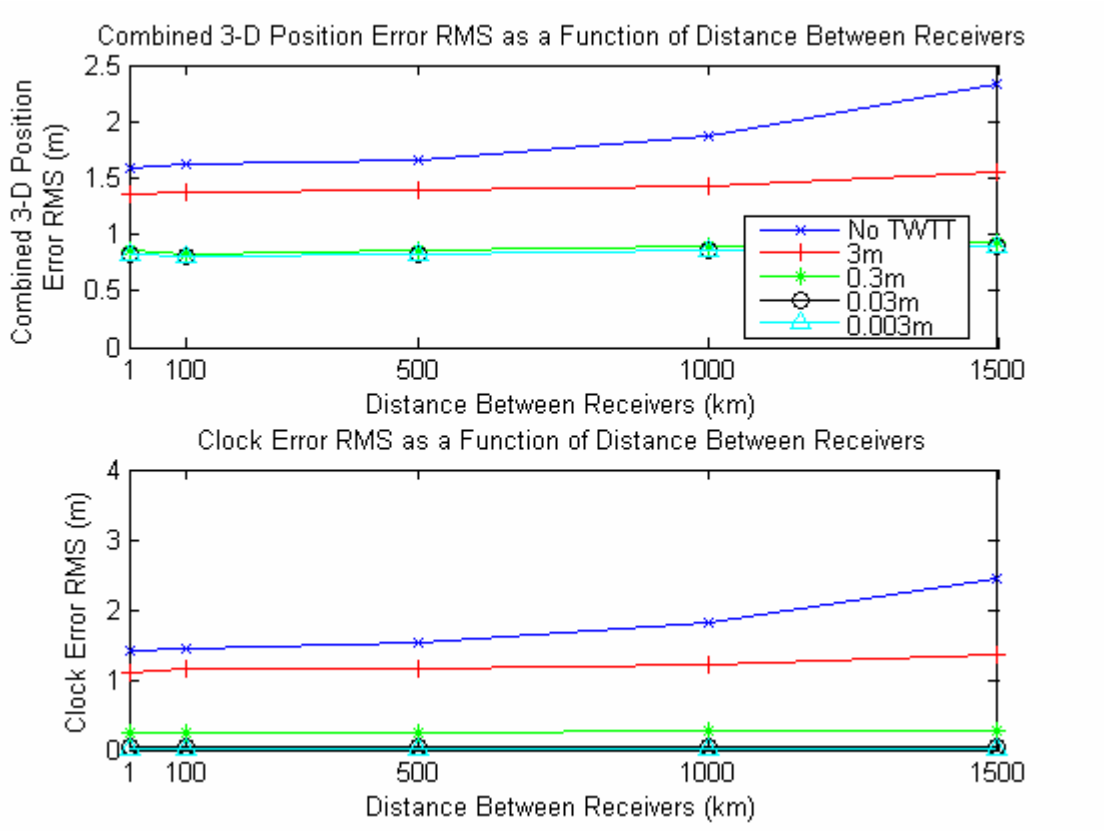

Figure 4.5.2 Combined 3-D Position Error RMS and Clock Error RMS vs. Receiver Separation (TWTT Time and Range Measurements)

It appears that in this simulation, the separation distance between receivers with an altitude of 1,000 km has to stay within approximately ¼ of the Earth's radius in order for there to be a sufficient number of common satellites in view of the receivers. Anything greater than this distance and there are generally not enough common satellites to obtain a solution.

Figures 4.5.3 and 4.5.4 are the RMS position errors in each axis as a function of the separation distance between the receivers. As shown, the error in the x (vertical) axis is the dominant axis contributing to the overall positioning solution error. The reason for this phenomenon was described in Section 4.2.

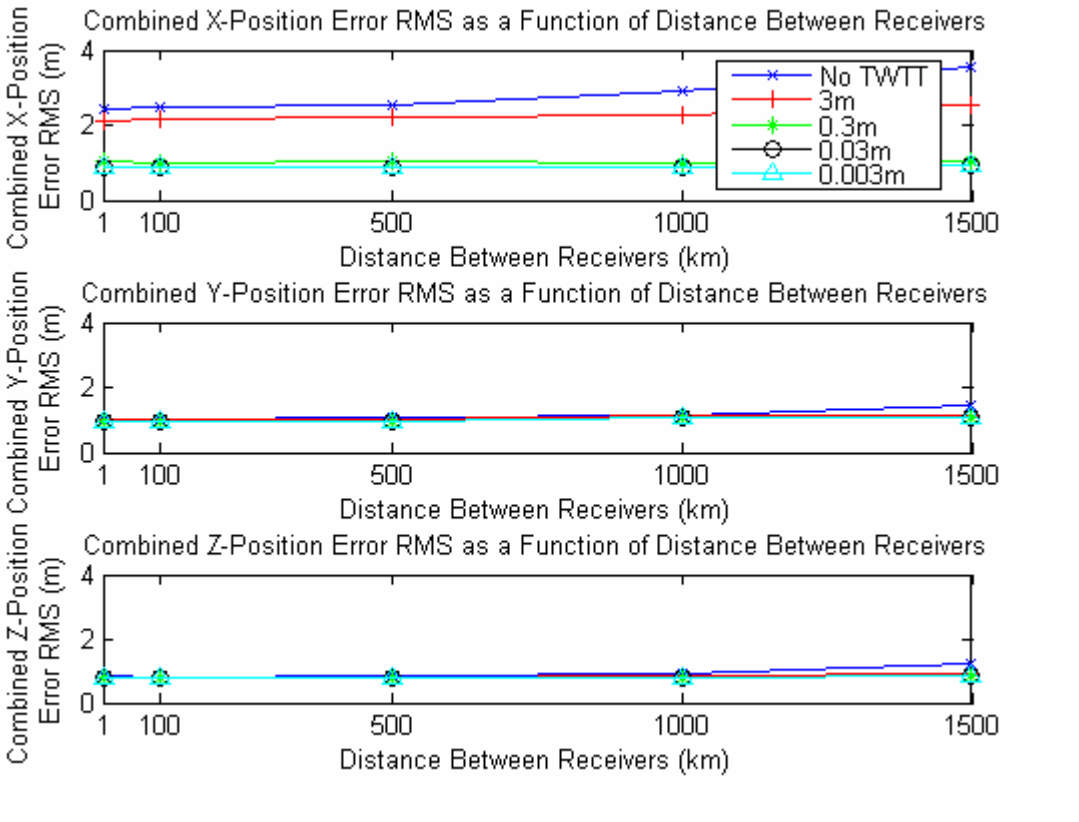

Figure 4.5.3 RMS Position Error vs. Receiver Separation in Each Axis
(TWTT Time Measurements Only)

The results show that networks where the receivers are separated by less than approximately 500 km will obtain similar relative positioning solutions. Receivers separated by more than 500 km will get an increasingly inferior solution as the separation distance increases when using only GPS measurements. If the observables include TWTT measurements, the solution increases slightly with receiver separation but not to the same extent as the GPS-only scenario. For example, the 3-D positioning error RMS for the GPS-only case increases by 32% when the separation distance is increased from 1 km to 1,500 km. Similarly, when increasing the receiver separation distance from 1 km to 1,500 km, the 3-D positioning error RMS for TWTT(A) + Ranging increases by 12%,

and for TWTT(B,C, and D) + Ranging all increase by approximately 8%. Finally, in this simulation, it appears that receivers in a network must be separated by less than one fourth of the radius of the Earth in order to have a sufficient number of common satellites in view to obtain a positioning solution.

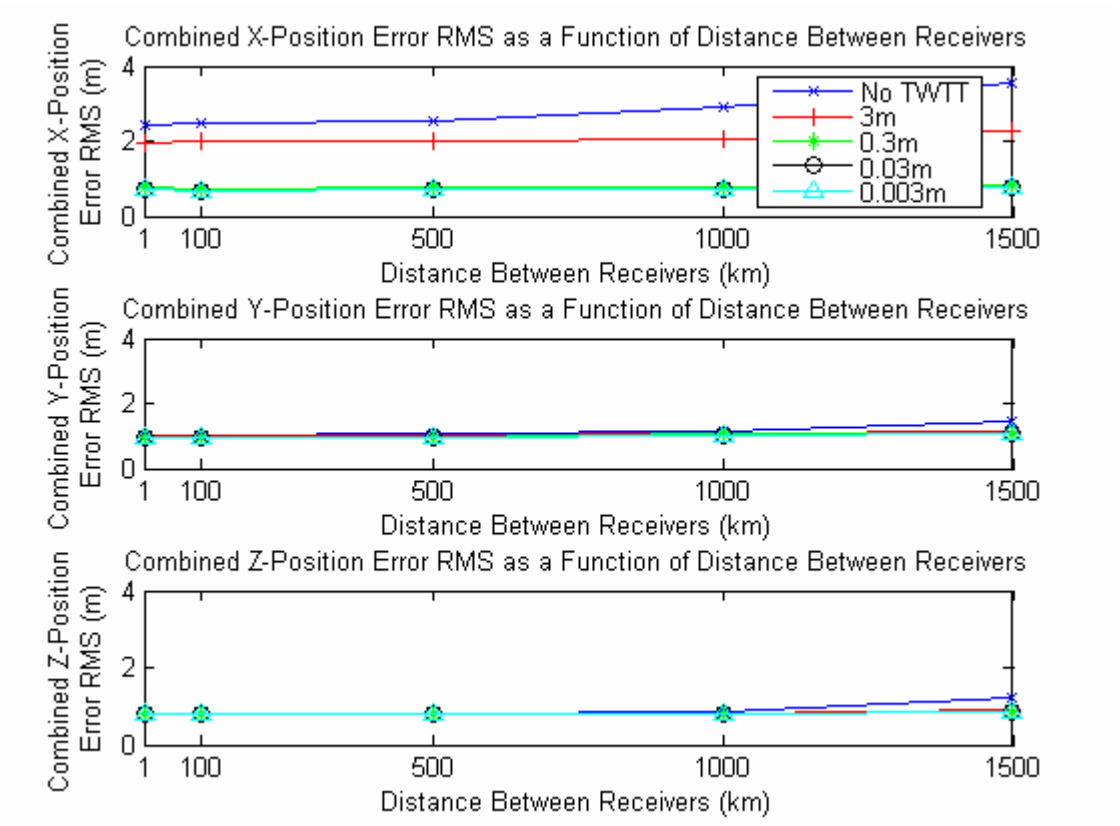

Figure 4.5.4 RMS Position Error vs. Receiver Separation in Each Axis
(TWTT Time and Range Measurements)

The results of this trade study were as expected: that system performance is dependent on the separation distance between the receivers. The best solutions are obtained when the receivers are separated by less than 500 km. As the separation distance is increased, the advantages of using TWTT-augmented GPS measurements become more evident. This is because the system is not relying solely on differential

GPS when the TWTT measurements are included. The next trade study that was performed was varying the TWTT satellite location as is described in the following section.

4.6 Trade Study 4: Vary the Location of the TWTT Satellite

This trade study was run to determine if the relative positioning solution is dependent on the TWTT satellite location. It was expected that as the TWTT position moved off-center from directly above the receiver network, the overall performance of the system would decline. This decline in performance is expected due to the change in geometry between the TWTT satellite and the receiver network.

The six-receiver baseline configuration was used as a network. The TWTT satellite was initially located directly over the network (in geostationary orbit above the intersection of the equator and the Prime Meridian). The TWTT satellite was then moved in 15 degree increments to 60 degrees longitude. This trade study is only applicable to the case where the TWTT ranging is included in the observables. If it is not included, there are no ranging measurements that are dependent on the location of the TWTT satellite; therefore, the TWTT satellite location does not affect the overall solution.

Figures 4.6.1 shows the 3-D position error RMS and clock error RMS as functions of TWTT satellite location for the case where the TWTT ranging measurements are included. As seen in Figure 4.6.1, the overall 3-D position error RMS is increased in the cases of TWTT(A) and TWTT(B) as the TWTT satellite is moved off-center from the network. The TWTT(A) solution is increased by 3.2%, the TWTT(B) solution is

increased by 1.9%. The TWTT (C) and TWTT(D) solutions are actually decreased by 1.2%. This phenomenon can be explained by examining Figure 4.6.2. The clock error RMS solutions Figure 4.6.1 show an increase as the TWTT(A) and TWTT(B) of 4.3% and 11.3%, respectively as the TWTT satellite is moved away from the receiver network. The clock error RMS solutions for TWTT(C) and TWTT(D) show no change as the TWTT satellite is moved.

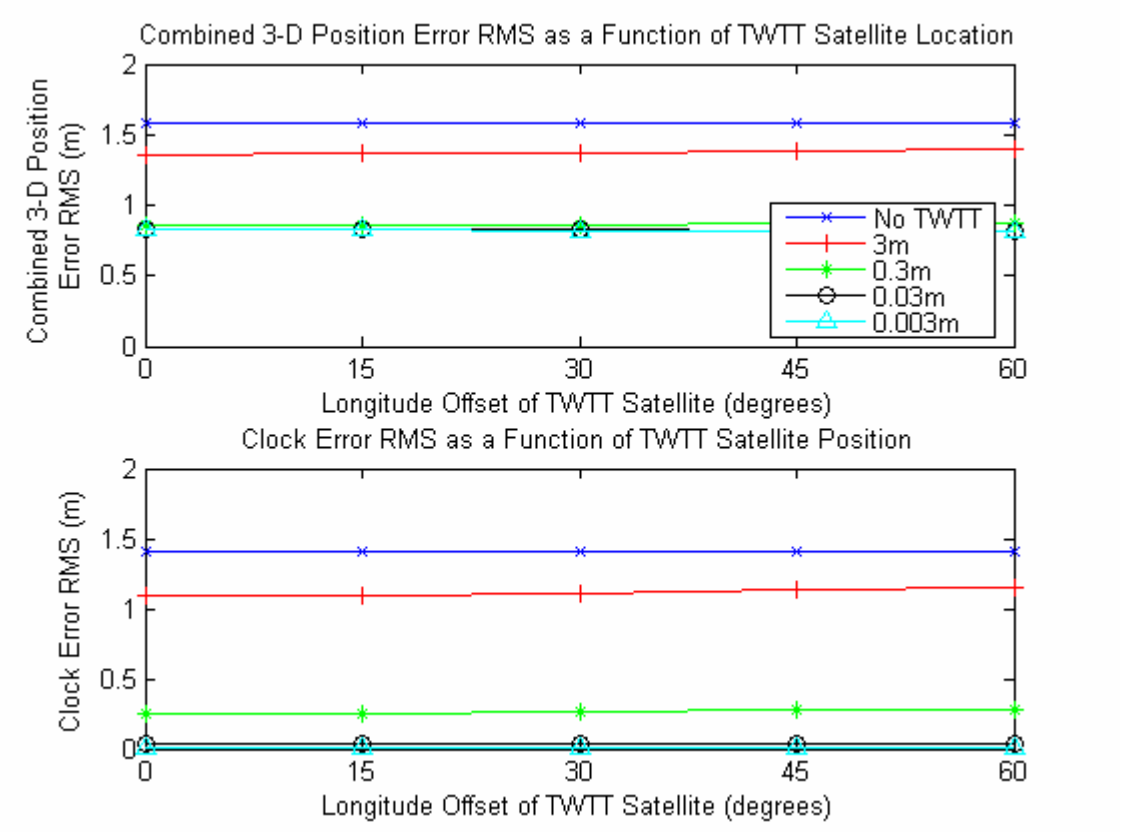

Figure 4.6.1 Combined 3-D Position Error RMS and Clock Error RMS vs. TWTT Satellite Location (TWTT Time and Range Measurements)

As seen in Figure 4.6.2, the RMS position error in the y-direction is actually slightly improved by moving the TWTT satellite East in Longitude (in the positive y-

direction) for the TWTT(C) and TWTT(D) scenarios. For the cases of TWTT(A) and TWTT(B), the TWTT measurement is not accurate enough to pick up the improvement in the y-direction, however, the measurements pick up the degraded performance in the x-direction and therefore the overall 3-D solution is degraded. This is due to the fact that the y-direction and z-direction errors are orders of magnitude smaller than the error in the x-direction, so the TWTT measurements have to be very precise in order to pick up the improvement in those directions. The TWTT(C) and TWTT(D) scenarios see the improvement in the y-direction error RMS, and that improvement is actually greater than the degraded performance in the x-direction, so the overall solution is slightly improved by approximately 1.2%.

Figure 4.6.3 below shows the 3-D relative positioning and RMS clock error results when the TWTT satellite is located directly above the receiver network as well as offset +/- 30 degrees in both longitude and latitude. Realistically it is not possible to vary a geostationary satellite's latitude as geostationary orbits must lie directly above the equator. This testing was run, however, to quantify the effects of moving the satellite location in the positive and negative latitude directions in the event of the use of a satellite network or a satellite in a lower orbit.

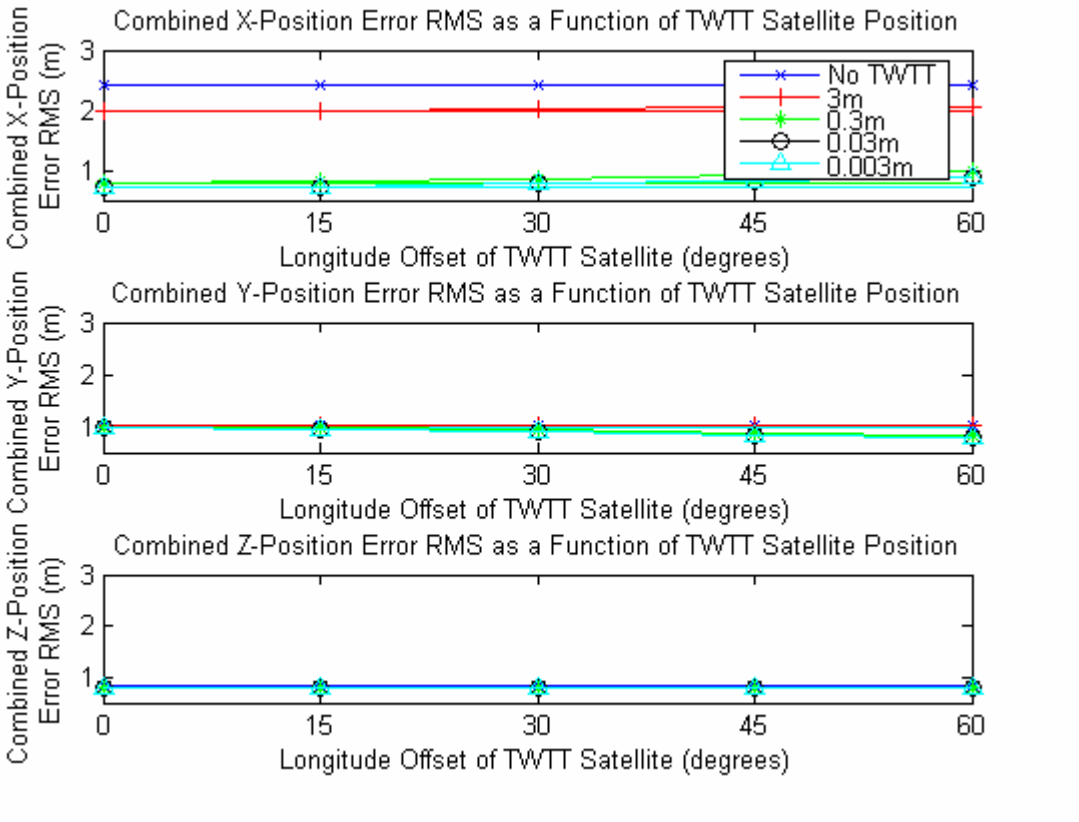

Figure 4.6.2 Position Error RMS vs. TWTT Satellite Location in Each Axis (TWTT Time and Range Measurements)

As expected, the results are the same when the TWTT satellite is offset in latitude *or* longitude, but the results for the longitude adjustment are slightly better than those with the latitude adjustment. This is not a significant improvement and is most likely due to the geometry of the satellites and receivers.

The direction of the TWTT satellite offset is the direction that is improved in the solution for each axis. However, that improvement is very small relative to the degraded performance in the x-direction and is only seen in the very precise TWTT scenarios. The worst direction for error in DGPS is in the vertical direction; therefore, the maximum 3-D

improvement can be obtained by placing the TWTT satellite directly above the receiver network.

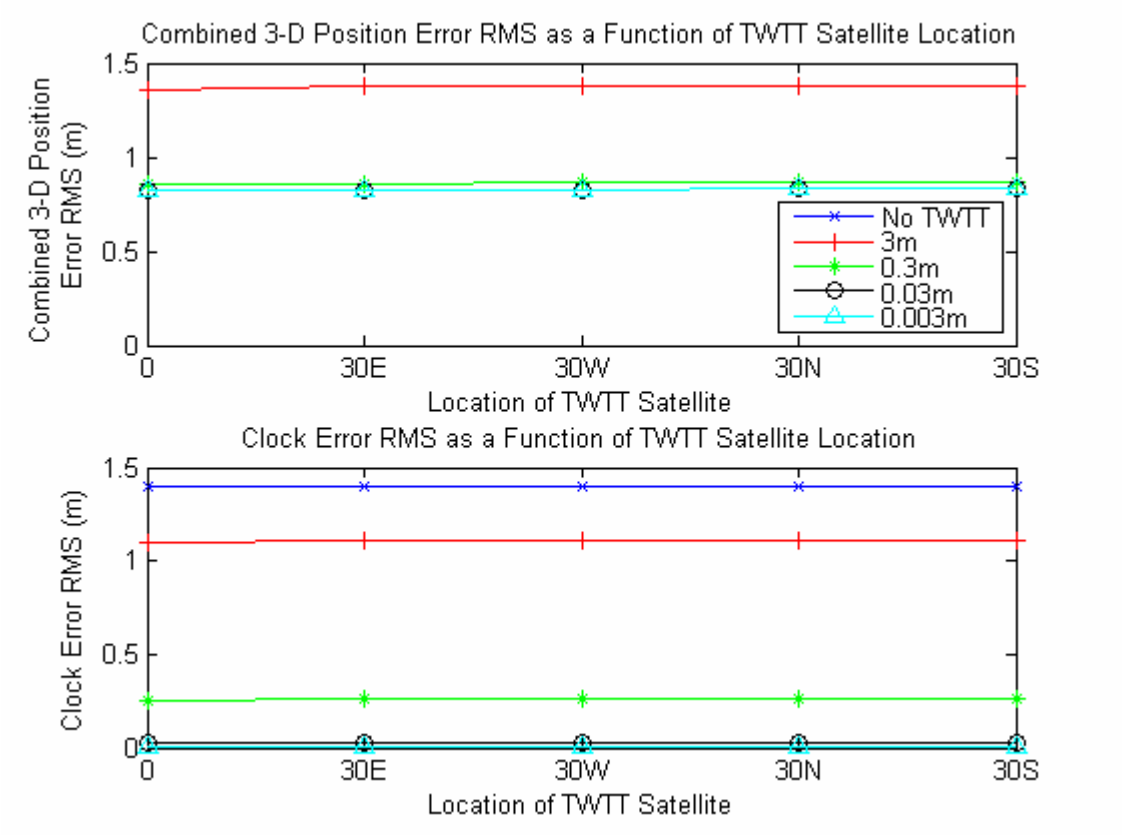

Figure 4.6.3 Combined 3-D Position Error RMS and Clock Error RMS vs. TWTT Satellite Location (TWTT Time and Range Measurements)

Figure 4.6.4 shows the position error RMS in each axis as a function of TWTT satellite location. It shows that the direction in which the TWTT satellite is being moved is the direction in which an improvement can be seen. When the TWTT satellite location is varied in latitude, an improvement is seen in the z-direction; when the TWTT satellite location is varied in longitude, the improvement is seen in the y-direction.

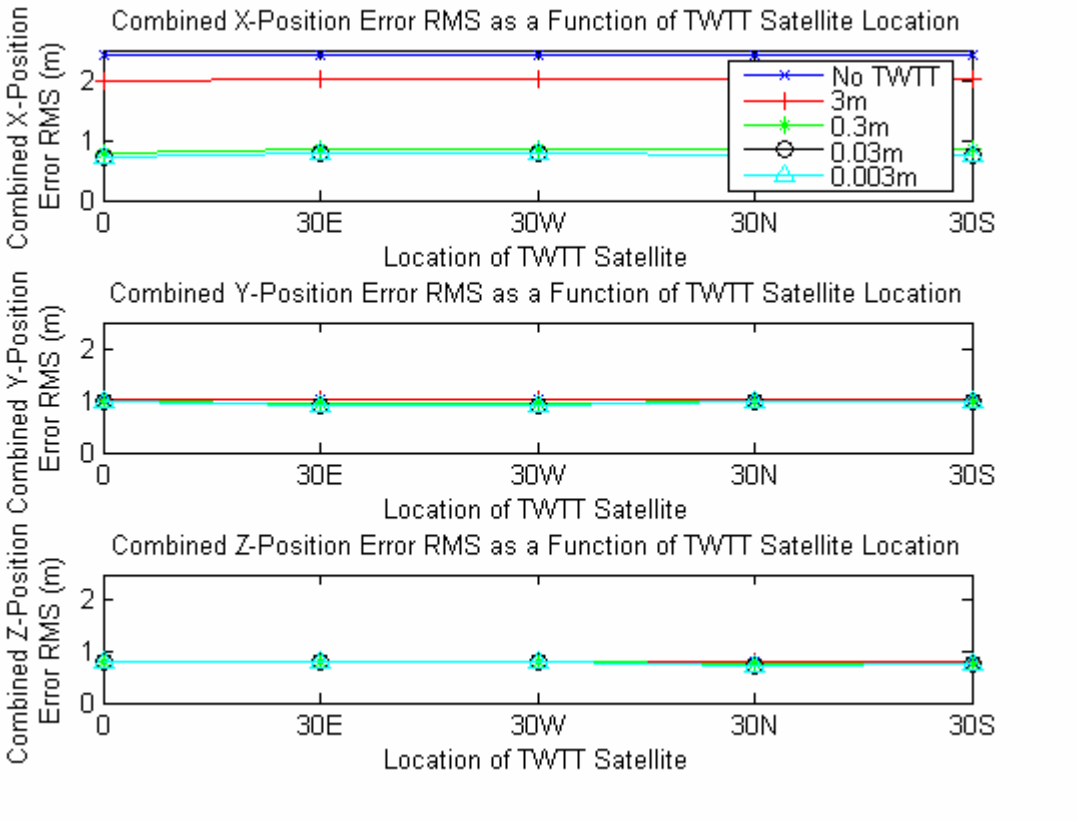

Figure 4.6.4 Position Error RMS vs. TWTT Satellite Location in Each Axis (TWTT Time and Range Measurements)

The results as were shown in Figures 4.6.1 and 4.6.3 indicate that the overall 3-D positioning solution is optimized when the TWTT satellite is located directly above the receiver network. This confirmed the original hypothesis for the system.

4.7 Trade Study 5: Vary the Satellite Elevation Cutoff

This trade study was performed to determine the impact of the satellite elevation cutoff angle on the relative positioning solution. It is expected that as the elevation angle cutoff is increased, the system performance will decrease due to the reduction in the number of satellites visible to the receivers and the reduction of the amount of time that

the satellites are visible to the receivers. The satellite elevation cutoff angle is the minimum angle at which the satellites can be viewed by the receivers. This angle limits the maximum in-view times of the satellites as shown in Figure 4.7.1, where El is the satellite elevation cutoff angle.

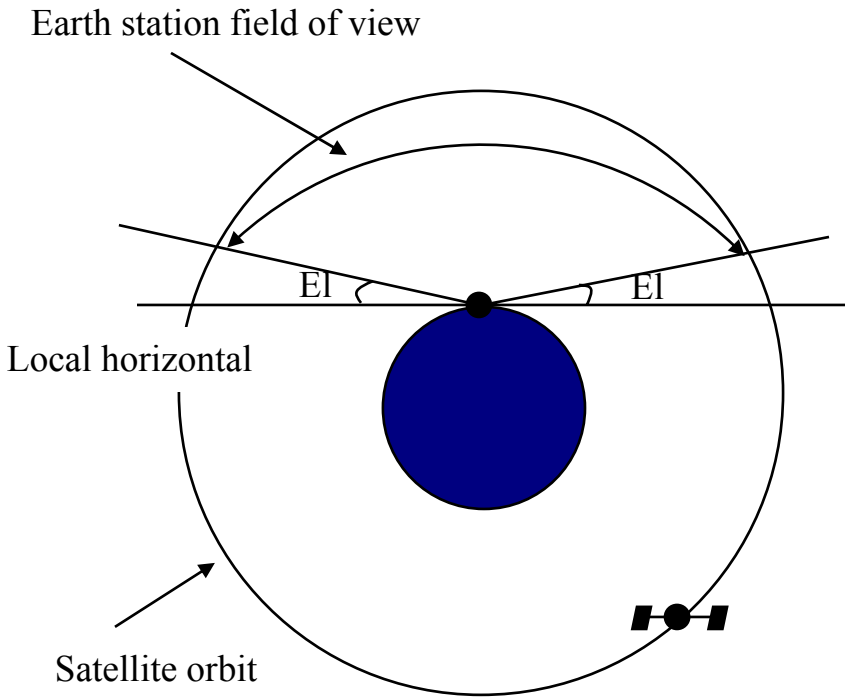

Figure 4.7.1 Satellite Elevation Angle Limits the In-view Time of a Satellite

Figures 4.7.2 and 4.7.3 show the combined 3-D position error RMS and clock error RMS as functions of the satellite elevation cutoff angle when the TWTT ranging measurements are not included and when they are, respectively.

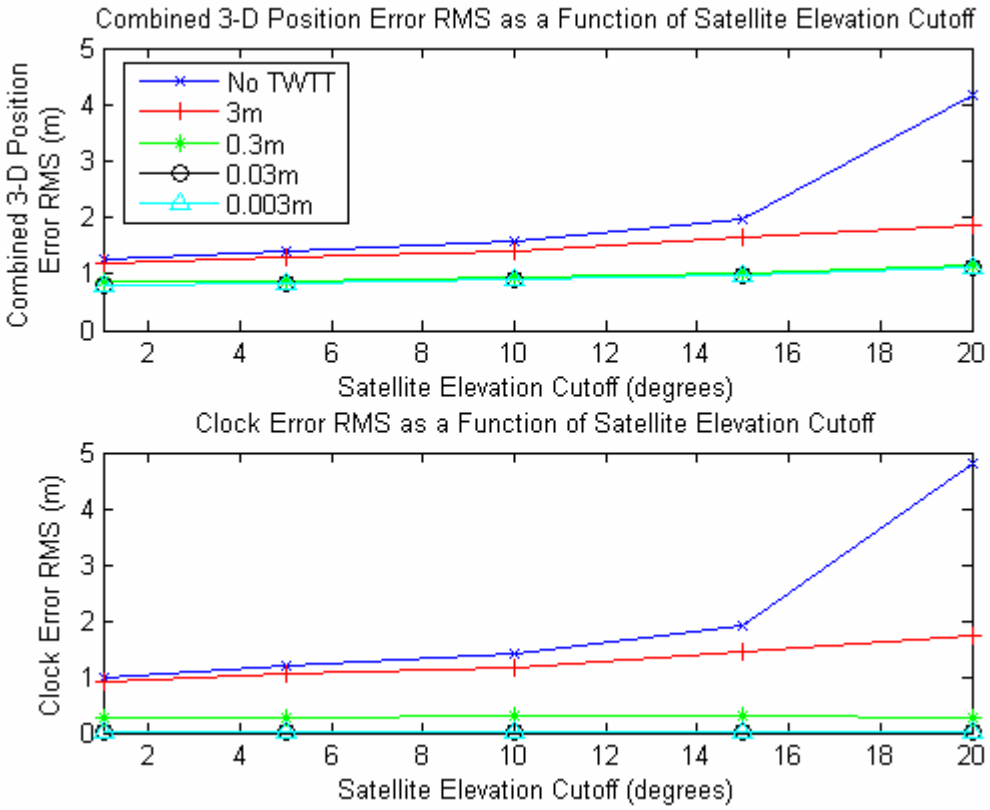

Figure 4.7.2 Combined 3-D Position Error RMS and Clock Error RMS vs. Satellite Elevation Cutoff (TWTT Time Measurements Only)

As shown in the Figures 4.7.2 and 4.7.3, as the satellite elevation cutoff is increased, the 3-D position solutions get worse. This is due to the decrease in number of visible GPS satellites as the cutoff angle is increased. The GPS-only solution is affected the most by this limitation because it is dependent solely on the GPS satellite constellation, and four satellites are required to obtain a complete solution. The solutions using TWTT measurements are affected, but not as significantly due to the fact that they're using the TWTT satellite measurements as observables, are not completely dependent on the GPS satellite constellation, and effectively reduce by 2 the number of GPS satellites needed to obtain the solution. Therefore, as shown, one is able to maintain

performance by using TWTT measurements in addition to GPS measurements even with a high elevation cutoff angle.

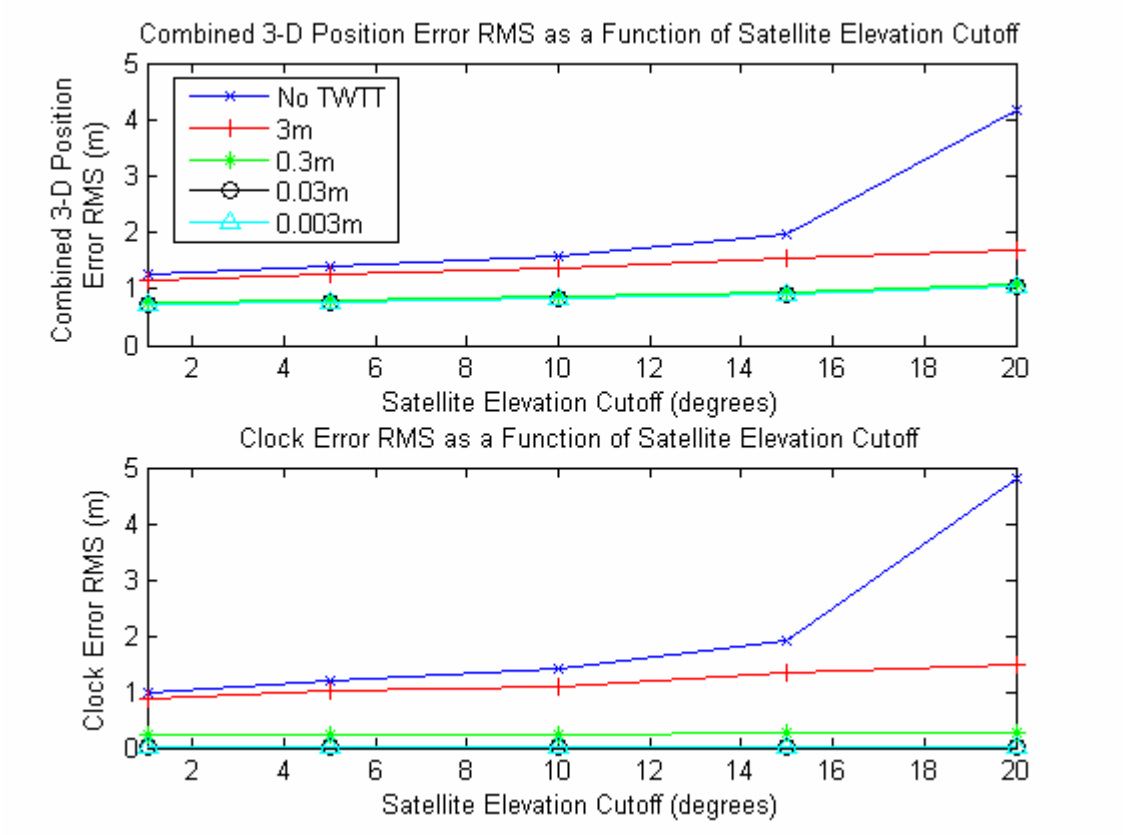

Figure 4.7.3 Combined 3-D Position Error RMS and Clock Error RMS vs. Satellite Elevation Cutoff (TWTT Time and Range Measurements)

Above a satellite elevation cutoff of 15 degrees, the GPS-only solution degrades rapidly. The GPS solutions that are augmented with TWTT measurements continue to increase slightly; however, there is not the rapid increase as is seen in the GPS-only solution. This is evident that there is an enormous benefit to using TWTT-augmented GPS measurements when it is necessary to have a high elevation cutoff.

Comparing Figures 4.7.2 and 4.7.3, it is again seen that including the TWTT ranging measurements in the observables improves the solution slightly. The RMS clock

errors are similarly affected whether the TWTT ranging measurements are included or not.

The GPS-only measurements get considerably worse at 20 degrees – much worse than would be expected. Upon further investigation, it was discovered that this poor performance of the system at a 20 degree elevation cutoff is due to several 'bad' time epochs where there is an un-observability due to an unusual satellite configuration. The way the current simulation is set up, all epochs need to have a valid result. Figure 4.7.4 is the delta position error RMS in each axis for the GPS-only scenario at 10 degrees. As shown, the errors are small and appear to be white Gaussian noise. Figure 4.7.5 is the delta position error RMS in each axis for the GPS-only scenario at 20 degrees. Notice all of the spikes indicating bad epochs. The results of these epochs are being used in the simulation along with the good epochs. This simulation does not account for bad epochs within the batch filter, so future work could include changing how the batch filter is being implemented to disregard any bad epochs. The data being used is real data and is therefore valid; therefore, this simulation demonstrates the importance of including TWTT measurements in the observables and reducing the dependency on GPS satellite configuration.

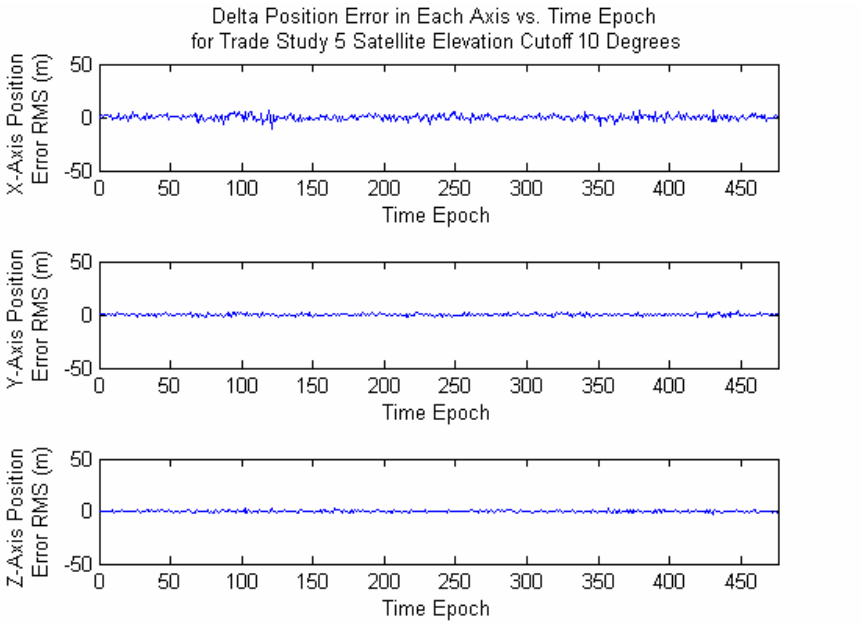

Figure 4.7.4 Delta Position Error RMS in Each Axis vs. Time Epoch for Satellite Elevation Cutoff of 10 Degrees (TWTT Time and Range Measurements)

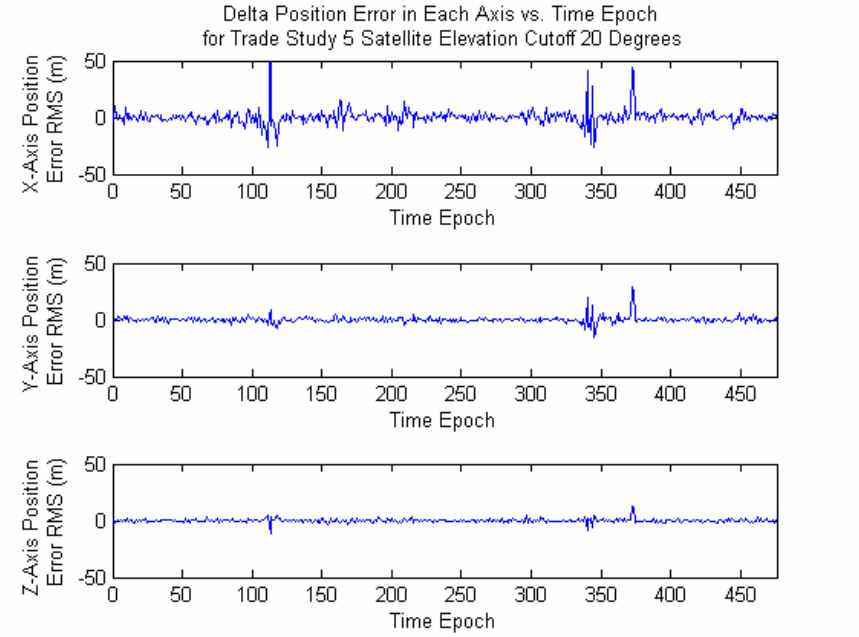

Figure 4.7.5 Delta Position Error RMS in Each Axis vs. Time Epoch for Satellite Elevation Cutoff of 20 Degrees (TWTT Time and Range Measurements)

Figures 4.7.6 and 4.7.7 both show that the RMS in the x-direction are the most affected by varying the satellite elevation cutoff, then the y-direction RMS and finally the z-direction RMS. This is due to the geometry of the receivers and satellites.

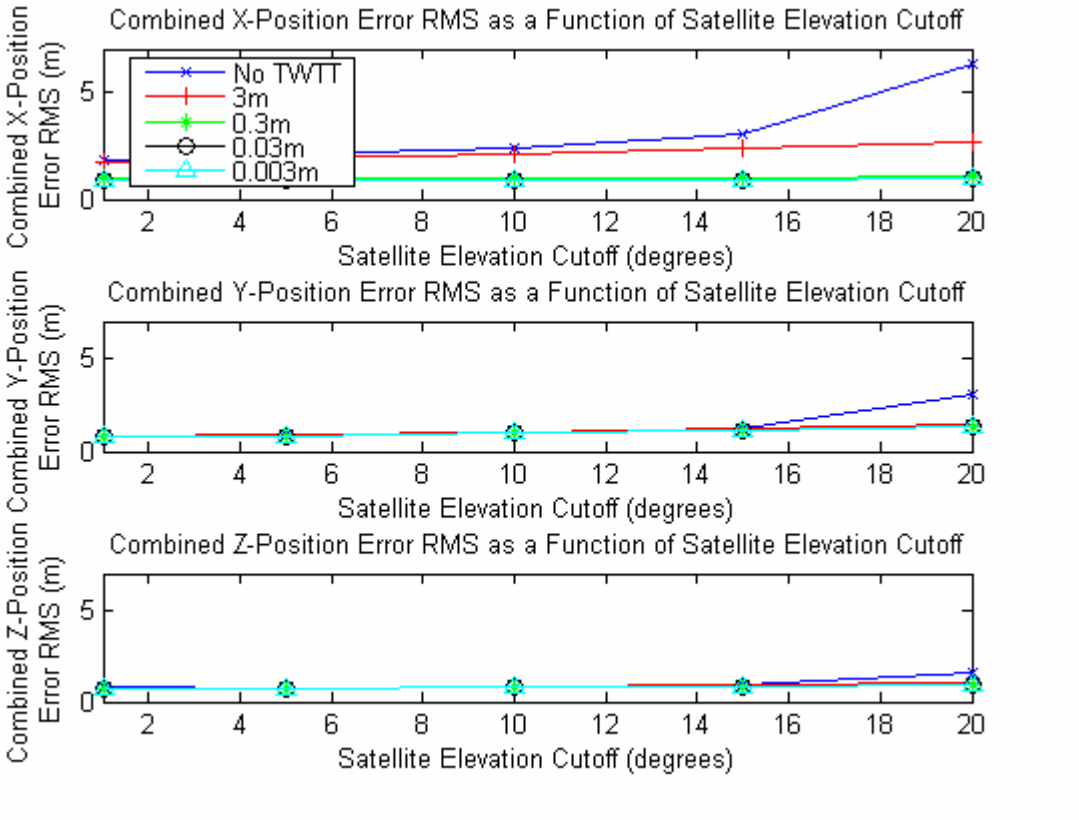

Figure 4.7.6 Position Error RMS vs. Satellite Elevation Cutoff in Each Axis (TWTT Time Measurements Only)

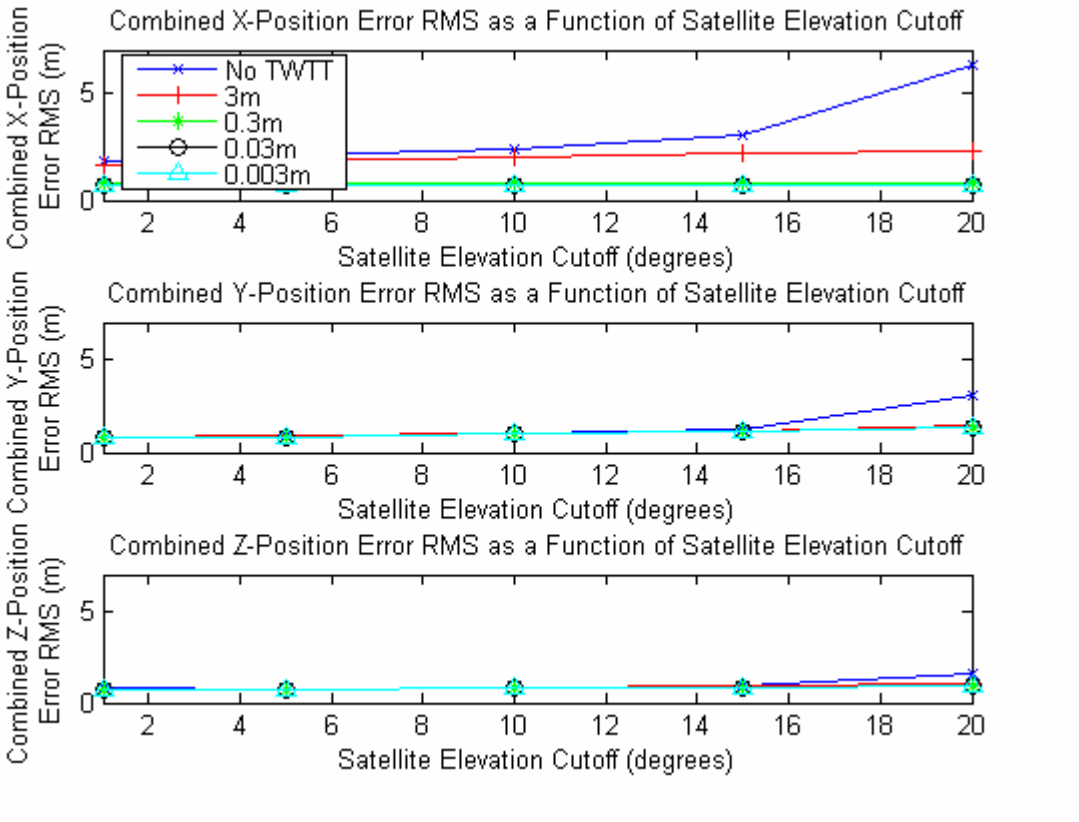

Figure 4.7.7 Position Error RMS vs. Satellite Elevation Cutoff in Each Axis (TWTT Time and Range Measurements)

As expected, the results of this trade study show that the overall position error increases as the satellite elevation cutoff increases. Above approximately 15 degrees the GPS-only solution is considerably worse than the solution augmented with TWTT measurements due to satellite visibility and the requirement for four GPS satellites to obtain a positioning solution. Performance is able to be maintained when using TWTT measurements in addition to GPS measurements, even at a high elevation cutoff angle. The results show that there is a considerable benefit to using the TWTT-augmented GPS measurements when a high elevation cutoff is required.

4.8 Summary

This chapter discussed the results of the simulation and provided an in-depth analysis of the results. First, the baseline results were described in detail. Next, results of each of the trade studies performed were discussed and analyzed. The first trade study performed was using two different days' ephemeris and comparing their results. The results of this trade study prove that the simulation is valid regardless of the day's ephemeris used. The second trade study was to vary the number of independent receivers used. The results confirmed that the overall positioning solution is not significantly impacted by changing the number of independent receivers in a network. This trade study also verified that there are no hidden correlations between the receivers present in the simulation. The third trade study looked at varying the separation distance between the receivers. As expected, the 3-D positioning solution can be optimized by minimizing the distance between the receivers. Separation distances less than approximately 500 km yield similar results, and as distance increases above 500 km, it is more advantageous to use a TWTT-augmented system as the solution is increasingly superior to the GPS-only solution. The fourth trade study investigated the impact of varying the location of the TWTT satellite. Results confirmed that the 3-D positioning solution is optimized when the TWTT satellite is located directly above the receiver network. Finally, the fifth trade study varied the satellite elevation cutoff to determine the solution's dependence on it. Results from the trade study show that the performance of the overall solution is dependent on the satellite elevation cutoff and can be optimized as the cutoff is minimized. It was also shown that at systems with higher elevation cutoff requirements

are significantly improved by using TWTT measurements in addition to the GPS measurements.

Chapter 5 will summarize conclusions and give recommendations for further research thrusts in this area.

V. Conclusions and Recommendations

5.1 Conclusions

The thrust of this research was to determine the impact of combining precise TWTT time and ranging measurements with GPS. The results indicate that up to 48% improvement can be achieved by including precise TWTT measurements as observables in addition to single-differenced GPS pseudorange measurements. A 40% improvement can be seen when using TWTT-augmented single-differenced carrier-phase measurements when compared to using double-differenced carrier-phase measurements alone. The baseline results as well as the results of each trade study are described below as well as a table summarizing the overall results.

5.1.1 Baseline Results

The baseline results in Chapter 4 show that including the TWTT ranging measurements in the observables in addition to the TWTT time-difference measurements reduces the positioning and clock errors further than only including the TWTT time-difference measurements. When comparing the GPS pseudorange-only case with highest accuracy TWTT case ($\Delta\rho$ + TT(D) + TWTT Ranging), the TWTT reduces the positioning error by over 70% in the x-direction alone, nearly 48% in the combined 3-D position, and reduces the clock error by over 99%. Even when using a TWTT accuracy of 3m and using the ranging measurements, the pseudorange-based positioning errors are reduced by over 10% and the clock errors are reduced by 22%. Including the TWTT ranging measurements improves the 3-D relative positioning solution by approximately 4-9% over solely using the TWTT time-differencing measurements. A special case was

run combining the TWTT measurements with GPS carrier-phase measurements, and slight improvements were seen. Due to the fact that the carrier phase measurements are more precise than the pseudorange measurements, the impact of the TWTT measurements on the solution is not as evident. The point of comparison for phase-based positioning is to compare between double differenced phase results (3-D RMS value of 0.072 m) with single-differenced phase results with TT(D) (3-D RMS value of 0.043 m). This is effectively an improvement of almost 40% in already-precise carrier-phase-based positioning. The relative positioning in the x-direction is improved by nearly 65% when using TT(D).

5.1.2 Trade Study 1

The first trade study compared results obtained using two different days' broadcast and precise ephemeris. The point values obtained vary by up to 6% between the two days and the relative improvements are generally within 5% for values compared between the different days. Comparing the results confirms that the results obtained are valid regardless of which day's ephemeris is used.

5.1.3 Trade Study 2

The second trade study looked at varying the number of receivers used in the network. The results show variation of up to 15% in the 3-D positioning accuracy as the number of receivers is varied, but there is no common trend that is followed. The variation seen is most likely due to the changed network geometry or due to the fact that the random number seed in the simulation is called a different number of times for different numbers of receivers. The results confirm the expectation that the overall

positioning solution is not significantly impacted by varying the number of independent receivers.

5.1.4 Trade Study 3

The third trade study performed was varying the separation distance between the receivers. The results show that networks where the receivers are separated by less than approximately 500 km obtain similar relative positioning solutions. Receivers separated by more than 500 km get an increasingly inferior solution as the separation distance increases when using only GPS measurements. If the observables include TWTT measurements, the solution increases slightly with receiver separation but not to the same extent as the GPS-only scenario. The 3-D positioning accuracy when only using GPS single-differenced pseudorange measurements with a separation distance of 1 km is 1.587 km and with a separation distance of 1,500 km it is 2.331 km. That is a decrease of approximately 32% in performance. When the most precise TWTT measurement is used, the 3-D positioning accuracy is 0.889 km with a separation distance of 1 km and 0.965 km with a separation distance of 1,500 km. That is a decrease of approximately 7.8% in performance. Therefore, the results indicate that the overall positioning solution is optimized as the separation distance between receivers is decreased, and if it is necessary to maintain large separation distances between receivers, significantly better performance will be achieved when using TWTT-augmented measurements.

5.1.5 Trade Study 4

Trade study four was performed to determine if the location of the TWTT satellite has an impact on the relative positioning solution. It shows that if the TWTT

measurements including ranging are included in the simulation, then as the TWTT satellite moves off-center from the network, the overall positioning solution is degraded by up to 3%. The RMS position error in the direction in which the satellite is being relocated actually improves, but generally not enough to compensate for the degraded performance in the x-direction (pointing straight up from the network). The results show that if the goal is to optimize the 3-D solution then it is ideal to have the TWTT satellite located directly above the receiver network. If the TWTT timing measurements are used (with no ranging measurements) then the solution does not change regardless of the location of the TWTT satellite.

5.1.6 Trade Study 5

Finally, the last trade study performed was to determine the effects of varying the satellite elevation cutoff. The results show that the overall solution increases as the satellite elevation cutoff increases, but above approximately 15 degrees the GPS-only solution is significantly worse than the solution augmented with TWTT measurements. When the elevation cutoff angle is varied from 1 to 20 degrees, the GPS only solution degrades by over 60% whereas the least precise TWTT solution decreases by only 36%. Therefore, the overall positioning solution is optimized as the cutoff elevation angle is minimized, and there is a considerable benefit to using the TWTT-augmented GPS measurements when a high elevation cutoff is required.

The results of the five trade studies have been explained, and tables summarizing their consolidated results are provided in the next section.

5.1.7 Consolidated Results

Below are two tables summarizing the results of the research. Across the top of the first table are five of the different simulations run (single-differenced pseudorange only and TWTT – No Ranging) and across the top of the second table are the other four (the single-differenced pseudorange only case re-stated for convenient comparison and the TWTT – With Ranging). The first column in each table describes the scenario as defined in the trade studies; the corresponding trade study is indicated in brackets. The values shown in the table are the 3-D RMS values obtained in units of kilometers.

Table 5.1.1 Consolidated Results for 3-D Position Error (m) - No TWTT Ranging

Scenario	$\Delta\rho$ only	$\Delta\rho$ + TT(A)	$\Delta\rho$ + TT(B)	$\Delta\rho$ + TT(C)	$\Delta\rho$ + TT(D)
Base	1.587	1.415	0.935	0.890	0.889
2 Receivers [2]	1.631	1.527	0.909	0.869	0.869
4 Receivers [2]	1.512	1.401	0.924	0.882	0.882
6 Receivers [2]	1.587	1.415	0.935	0.890	0.889
8 Receivers [2]	1.571	1.397	0.920	0.877	0.876
10 Receivers [2]	1.599	1.417	0.930	0.886	0.885
1km Receiver Separation [3]	1.587	1.415	0.935	0.890	0.889
100km Receiver Separation [3]	1.617	1.439	0.914	0.872	0.872
500km Receiver Separation [3]	1.656	1.483	0.939	0.891	0.890
1,000km Receiver Separation [3]	1.875	1.538	0.968	0.927	0.927
1,500km Receiver Separation [3]	2.331	1.683	1.007	0.966	0.965
TWTT Satellite 0˚ Offset [4]	1.587	1.415	0.935	0.890	0.889
TWTT Satellite 15˚ Offset [4]	1.587	1.415	0.935	0.890	0.889
TWTT Satellite 30˚ Offset [4]	1.587	1.415	0.935	0.890	0.889
TWTT Satellite 45˚ Offset [4]	1.587	1.415	0.935	0.890	0.889
TWTT Satellite 60˚ Offset [4]	1.587	1.415	0.935	0.890	0.889
Satellite Elevation Cutoff 1˚ [5]	1.261	1.193	0.856	0.813	0.813
Satellite Elevation Cutoff 5˚ [5]	1.403	1.289	0.866	0.825	0.825
Satellite Elevation Cutoff 10˚ [5]	0.587	1.415	0.935	0.890	0.889
Satellite Elevation Cutoff 15˚ [5]	1.972	1.640	1.016	0.980	0.980
Satellite Elevation Cutoff 20˚ [5]	4.165	1.867	1.145	1.120	1.120

Table 5.1.2 Consolidated Results for 3-D Position Error (m) – With TWTT Ranging

Scenario	$\Delta\rho$ only	$\Delta\rho$ + TT(A) + Ranging	$\Delta\rho$ + TT(B) + Ranging	$\Delta\rho$ + TT(C) + Ranging	$\Delta\rho$ + TT(D) + Ranging
Base	1.587	1.358	0.856	0.829	0.828
2 Receivers [2]	1.631	1.527	0.909	0.869	0.869
4 Receivers [2]	1.512	1.355	0.854	0.829	0.830
6 Receivers [2]	1.587	1.358	0.856	0.829	0.828
8 Receivers [2]	1.571	1.328	0.828	0.805	0.805
10 Receivers [2]	1.599	1.347	0.838	0.813	0.813
1km Receiver Separation [3]	1.587	1.358	0.856	0.829	0.828
100km Receiver Separation [3]	1.617	1.378	0.831	0.809	0.809
500km Receiver Separation [3]	1.656	1.383	0.852	0.825	0.824
1,000km Receiver Separation [3]	1.875	1.431	0.889	0.862	0.862
1,500km Receiver Separation [3]	2.331	1.546	0.927	0.901	0.900
TWTT Satellite 0˚ Offset [4]	1.587	1.358	0.856	0.829	0.828
TWTT Satellite 15˚ Offset [4]	1.587	1.362	0.857	0.826	0.825
TWTT Satellite 30˚ Offset [4]	1.587	1.373	0.860	0.823	0.822
TWTT Satellite 45˚ Offset [4]	1.587	1.389	0.866	0.820	0.819
TWTT Satellite 60˚ Offset [4]	1.587	1.403	0.873	0.819	0.818
Satellite Elevation Cutoff 1˚ [5]	1.261	1.160	0.771	0.744	0.744
Satellite Elevation Cutoff 5˚ [5]	1.403	1.248	0.785	0.760	0.760
Satellite Elevation Cutoff 10˚ [5]	0.587	1.358	0.856	0.829	0.828
Satellite Elevation Cutoff 15˚ [5]	1.972	1.531	0.758	0.912	0.912
Satellite Elevation Cutoff 20˚ [5]	4.165	1.684	1.074	1.054	1.054

Using the two tables above, one can see the benefits of using TWTT-augmented GPS measurements in the different scenarios run. The effects of varying different parameters can be seen in each of the different situations. The significance of the results of this research is laid out in the following section.

5.2 Significance of Research

The significance of this research is three-fold. First, the results show an improvement of 48% in the 3-D relative positioning solution when using precise TWTT measurements in addition to GPS pseudorange measurements. An improvement of 40% over double-differenced carrier-phase measurements can be obtained when integrating precise TWTT measurements with single-differenced carrier-phase measurements. These are both substantial improvements over solely using GPS measurements for positioning solutions. This has major implications for both civilian and military users. By integrating the TWTT measurements with GPS measurements, the lives of civilians who dial '911' on their cell phones may be saved because the emergency personnel could precisely locate them; fewer civilian casualties could result in wars due to more precise munitions; and networks of vehicles can be implemented in more constrained situations without fear of collisions with one another.

Second, this research generated a new source of measurements from the TWTT technique. This is the first known proposal of using the TWTT ranging measurements as pseudorange measurements to determine position. By using these measurements in addition to GPS measurements, it reduces by two the number of GPS satellites required

to obtain a positioning solution. In effect, it suggests that a communications network can be turned into a positioning system.

Third, the results of the first trade study indicate that the simulation is not limited to any particular day's ephemeris, but it is valid for any day of the year. The second trade study shows that as expected, overall positioning solution can not be optimized by varying the number of independent receivers in a network. The results of the third trade study confirm that the overall positioning solution is optimized when the receivers in the network are separated by small distances. This trade study also shows that as the separation distance between receivers increase, there is a substantial improvement in the positioning solution when using TWTT-augmented GPS measurements. The fourth trade study shows that the overall positioning solution is optimized when the TWTT satellite is located directly above the receiver network. Finally, the results of the fifth trade study are such that the 3-D positioning solution is optimized when the satellite elevation cutoff angle is minimized. Also, as the satellite elevation angle is increased, there is a remarkable improvement in the solution when using TWTT measurements in addition to the GPS measurements.

All of these results signify potential in this area of research. The following section contains recommendations for future research.

5.3 Recommendations for Future Research

It is recommended that more attention be brought to the possibility of improving relative positioning solutions by augmenting GPS measurements with TWTT time and

range measurements. The simulation developed for this research provides evidence that there is a huge potential benefit in doing so. A more rigorous examination of the problem must be performed. This can be done by further developing the simulation and ultimately field testing the TWTT/GPS system. Also, through the course of this research, the possibility of a TWTT-only approach to navigation is possible. Each of these suggestions is described in the following sections.

5.3.1 Improve Simulation Fidelity

The deterministic effects such as motion-related errors and the effects of the Sagnac delay were not modeled in this simulation. The propagation delays caused by using different uplink and downlink frequencies should be investigated and modeled as should the atmospheric effects on those frequencies. The propagation delays resulting from using D-TWTT as opposed to S-TWTT were not included in the simulation, but should be modeled. It was assumed that the deterministic effects could be calculated and removed for simplicity in this simulation. The deterministic errors should not have an impact on the overall position solution accuracy. When using real-time data, however, deterministic errors would have to be accounted for, because they would be present in the measurements.

This simulation used stationary receivers in the scenarios. The satellites in the GPS network were constantly moving along their individual trajectories, so the pseudorange and carrier-phase measurements between the satellites and receivers were continuously changing as well. The measurements between the TWTT satellite and the receivers, however, stayed relatively constant. A more realistic simulation would include

position and velocity vectors for the receivers to simulate moving vehicles. This is now possible with the successful testing of dynamic TWTT. The simulation should also look at cases where the receivers are not all in the same vertical plane, but are located at different elevations. Again, this will change the resulting values, but the general trends of the results will be the same.

This simulation looked at determining the relative positions between a reference receiver and the remaining independent receivers. The results showed that the number of independent receivers does not significantly impact the accuracy of the 3-D positioning solution. It is expected that if the receivers are not independent, that relative positioning measurements are used between all of the receivers; the overall positioning solution will be improved as the number of dependent receivers increases.

5.3.2 Field Test Combined TWTT / GPS System

Once a realistic, working simulation has been created and tested, the next logical step is to actually field test a combined TWTT / GPS system. This requires the calculation and removal of the deterministic terms, and careful calibration and/or estimation of the instrument biases, which can be calibrated using GPS.

5.3.3 Investigate a TWTT-only Approach to Navigation

The possibility of using TWTT systems for navigation emerged while doing this research. It appears that an entirely non-GPS navigation system can be created by using only TWTT measurements. The approach to navigation using satellites meant for other means (for example communication satellites) should be investigated further.

5.4 Summary

This research examined the implications of integrating TWTT measurements with GPS measurements. Trade studies were performed in order to lay out the trade space of the problem and determine possible methods for optimizing the system. The results show that the overall 3-D positioning solution can be considerably improved by including the TWTT measurements (48% with pseudorange measurements and 40% with carrier-phase measurements) and further investigations into this area of research should be carried out.

Appendix A—Numerical Simulation Results

Baseline Results

Single Differenced PR / No TWTT
Combined Pos RMS x=2.855 y=1.107 z=0.862
Combined 3-D Pos RMS: 1.837 Clock RMS: 1.599

Single Differenced PR / TWTT A
Combined Pos RMS x=2.131 y=1.089 z=0.837
Combined 3-D Pos RMS: 1.464 Clock RMS: 1.169

Single Differenced PR / TWTT B
Combined Pos RMS x=0.830 y=1.061 z=0.819
Combined 3-D Pos RMS: 0.910 Clock RMS: 0.252

Single Differenced PR / TWTT C
Combined Pos RMS x=0.743 y=1.057 z=0.816
Combined 3-D Pos RMS: 0.882 Clock RMS: 0.030

Single Differenced PR / TWTT D
Combined Pos RMS x=0.741 y=1.057 z=0.816
Combined 3-D Pos RMS: 0.882 Clock RMS: 0.003

Single Differenced PR / TWTT A / No Ranging
Combined Pos RMS x=2.342 y=1.095 z=0.841
Combined 3-D Pos RMS: 1.570 Clock RMS: 1.267

Single Differenced PR / TWTT B / No Ranging
Combined Pos RMS x=1.083 y=1.065 z=0.821
Combined 3-D Pos RMS: 0.997 Clock RMS: 0.288

Single Differenced PR / TWTT C / No Ranging
Combined Pos RMS x=0.959 y=1.062 z=0.821
Combined 3-D Pos RMS: 0.952 Clock RMS: 0.030

Single Differenced PR / TWTT D / No Ranging
Combined Pos RMS x=0.956 y=1.061 z=0.821
Combined 3-D Pos RMS: 0.951 Clock RMS: 0.003

Single Differenced PM / No TWTT
Combined Pos RMS x=0.147 y=0.059 z=0.046
Combined 3-D Pos RMS: 0.095 Clock RMS: 0.083

Single Differenced PM / TWTT A
Combined Pos RMS x=0.147 y=0.059 z=0.046
Combined 3-D Pos RMS: 0.095 Clock RMS: 0.083

Single Differenced PM / TWTT B
Combined Pos RMS x=0.146 y=0.059 z=0.046
Combined 3-D Pos RMS: 0.094 Clock RMS: 0.082

Single Differenced PM / TWTT C
Combined Pos RMS x=0.089 y=0.057 z=0.044
Combined 3-D Pos RMS: 0.066 Clock RMS: 0.049

Single Differenced PM / TWTT D
Combined Pos RMS x=0.038 y=0.056 z=0.044
Combined 3-D Pos RMS: 0.046 Clock RMS: 0.007

Single Differenced PM / TWTT A / No Ranging
Combined Pos RMS x=0.147 y=0.059 z=0.046
Combined 3-D Pos RMS: 0.095 Clock RMS: 0.083

Single Differenced PM / TWTT B / No Ranging
Combined Pos RMS x=0.146 y=0.059 z=0.046
Combined 3-D Pos RMS: 0.095 Clock RMS: 0.082

Single Differenced PM / TWTT C / No Ranging
Combined Pos RMS x=0.105 y=0.057 z=0.045
Combined 3-D Pos RMS: 0.074 Clock RMS: 0.056

Single Differenced PM / TWTT D / No Ranging
Combined Pos RMS x=0.050 y=0.056 z=0.044
Combined 3-D Pos RMS: 0.050 Clock RMS: 0.005

Double Differenced PM / No TWTT
Combined Pos RMS x=0.115 y=0.058 z=0.045
Combined 3-D Pos RMS: 0.079 Clock RMS: 0.003

Trade Study 1 – Results for 5 May 1994

Single Differenced PR / No TWTT
Combined Pos RMS x=2.426 y=1.078 z=0.834
Combined 3-D Pos RMS: 1.607 Clock RMS: 1.426

Single Differenced PR / TWTT A
Combined Pos RMS x=1.946 y=1.073 z=0.819
Combined 3-D Pos RMS: 1.367 Clock RMS: 1.109

Single Differenced PR / TWTT B
Combined Pos RMS x=0.763 y=1.054 z=0.796
Combined 3-D Pos RMS: 0.881 Clock RMS: 0.248

Single Differenced PR / TWTT C
Combined Pos RMS x=0.693 y=1.051 z=0.794
Combined 3-D Pos RMS: 0.860 Clock RMS: 0.030

Single Differenced PR / TWTT D
Combined Pos RMS x=0.693 y=1.051 z=0.794
Combined 3-D Pos RMS: 0.859 Clock RMS: 0.003

Single Differenced PR / TWTT A / No Ranging
Combined Pos RMS x=2.085 y=1.073 z=0.822
Combined 3-D Pos RMS: 1.435 Clock RMS: 1.178

Single Differenced PR / TWTT B / No Ranging
Combined Pos RMS x=1.015 y=1.056 z=0.796
Combined 3-D Pos RMS: 0.963 Clock RMS: 0.288

Single Differenced PR / TWTT C / No Ranging
Combined Pos RMS x=0.895 y=1.054 z=0.795
Combined 3-D Pos RMS: 0.921 Clock RMS: 0.030

Single Differenced PR / TWTT D / No Ranging
Combined Pos RMS x=0.893 y=1.054 z=0.795
Combined 3-D Pos RMS: 0.920 Clock RMS: 0.003

Single Differenced PM / No TWTT
Combined Pos RMS x=0.129 y=0.062 z=0.044
Combined 3-D Pos RMS: 0.087 Clock RMS: 0.076

Single Differenced PM / TWTT A
Combined Pos RMS x=0.129 y=0.062 z=0.044
Combined 3-D Pos RMS: 0.087 Clock RMS: 0.076

Single Differenced PM / TWTT B
Combined Pos RMS x=0.129 y=0.062 z=0.044
Combined 3-D Pos RMS: 0.086 Clock RMS: 0.075

Single Differenced PM / TWTT C
Combined Pos RMS x=0.087 y=0.061 z=0.043
Combined 3-D Pos RMS: 0.066 Clock RMS: 0.048

Single Differenced PM / TWTT D
Combined Pos RMS x=0.036 y=0.060 z=0.042
Combined 3-D Pos RMS: 0.047 Clock RMS: 0.007

Single Differenced PM / TWTT A / No Ranging
Combined Pos RMS x=0.129 y=0.062 z=0.044
Combined 3-D Pos RMS: 0.087 Clock RMS: 0.076

Single Differenced PM / TWTT B / No Ranging
Combined Pos RMS x=0.129 y=0.062 z=0.044
Combined 3-D Pos RMS: 0.086 Clock RMS: 0.075

Single Differenced PM / TWTT C / No Ranging
Combined Pos RMS x=0.099 y=0.061 z=0.043
Combined 3-D Pos RMS: 0.071 Clock RMS: 0.054

Single Differenced PM / TWTT D / No Ranging
Combined Pos RMS x=0.048 y=0.060 z=0.042
Combined 3-D Pos RMS: 0.050 Clock RMS: 0.005

Double Differenced PM / No TWTT
Combined Pos RMS x=0.101 y=0.062 z=0.044
Combined 3-D Pos RMS: 0.073 Clock RMS: 0.003

Trade Study 2 – Vary the Number of Receivers

Single Differenced PR / No TWTT, N = 2
Combined Pos RMS x=2.517 y=1.007 z=0.792
Combined 3-D Pos RMS: 1.631 Clock RMS: 1.448

Single Differenced PR / No TWTT, N = 4
Combined Pos RMS x=2.262 y=1.026 z=0.830
Combined 3-D Pos RMS: 1.512 Clock RMS: 1.322

Single Differenced PR / No TWTT, N = 6
Combined Pos RMS x=2.417 y=1.022 z=0.820
Combined 3-D Pos RMS: 1.587 Clock RMS: 1.400

Single Differenced PR / No TWTT, N = 8
Combined Pos RMS x=2.396 y=0.986 z=0.832
Combined 3-D Pos RMS: 1.571 Clock RMS: 1.363

Single Differenced PR / No TWTT, N = 10
Combined Pos RMS x=2.447 y=1.026 z=0.796
Combined 3-D Pos RMS: 1.599 Clock RMS: 1.423

Single Differenced PR / TWTT A, N = 2
Combined Pos RMS x=2.321 y=0.997 z=0.786
Combined 3-D Pos RMS: 1.527 Clock RMS: 1.331

Single Differenced PR / TWTT A, N = 4
Combined Pos RMS x=1.949 y=1.011 z=0.827
Combined 3-D Pos RMS: 1.355 Clock RMS: 1.122

Single Differenced PR / TWTT A, N = 6
Combined Pos RMS x=1.969 y=1.005 z=0.804
Combined 3-D Pos RMS: 1.358 Clock RMS: 1.096

Single Differenced PR / TWTT A, N = 8
Combined Pos RMS x=1.917 y=0.969 z=0.824
Combined 3-D Pos RMS: 1.328 Clock RMS: 1.058

Single Differenced PR / TWTT A, N = 10
Combined Pos RMS x=1.949 y=1.009 z=0.791
Combined 3-D Pos RMS: 1.347 Clock RMS: 1.086

Single Differenced PR / TWTT B, N = 2
Combined Pos RMS x=0.988 y=0.951 z=0.773
Combined 3-D Pos RMS: 0.909 Clock RMS: 0.312

Single Differenced PR / TWTT B, N = 4
Combined Pos RMS x=0.771 y=0.959 z=0.819
Combined 3-D Pos RMS: 0.854 Clock RMS: 0.258

Single Differenced PR / TWTT B, N = 6
Combined Pos RMS x=0.793 y=0.975 z=0.787
Combined 3-D Pos RMS: 0.856 Clock RMS: 0.250

Single Differenced PR / TWTT B, N = 8
Combined Pos RMS x=0.724 y=0.933 z=0.813
Combined 3-D Pos RMS: 0.828 Clock RMS: 0.243

Single Differenced PR / TWTT B, N = 10
Combined Pos RMS x=0.755 y=0.971 z=0.770
Combined 3-D Pos RMS: 0.838 Clock RMS: 0.245

Single Differenced PR / TWTT C, N = 2
Combined Pos RMS x=0.872 y=0.950 z=0.775
Combined 3-D Pos RMS: 0.869 Clock RMS: 0.032

Single Differenced PR / TWTT C, N = 4
Combined Pos RMS x=0.696 y=0.954 z=0.819
Combined 3-D Pos RMS: 0.829 Clock RMS: 0.031

Single Differenced PR / TWTT C, N = 6
Combined Pos RMS x=0.708 y=0.971 z=0.785
Combined 3-D Pos RMS: 0.829 Clock RMS: 0.030

Single Differenced PR / TWTT C, N = 8
Combined Pos RMS x=0.656 y=0.926 z=0.811
Combined 3-D Pos RMS: 0.805 Clock RMS: 0.030

Single Differenced PR / TWTT C, N = 10
Combined Pos RMS x=0.684 y=0.964 z=0.767
Combined 3-D Pos RMS: 0.813 Clock RMS: 0.030

Single Differenced PR / TWTT D, N = 2
Combined Pos RMS x=0.873 y=0.950 z=0.776
Combined 3-D Pos RMS: 0.869 Clock RMS: 0.003

Single Differenced PR / TWTT D, N = 4
Combined Pos RMS x=0.696 y=0.954 z=0.819
Combined 3-D Pos RMS: 0.830 Clock RMS: 0.003

Single Differenced PR / TWTT D, N = 6
Combined Pos RMS x=0.705 y=0.971 z=0.786
Combined 3-D Pos RMS: 0.828 Clock RMS: 0.003

Single Differenced PR / TWTT D, N = 8
Combined Pos RMS x=0.655 y=0.926 z=0.811
Combined 3-D Pos RMS: 0.805 Clock RMS: 0.003

Single Differenced PR / TWTT D, N = 10
Combined Pos RMS x=0.683 y=0.963 z=0.767
Combined 3-D Pos RMS: 0.813 Clock RMS: 0.003

Single Differenced PR / TWTT A / No Ranging, N = 2
Combined Pos RMS x=2.321 y=0.997 z=0.786
Combined 3-D Pos RMS: 1.527 Clock RMS: 1.331

Single Differenced PR / TWTT A / No Ranging, N = 4
Combined Pos RMS x=2.043 y=1.014 z=0.829
Combined 3-D Pos RMS: 1.401 Clock RMS: 1.170

Single Differenced PR / TWTT A / No Ranging, N = 6
Combined Pos RMS x=2.085 y=1.008 z=0.805
Combined 3-D Pos RMS: 1.415 Clock RMS: 1.158

Single Differenced PR / TWTT A / No Ranging, N = 8
Combined Pos RMS x=2.057 y=0.970 z=0.825
Combined 3-D Pos RMS: 1.397 Clock RMS: 1.129

Single Differenced PR / TWTT A / No Ranging, N = 10
Combined Pos RMS x=2.089 y=1.013 z=0.794
Combined 3-D Pos RMS: 1.417 Clock RMS: 1.158

Single Differenced PR / TWTT B / No Ranging, N = 2
Combined Pos RMS x=0.988 y=0.951 z=0.773
Combined 3-D Pos RMS: 0.909 Clock RMS: 0.312

Single Differenced PR / TWTT B / No Ranging, N = 4
Combined Pos RMS x=0.979 y=0.964 z=0.820
Combined 3-D Pos RMS: 0.924 Clock RMS: 0.295

Single Differenced PR / TWTT B / No Ranging, N = 6
Combined Pos RMS x=1.025 y=0.977 z=0.787
Combined 3-D Pos RMS: 0.935 Clock RMS: 0.290

Single Differenced PR / TWTT B / No Ranging, N = 8
Combined Pos RMS x=1.004 y=0.935 z=0.812
Combined 3-D Pos RMS: 0.920 Clock RMS: 0.287

Single Differenced PR / TWTT B / No Ranging, N = 10
Combined Pos RMS x=1.023 y=0.975 z=0.771
Combined 3-D Pos RMS: 0.930 Clock RMS: 0.287

Single Differenced PR / TWTT C / No Ranging, N = 2
Combined Pos RMS x=0.872 y=0.950 z=0.775
Combined 3-D Pos RMS: 0.869 Clock RMS: 0.032

Single Differenced PR / TWTT C / No Ranging, N = 4
Combined Pos RMS x=0.860 y=0.960 z=0.820
Combined 3-D Pos RMS: 0.882 Clock RMS: 0.031

Single Differenced PR / TWTT C / No Ranging, N = 6
Combined Pos RMS x=0.898 y=0.975 z=0.787
Combined 3-D Pos RMS: 0.890 Clock RMS: 0.030

Single Differenced PR / TWTT C / No Ranging, N = 8
Combined Pos RMS x=0.882 y=0.933 z=0.812
Combined 3-D Pos RMS: 0.877 Clock RMS: 0.030

Single Differenced PR / TWTT C / No Ranging, N = 10
Combined Pos RMS x=0.905 y=0.971 z=0.769
Combined 3-D Pos RMS: 0.886 Clock RMS: 0.030

Single Differenced PR / TWTT D / No Ranging, N = 2
Combined Pos RMS x=0.873 y=0.950 z=0.776
Combined 3-D Pos RMS: 0.869 Clock RMS: 0.003

Single Differenced PR / TWTT D / No Ranging, N = 4
Combined Pos RMS x=0.860 y=0.960 z=0.820
Combined 3-D Pos RMS: 0.882 Clock RMS: 0.003

Single Differenced PR / TWTT D / No Ranging, N = 6
Combined Pos RMS x=0.895 y=0.975 z=0.787
Combined 3-D Pos RMS: 0.889 Clock RMS: 0.003

Single Differenced PR / TWTT D / No Ranging, N = 8
Combined Pos RMS x=0.880 y=0.933 z=0.812
Combined 3-D Pos RMS: 0.876 Clock RMS: 0.003

Single Differenced PR / TWTT D / No Ranging, N = 10
Combined Pos RMS x=0.903 y=0.971 z=0.769
Combined 3-D Pos RMS: 0.885 Clock RMS: 0.003

Trade Study 3 – Vary the Separation Distance Between Receivers

Single Differenced PR / No TWTT, Distance = 1 km
Combined Pos RMS x=2.417 y=1.022 z=0.820
Combined 3-D Pos RMS: 1.587 Clock RMS: 1.400

Single Differenced PR / No TWTT, Distance = 100 km
Combined Pos RMS x=2.484 y=1.008 z=0.809
Combined 3-D Pos RMS: 1.617 Clock RMS: 1.432

Single Differenced PR / No TWTT, Distance = 500 km
Combined Pos RMS x=2.535 y=1.063 z=0.819
Combined 3-D Pos RMS: 1.656 Clock RMS: 1.528

Single Differenced PR / No TWTT, Distance = 1,000 km
Combined Pos RMS x=2.908 y=1.152 z=0.878
Combined 3-D Pos RMS: 1.875 Clock RMS: 1.817

Single Differenced PR / No TWTT, Distance = 1,500 km
Combined Pos RMS x=3.568 y=1.447 z=1.215
Combined 3-D Pos RMS: 2.331 Clock RMS: 2.434

Single Differenced PR / TWTT A, Distance = 1 km
Combined Pos RMS x=1.969 y=1.005 z=0.804
Combined 3-D Pos RMS: 1.358 Clock RMS: 1.096

Single Differenced PR / TWTT A, Distance = 100 km
Combined Pos RMS x=2.020 y=0.992 z=0.795
Combined 3-D Pos RMS: 1.378 Clock RMS: 1.143

Single Differenced PR / TWTT A, Distance = 500 km
Combined Pos RMS x=2.012 y=1.024 z=0.803
Combined 3-D Pos RMS: 1.383 Clock RMS: 1.165

Single Differenced PR / TWTT A, Distance = 1,000 km
Combined Pos RMS x=2.061 y=1.099 z=0.831
Combined 3-D Pos RMS: 1.431 Clock RMS: 1.208

Single Differenced PR / TWTT A, Distance = 1,500 km
Combined Pos RMS x=2.248 y=1.137 z=0.905
Combined 3-D Pos RMS: 1.546 Clock RMS: 1.345

Single Differenced PR / TWTT B, Distance = 1 km
Combined Pos RMS x=0.793 y=0.975 z=0.787
Combined 3-D Pos RMS: 0.856 Clock RMS: 0.250

Single Differenced PR / TWTT B, Distance = 100 km
Combined Pos RMS x=0.739 y=0.956 z=0.782
Combined 3-D Pos RMS: 0.831 Clock RMS: 0.256

Single Differenced PR / TWTT B, Distance = 500 km
Combined Pos RMS x=0.778 y=0.975 z=0.788
Combined 3-D Pos RMS: 0.852 Clock RMS: 0.256

Single Differenced PR / TWTT B, Distance = 1,000 km
Combined Pos RMS x=0.775 y=1.056 z=0.810
Combined 3-D Pos RMS: 0.889 Clock RMS: 0.265

Single Differenced PR / TWTT B, Distance = 1,500 km
Combined Pos RMS x=0.832 y=1.075 z=0.854
Combined 3-D Pos RMS: 0.927 Clock RMS: 0.267

Single Differenced PR / TWTT C, Distance = 1 km
Combined Pos RMS x=0.708 y=0.971 z=0.785
Combined 3-D Pos RMS: 0.829 Clock RMS: 0.030

Single Differenced PR / TWTT C, Distance = 100 km
Combined Pos RMS x=0.670 y=0.952 z=0.781
Combined 3-D Pos RMS: 0.809 Clock RMS: 0.031

Single Differenced PR / TWTT C, Distance = 500 km
Combined Pos RMS x=0.699 y=0.966 z=0.788
Combined 3-D Pos RMS: 0.825 Clock RMS: 0.031

Single Differenced PR / TWTT C, Distance = 1,000 km
Combined Pos RMS x=0.697 y=1.045 z=0.808
Combined 3-D Pos RMS: 0.862 Clock RMS: 0.031

Single Differenced PR / TWTT C, Distance = 1,500 km
Combined Pos RMS x=0.757 y=1.068 z=0.849
Combined 3-D Pos RMS: 0.901 Clock RMS: 0.030

Single Differenced PR / TWTT D, Distance = 1 km
Combined Pos RMS x=0.705 y=0.971 z=0.786
Combined 3-D Pos RMS: 0.828 Clock RMS: 0.003

Single Differenced PR / TWTT D, Distance = 100 km
Combined Pos RMS x=0.670 y=0.952 z=0.781
Combined 3-D Pos RMS: 0.809 Clock RMS: 0.003

Single Differenced PR / TWTT D, Distance = 500 km
Combined Pos RMS x=0.697 y=0.965 z=0.788
Combined 3-D Pos RMS: 0.824 Clock RMS: 0.003

Single Differenced PR / TWTT D, Distance = 1,000 km
Combined Pos RMS x=0.696 y=1.045 z=0.808
Combined 3-D Pos RMS: 0.862 Clock RMS: 0.003

Single Differenced PR / TWTT D, Distance = 1,500 km
Combined Pos RMS x=0.755 y=1.068 z=0.849
Combined 3-D Pos RMS: 0.900 Clock RMS: 0.003

Single Differenced PR / TWTT A / No Ranging, Distance = 1 km
Combined Pos RMS x=2.085 y=1.008 z=0.805
Combined 3-D Pos RMS: 1.415 Clock RMS: 1.158

Single Differenced PR / TWTT A / No Ranging, Distance = 100 km
Combined Pos RMS x=2.141 y=0.995 z=0.797
Combined 3-D Pos RMS: 1.439 Clock RMS: 1.206

Single Differenced PR / TWTT A / No Ranging, Distance = 500 km
Combined Pos RMS x=2.208 y=1.035 z=0.807
Combined 3-D Pos RMS: 1.483 Clock RMS: 1.273

Single Differenced PR / TWTT A / No Ranging, Distance = 1,000 km
Combined Pos RMS x=2.270 y=1.112 z=0.838
Combined 3-D Pos RMS: 1.538 Clock RMS: 1.335

Single Differenced PR / TWTT A / No Ranging, Distance = 1,500 km
Combined Pos RMS x=2.515 y=1.152 z=0.921
Combined 3-D Pos RMS: 1.683 Clock RMS: 1.516

Single Differenced PR / TWTT B / No Ranging, Distance = 1 km
Combined Pos RMS x=1.025 y=0.977 z=0.787
Combined 3-D Pos RMS: 0.935 Clock RMS: 0.290

Single Differenced PR / TWTT B / No Ranging, Distance = 100 km
Combined Pos RMS x=0.988 y=0.957 z=0.783
Combined 3-D Pos RMS: 0.914 Clock RMS: 0.298

Single Differenced PR / TWTT B / No Ranging, Distance = 500 km
Combined Pos RMS x=1.028 y=0.981 z=0.790
Combined 3-D Pos RMS: 0.939 Clock RMS: 0.298

Single Differenced PR / TWTT B / No Ranging, Distance = 1,000 km
Combined Pos RMS x=1.011 y=1.063 z=0.812
Combined 3-D Pos RMS: 0.968 Clock RMS: 0.299

Single Differenced PR / TWTT B / No Ranging, Distance = 1,500 km
Combined Pos RMS x=1.059 y=1.088 z=0.859
Combined 3-D Pos RMS: 1.007 Clock RMS: 0.298

Single Differenced PR / TWTT C / No Ranging, Distance = 1 km
Combined Pos RMS x=0.898 y=0.975 z=0.787
Combined 3-D Pos RMS: 0.890 Clock RMS: 0.030

Single Differenced PR / TWTT C / No Ranging, Distance = 100 km
Combined Pos RMS x=0.868 y=0.956 z=0.783
Combined 3-D Pos RMS: 0.872 Clock RMS: 0.031

Single Differenced PR / TWTT C / No Ranging, Distance = 500 km
Combined Pos RMS x=0.896 y=0.977 z=0.790
Combined 3-D Pos RMS: 0.891 Clock RMS: 0.031

Single Differenced PR / TWTT C / No Ranging, Distance = 1,000 km
Combined Pos RMS x=0.897 y=1.058 z=0.809
Combined 3-D Pos RMS: 0.927 Clock RMS: 0.031

Single Differenced PR / TWTT C / No Ranging, Distance = 1,500 km
Combined Pos RMS x=0.940 y=1.086 z=0.856
Combined 3-D Pos RMS: 0.966 Clock RMS: 0.030

Single Differenced PR / TWTT D / No Ranging, Distance = 1 km
Combined Pos RMS x=0.895 y=0.975 z=0.787
Combined 3-D Pos RMS: 0.889 Clock RMS: 0.003

Single Differenced PR / TWTT D / No Ranging, Distance = 100 km
Combined Pos RMS x=0.867 y=0.956 z=0.783
Combined 3-D Pos RMS: 0.872 Clock RMS: 0.003

Single Differenced PR / TWTT D / No Ranging, Distance = 500 km
Combined Pos RMS x=0.893 y=0.977 z=0.790
Combined 3-D Pos RMS: 0.890 Clock RMS: 0.003

Single Differenced PR / TWTT D / No Ranging, Distance = 1,000 km
Combined Pos RMS x=0.896 y=1.058 z=0.808
Combined 3-D Pos RMS: 0.927 Clock RMS: 0.003

Single Differenced PR / TWTT D / No Ranging, Distance = 1,500 km
Combined Pos RMS x=0.938 y=1.086 z=0.856
Combined 3-D Pos RMS: 0.965 Clock RMS: 0.003

Trade Study 4 – Vary the Location of the TWTT Satellite

Single Differenced PR / No TWTT, TWTT Satellite Location 1
Combined Pos RMS x=2.417 y=1.022 z=0.820
Combined 3-D Pos RMS: 1.587 Clock RMS: 1.400

Single Differenced PR / No TWTT, TWTT Satellite Location 2
Combined Pos RMS x=2.417 y=1.022 z=0.820
Combined 3-D Pos RMS: 1.587 Clock RMS: 1.400

Single Differenced PR / No TWTT, TWTT Satellite Location 3
Combined Pos RMS x=2.417 y=1.022 z=0.820
Combined 3-D Pos RMS: 1.587 Clock RMS: 1.400

Single Differenced PR / No TWTT, TWTT Satellite Location 4
Combined Pos RMS x=2.417 y=1.022 z=0.820
Combined 3-D Pos RMS: 1.587 Clock RMS: 1.400

Single Differenced PR / No TWTT, TWTT Satellite Location 5
Combined Pos RMS x=2.417 y=1.022 z=0.820
Combined 3-D Pos RMS: 1.587 Clock RMS: 1.400

Single Differenced PR / TWTT A, TWTT Satellite Location 1
Combined Pos RMS x=1.969 y=1.005 z=0.804
Combined 3-D Pos RMS: 1.358 Clock RMS: 1.096

Single Differenced PR / TWTT A, TWTT Satellite Location 2
Combined Pos RMS x=1.977 y=1.005 z=0.804
Combined 3-D Pos RMS: 1.362 Clock RMS: 1.100

Single Differenced PR / TWTT A, TWTT Satellite Location 3
Combined Pos RMS x=2.001 y=1.004 z=0.804
Combined 3-D Pos RMS: 1.373 Clock RMS: 1.112

Single Differenced PR / TWTT A, TWTT Satellite Location 4
Combined Pos RMS x=2.034 y=1.003 z=0.804
Combined 3-D Pos RMS: 1.389 Clock RMS: 1.129

Single Differenced PR / TWTT A, TWTT Satellite Location 5
Combined Pos RMS x=2.064 y=1.001 z=0.805
Combined 3-D Pos RMS: 1.403 Clock RMS: 1.145

Single Differenced PR / TWTT B, TWTT Satellite Location 1
Combined Pos RMS x=0.793 y=0.975 z=0.787
Combined 3-D Pos RMS: 0.856 Clock RMS: 0.250

Single Differenced PR / TWTT B, TWTT Satellite Location 2
Combined Pos RMS x=0.810 y=0.962 z=0.787
Combined 3-D Pos RMS: 0.857 Clock RMS: 0.253

Single Differenced PR / TWTT B, TWTT Satellite Location 3
Combined Pos RMS x=0.859 y=0.930 z=0.787
Combined 3-D Pos RMS: 0.860 Clock RMS: 0.261

Single Differenced PR / TWTT B, TWTT Satellite Location 4
Combined Pos RMS x=0.923 y=0.884 z=0.786
Combined 3-D Pos RMS: 0.866 Clock RMS: 0.272

Single Differenced PR / TWTT B, TWTT Satellite Location 5
Combined Pos RMS x=0.983 y=0.839 z=0.785
Combined 3-D Pos RMS: 0.873 Clock RMS: 0.282

Single Differenced PR / TWTT C, TWTT Satellite Location 1
Combined Pos RMS x=0.708 y=0.971 z=0.785
Combined 3-D Pos RMS: 0.829 Clock RMS: 0.030

Single Differenced PR / TWTT C, TWTT Satellite Location 2
Combined Pos RMS x=0.729 y=0.949 z=0.785
Combined 3-D Pos RMS: 0.826 Clock RMS: 0.030

Single Differenced PR / TWTT C, TWTT Satellite Location 3
Combined Pos RMS x=0.778 y=0.900 z=0.785
Combined 3-D Pos RMS: 0.823 Clock RMS: 0.030

Single Differenced PR / TWTT C, TWTT Satellite Location 4
Combined Pos RMS x=0.831 y=0.844 z=0.784
Combined 3-D Pos RMS: 0.820 Clock RMS: 0.030

Single Differenced PR / TWTT C, TWTT Satellite Location 5
Combined Pos RMS x=0.871 y=0.798 z=0.784
Combined 3-D Pos RMS: 0.819 Clock RMS: 0.030

Single Differenced PR / TWTT D, TWTT Satellite Location 1
Combined Pos RMS x=0.705 y=0.971 z=0.786
Combined 3-D Pos RMS: 0.828 Clock RMS: 0.003

Single Differenced PR / TWTT D, TWTT Satellite Location 2
Combined Pos RMS x=0.727 y=0.948 z=0.785
Combined 3-D Pos RMS: 0.825 Clock RMS: 0.003

Single Differenced PR / TWTT D, TWTT Satellite Location 3
Combined Pos RMS x=0.776 y=0.900 z=0.785
Combined 3-D Pos RMS: 0.822 Clock RMS: 0.003

Single Differenced PR / TWTT D, TWTT Satellite Location 4
Combined Pos RMS x=0.829 y=0.844 z=0.784
Combined 3-D Pos RMS: 0.819 Clock RMS: 0.003

Single Differenced PR / TWTT D, TWTT Satellite Location 5
Combined Pos RMS x=0.869 y=0.798 z=0.784
Combined 3-D Pos RMS: 0.818 Clock RMS: 0.003

Single Differenced PR / TWTT A / No Ranging, TWTT Satellite Location 1
Combined Pos RMS x=2.085 y=1.008 z=0.805
Combined 3-D Pos RMS: 1.415 Clock RMS: 1.158

Single Differenced PR / TWTT A / No Ranging, TWTT Satellite Location 2
Combined Pos RMS x=2.085 y=1.008 z=0.805
Combined 3-D Pos RMS: 1.415 Clock RMS: 1.158

Single Differenced PR / TWTT A / No Ranging, TWTT Satellite Location 3
Combined Pos RMS x=2.085 y=1.008 z=0.805
Combined 3-D Pos RMS: 1.415 Clock RMS: 1.158

Single Differenced PR / TWTT A / No Ranging, TWTT Satellite Location 4
Combined Pos RMS x=2.085 y=1.008 z=0.805
Combined 3-D Pos RMS: 1.415 Clock RMS: 1.158

Single Differenced PR / TWTT A / No Ranging, TWTT Satellite Location 5
Combined Pos RMS x=2.085 y=1.008 z=0.805
Combined 3-D Pos RMS: 1.415 Clock RMS: 1.158

Single Differenced PR / TWTT B / No Ranging, TWTT Satellite Location 1
Combined Pos RMS x=1.025 y=0.977 z=0.787
Combined 3-D Pos RMS: 0.935 Clock RMS: 0.290

Single Differenced PR / TWTT B / No Ranging, TWTT Satellite Location 2
Combined Pos RMS x=1.025 y=0.977 z=0.787
Combined 3-D Pos RMS: 0.935 Clock RMS: 0.290

Single Differenced PR / TWTT B / No Ranging, TWTT Satellite Location 3
Combined Pos RMS x=1.025 y=0.977 z=0.787
Combined 3-D Pos RMS: 0.935 Clock RMS: 0.290

Single Differenced PR / TWTT B / No Ranging, TWTT Satellite Location 4
Combined Pos RMS x=1.025 y=0.977 z=0.787
Combined 3-D Pos RMS: 0.935 Clock RMS: 0.290

Single Differenced PR / TWTT B / No Ranging, TWTT Satellite Location 5
Combined Pos RMS x=1.025 y=0.977 z=0.787
Combined 3-D Pos RMS: 0.935 Clock RMS: 0.290

Single Differenced PR / TWTT C / No Ranging, TWTT Satellite Location 1
Combined Pos RMS x=0.898 y=0.975 z=0.787
Combined 3-D Pos RMS: 0.890 Clock RMS: 0.030

Single Differenced PR / TWTT C / No Ranging, TWTT Satellite Location 2
Combined Pos RMS x=0.898 y=0.975 z=0.787
Combined 3-D Pos RMS: 0.890 Clock RMS: 0.030

Single Differenced PR / TWTT C / No Ranging, TWTT Satellite Location 3
Combined Pos RMS x=0.898 y=0.975 z=0.787
Combined 3-D Pos RMS: 0.890 Clock RMS: 0.030

Single Differenced PR / TWTT C / No Ranging, TWTT Satellite Location 4
Combined Pos RMS x=0.898 y=0.975 z=0.787
Combined 3-D Pos RMS: 0.890 Clock RMS: 0.030

Single Differenced PR / TWTT C / No Ranging, TWTT Satellite Location 5
Combined Pos RMS x=0.898 y=0.975 z=0.787
Combined 3-D Pos RMS: 0.890 Clock RMS: 0.030

Single Differenced PR / TWTT D / No Ranging, TWTT Satellite Location 1
Combined Pos RMS x=0.895 y=0.975 z=0.787
Combined 3-D Pos RMS: 0.889 Clock RMS: 0.003

Single Differenced PR / TWTT D / No Ranging, TWTT Satellite Location 2
Combined Pos RMS x=0.895 y=0.975 z=0.787
Combined 3-D Pos RMS: 0.889 Clock RMS: 0.003

Single Differenced PR / TWTT D / No Ranging, TWTT Satellite Location 3
Combined Pos RMS x=0.895 y=0.975 z=0.787
Combined 3-D Pos RMS: 0.889 Clock RMS: 0.003

Single Differenced PR / TWTT D / No Ranging, TWTT Satellite Location 4
Combined Pos RMS x=0.895 y=0.975 z=0.787
Combined 3-D Pos RMS: 0.889 Clock RMS: 0.003

Single Differenced PR / TWTT D / No Ranging, TWTT Satellite Location 5
Combined Pos RMS x=0.895 y=0.975 z=0.787
Combined 3-D Pos RMS: 0.889 Clock RMS: 0.003

Trade Study 5 – Vary the Satellite Elevation Cutoff

Single Differenced PR / No TWTT, SV Cutoff Elevation = 1 degree
Combined Pos RMS x=1.866 y=0.839 z=0.766
Combined 3-D Pos RMS: 1.261 Clock RMS: 0.999

Single Differenced PR / No TWTT, SV Cutoff Elevation = 5 degrees
Combined Pos RMS x=2.126 y=0.895 z=0.763
Combined 3-D Pos RMS: 1.403 Clock RMS: 1.194

Single Differenced PR / No TWTT, SV Cutoff Elevation = 10 degrees
Combined Pos RMS x=2.417 y=1.022 z=0.820
Combined 3-D Pos RMS: 1.587 Clock RMS: 1.400

Single Differenced PR / No TWTT, SV Cutoff Elevation = 15 degrees
Combined Pos RMS x=3.052 y=1.222 z=0.928
Combined 3-D Pos RMS: 1.972 Clock RMS: 1.922

Single Differenced PR / No TWTT, SV Cutoff Elevation = 20 degrees
Combined Pos RMS x=6.317 y=3.090 z=1.610
Combined 3-D Pos RMS: 4.165 Clock RMS: 4.812

Single Differenced PR / TWTT A, SV Cutoff Elevation = 1 degree
Combined Pos RMS x=1.668 y=0.824 z=0.759
Combined 3-D Pos RMS: 1.160 Clock RMS: 0.875

Single Differenced PR / TWTT A, SV Cutoff Elevation = 5 degrees
Combined Pos RMS x=1.820 y=0.885 z=0.761
Combined 3-D Pos RMS: 1.248 Clock RMS: 1.003

Single Differenced PR / TWTT A, SV Cutoff Elevation = 10 degrees
Combined Pos RMS x=1.969 y=1.005 z=0.804
Combined 3-D Pos RMS: 1.358 Clock RMS: 1.096

Single Differenced PR / TWTT A, SV Cutoff Elevation = 15 degrees
Combined Pos RMS x=2.206 y=1.181 z=0.879
Combined 3-D Pos RMS: 1.531 Clock RMS: 1.330

Single Differenced PR / TWTT A, SV Cutoff Elevation = 20 degrees
Combined Pos RMS x=2.315 y=1.472 z=0.991
Combined 3-D Pos RMS: 1.684 Clock RMS: 1.497

Single Differenced PR / TWTT B, SV Cutoff Elevation = 1 degree
Combined Pos RMS x=0.769 y=0.800 z=0.743
Combined 3-D Pos RMS: 0.771 Clock RMS: 0.244

Single Differenced PR / TWTT B, SV Cutoff Elevation = 5 degrees
Combined Pos RMS x=0.750 y=0.849 z=0.753
Combined 3-D Pos RMS: 0.785 Clock RMS: 0.249

Single Differenced PR / TWTT B, SV Cutoff Elevation = 10 degrees
Combined Pos RMS x=0.793 y=0.975 z=0.787
Combined 3-D Pos RMS: 0.856 Clock RMS: 0.250

Single Differenced PR / TWTT B, SV Cutoff Elevation = 15 degrees
Combined Pos RMS x=0.758 y=1.151 z=0.847
Combined 3-D Pos RMS: 0.934 Clock RMS: 0.260

Single Differenced PR / TWTT B, SV Cutoff Elevation = 20 degrees
Combined Pos RMS x=0.806 y=1.385 z=0.945
Combined 3-D Pos RMS: 1.074 Clock RMS: 0.257

Single Differenced PR / TWTT C, SV Cutoff Elevation = 1 degree
Combined Pos RMS x=0.692 y=0.796 z=0.741
Combined 3-D Pos RMS: 0.744 Clock RMS: 0.030

Single Differenced PR / TWTT C, SV Cutoff Elevation = 5 degrees
Combined Pos RMS x=0.678 y=0.843 z=0.752
Combined 3-D Pos RMS: 0.760 Clock RMS: 0.030

Single Differenced PR / TWTT C, SV Cutoff Elevation = 10 degrees
Combined Pos RMS x=0.708 y=0.971 z=0.785
Combined 3-D Pos RMS: 0.829 Clock RMS: 0.030

Single Differenced PR / TWTT C, SV Cutoff Elevation = 15 degrees
Combined Pos RMS x=0.685 y=1.146 z=0.844
Combined 3-D Pos RMS: 0.912 Clock RMS: 0.030

Single Differenced PR / TWTT C, SV Cutoff Elevation = 20 degrees
Combined Pos RMS x=0.746 y=1.375 z=0.941
Combined 3-D Pos RMS: 1.054 Clock RMS: 0.029

Single Differenced PR / TWTT D, SV Cutoff Elevation = 1 degree
Combined Pos RMS x=0.691 y=0.796 z=0.741
Combined 3-D Pos RMS: 0.744 Clock RMS: 0.003

Single Differenced PR / TWTT D, SV Cutoff Elevation = 5 degrees
Combined Pos RMS x=0.677 y=0.843 z=0.752
Combined 3-D Pos RMS: 0.760 Clock RMS: 0.003

Single Differenced PR / TWTT D, SV Cutoff Elevation = 10 degrees
Combined Pos RMS x=0.705 y=0.971 z=0.786
Combined 3-D Pos RMS: 0.828 Clock RMS: 0.003

Single Differenced PR / TWTT D, SV Cutoff Elevation = 15 degrees
Combined Pos RMS x=0.684 y=1.146 z=0.844
Combined 3-D Pos RMS: 0.912 Clock RMS: 0.003

Single Differenced PR / TWTT D, SV Cutoff Elevation = 20 degrees
Combined Pos RMS x=0.746 y=1.375 z=0.941
Combined 3-D Pos RMS: 1.054 Clock RMS: 0.003

Single Differenced PR / TWTT A / No Ranging, SV Cutoff Elevation = 1 degree
Combined Pos RMS x=1.735 y=0.826 z=0.760
Combined 3-D Pos RMS: 1.193 Clock RMS: 0.900

Single Differenced PR / TWTT A / No Ranging, SV Cutoff Elevation = 5 degrees
Combined Pos RMS x=1.900 y=0.888 z=0.763
Combined 3-D Pos RMS: 1.289 Clock RMS: 1.041

Single Differenced PR / TWTT A / No Ranging, SV Cutoff Elevation = 10 degrees
Combined Pos RMS x=2.085 y=1.008 z=0.805
Combined 3-D Pos RMS: 1.415 Clock RMS: 1.158

Single Differenced PR / TWTT A / No Ranging, SV Cutoff Elevation = 15 degrees
Combined Pos RMS x=2.422 y=1.187 z=0.892
Combined 3-D Pos RMS: 1.640 Clock RMS: 1.461

Single Differenced PR / TWTT A / No Ranging, SV Cutoff Elevation = 20 degrees
Combined Pos RMS x=2.684 y=1.490 z=1.014
Combined 3-D Pos RMS: 1.867 Clock RMS: 1.736

Single Differenced PR / TWTT B / No Ranging, SV Cutoff Elevation = 1 degree
Combined Pos RMS x=1.000 y=0.802 z=0.744
Combined 3-D Pos RMS: 0.856 Clock RMS: 0.274

Single Differenced PR / TWTT B / No Ranging, SV Cutoff Elevation = 5 degrees
Combined Pos RMS x=0.978 y=0.851 z=0.754
Combined 3-D Pos RMS: 0.866 Clock RMS: 0.282

Single Differenced PR / TWTT B / No Ranging, SV Cutoff Elevation = 10 degrees
Combined Pos RMS x=1.025 y=0.977 z=0.787
Combined 3-D Pos RMS: 0.935 Clock RMS: 0.290

Single Differenced PR / TWTT B / No Ranging, SV Cutoff Elevation = 15 degrees
Combined Pos RMS x=1.018 y=1.159 z=0.849
Combined 3-D Pos RMS: 1.016 Clock RMS: 0.296

Single Differenced PR / TWTT B / No Ranging, SV Cutoff Elevation = 20 degrees
Combined Pos RMS x=1.045 y=1.394 z=0.946
Combined 3-D Pos RMS: 1.145 Clock RMS: 0.285

Single Differenced PR / TWTT C / No Ranging, SV Cutoff Elevation = 1 degree
Combined Pos RMS x=0.890 y=0.801 z=0.742
Combined 3-D Pos RMS: 0.813 Clock RMS: 0.030

Single Differenced PR / TWTT C / No Ranging, SV Cutoff Elevation = 5 degrees
Combined Pos RMS x=0.870 y=0.847 z=0.752
Combined 3-D Pos RMS: 0.825 Clock RMS: 0.030

Single Differenced PR / TWTT C / No Ranging, SV Cutoff Elevation = 10 degrees
Combined Pos RMS x=0.898 y=0.975 z=0.787
Combined 3-D Pos RMS: 0.890 Clock RMS: 0.030

Single Differenced PR / TWTT C / No Ranging, SV Cutoff Elevation = 15 degrees
Combined Pos RMS x=0.906 y=1.160 z=0.847
Combined 3-D Pos RMS: 0.980 Clock RMS: 0.030

Single Differenced PR / TWTT C / No Ranging, SV Cutoff Elevation = 20 degrees
Combined Pos RMS x=0.965 y=1.392 z=0.944
Combined 3-D Pos RMS: 1.120 Clock RMS: 0.029

Single Differenced PR / TWTT D / No Ranging, SV Cutoff Elevation = 1 degree
Combined Pos RMS x=0.888 y=0.801 z=0.742
Combined 3-D Pos RMS: 0.813 Clock RMS: 0.003

Single Differenced PR / TWTT D / No Ranging, SV Cutoff Elevation = 5 degrees
Combined Pos RMS x=0.870 y=0.847 z=0.752
Combined 3-D Pos RMS: 0.825 Clock RMS: 0.003

Single Differenced PR / TWTT D / No Ranging, SV Cutoff Elevation = 10 degrees
Combined Pos RMS x=0.895 y=0.975 z=0.787
Combined 3-D Pos RMS: 0.889 Clock RMS: 0.003

Single Differenced PR / TWTT D / No Ranging, SV Cutoff Elevation = 15 degrees
Combined Pos RMS x=0.905 y=1.160 z=0.846
Combined 3-D Pos RMS: 0.980 Clock RMS: 0.003

Single Differenced PR / TWTT D / No Ranging, SV Cutoff Elevation = 20 degrees
Combined Pos RMS x=0.964 y=1.392 z=0.944
Combined 3-D Pos RMS: 1.120 Clock RMS: 0.003

Bibliography

[1] Steele, J., Markowitz, W., and Lidback A., "Telstar Time Synchronization," IEEE Trans. on Instrumentation and Measurement, Vol. IM-13, No. 4, December 1964.

[2] Markowitz W., Lidback A., Uyeda H., and Muramatsu L., "Clock Synchronization via Relay II Satellite," IEEE Trans. on Instrumentation and Measurement, Vol. IM-15, No. 4, December 1966.

[3] Celano, Beckman, Warriner, Francis, Gifford, and Howe, "Dynamic Two-Way Time Transfer to Moving Platforms," 2003 IEEE International Frequency Control Symposium, September 2003.

[4] Jespersen, J., Kamas, G., Gatterer, L., and Macdoran, P., "Satellite VHF transponder Time Synchronization," Proc. IEEE, Vol. 56, No. 7, July 1968.

[5] Mazur, W.E. Jr., "Dual Transponder Time Synchronization at C-Band Using ATS-3," Proc. IEEE, Vol. 60, No. 5, May 1972.

[6] Ramasastry, J., Rosenbaum, B., Michelini, R., and Kuegler, G., "Clock Synchronization Experiments Performed via the ATS-1 and ATS-3 satellites," IEEE Trans. on Instrumentation and Measurement, Vol. IM-22, No. 1, March 1973.

[7] Chi, A.R., and Byron, E., "Two-Way Time Transfer Experiment Using a Synchronous Satellite," Proceedings of the Seventh Annual Precise Time and Time Interval Planning Meeting, Washington D.C., December 1975.

[8] Saburi, Y., Yamamoto, M., and Harada, K., "High Precision Time Comparisons via Satellite and Observed Discrepancy of Synchronization," IEEE Trans. on Instrumentation and Measurement, Vol. IM-25, No. 4, December 1976.

[9] Hanson, D.W., "Fundamentals of Two-Way Time Transfers by Satellite," 43rd Annual Symposium on Frequency Control, 1989.

[10] Murray, Pritt, Blocker, Leavitt, Hooten, andGoring, "Time Transfer by Defense Communications Satellite," Proc. of 25th Annual Frequency Control Symposium, Atlantic City, NJ, April 1971.

[11] Kelso, "GPS Yuma Almanac," celestrak.com/GPS, August 2004.

[12] Brown, K., "The Theory of the GPS Composite Clock," Proc. of the ION GPS-91, September 2001.

[13] Woodfork, D., "The Use of X-Ray Pulsars for Aiding GPS Satellite Orbit Determination," Masters Thesis, AFIT, 2005.

[14] Brown, R. and Hwang, P., "Introduction to Random Signals and Applied Kalman Filtering," John Wiley and Sons Inc., New York, 1983.

[15] Brown, K., "Characterizations of OCS Kalman Filter Errors," Proc. of the ION GPS-91, September 1991.

[16] Hutsell, S., "Fine Tuning GPS Clock Estimation in the MCS," 26th Annual Precise Time and Time Interval (PTTI) Applications and Planning Meeting, December 1994.

[17] Costain, Daams, Boulanger, Hanson, and Klepczynski, "Two-Way Time Transfer Between NRC/USNO via the Hermes (CTS) Satellite," Proc. of the 10th Annual Precise Time and Time Interval Applications and Planning Meeting, Washington D.C., November 1978.

[18] Brunet, M., "Synchronization of Atomic Clocks Through the Symphonie Satellite," Radio Science, Vol. 14, No. 4, July – August 1979.

[19] Costain, Boulanger, Daams, Hanson, Beehler, Clements, Davis, Klepczynski, Veenstra, Kaiser, Guinot, Parcelier, Freon, and Brunet, "Two-way Time Transfer via Geostationary Satellites NCR/NBS, NRC/USNO and NBS/USNO via Hermes and NRC/LPTF (France) via Symphonie," Proc. of the 11th Annual Precise Time and Time Interval Applications and Planning Meeting, Washington D.C., November 1979.

[20] Mathur, B.S., Banerjee, P., Sood, P.C., Saxena, M. Kumar, N., and Suri, A. K., "Precise Time and Frequency Inter-comparison Between NPL, India and PTB, Federal Republic of Germany via satellite Symphonie-1," Proc. of the12th Annual Precise Time and Time Interval Applications and Planning Meeting, Washington D.C., December 1980, or Journal of IETE, Vol. 27, No. 10 October 1981.

[21] Veenstra, Kaiser, Costain, Klepczynski, and Allan, "Frequency and Time Coordination via Satellite," Comsat Technical Review, Vol. 11, No. 2, Fall 1981.

[22] Detoma, E. and Leschiutta, S., "Two-Way Sequential Time Synchronization: Preliminary Results from the SIRIO-1 Experiment," Proc. of the 12th Annual Precise Time and Time Interval Applications and Planning Meeting, Washington D.C., December 1980.

[23] Wiesel, W. E., "Modern Orbit Determination," Beavercreek, OH, Aphelion Press, 2003.

[24] Vallado, D. A., "The Fundamentals of Astrodynamics and Applications," New York, The McGraw-Hill Companies, Inc., 1997.

[25] National Research Council, "The Global Positioning System, a Shared National Asset, Recommendations for Technical Improvements and Enhancements," Technical Report, National Academy Press, Washington D.C. 1995.

[26] Lombardi, Nelson, Novick, and Zhang, "Time and Frequency Measurements Using the Global Positioning System," Cal Lab, the International Journal of Metrology, July-September 2001.

[27] Time and Frequency Division of the National Institute of Standards and Technology, "Time and Frequency Transfer Using the Phase of the GPS Carrier," tf.nist.gov/timefreq/time/carrierphase.htm.

[28] Misra, Pratap and Per Enge, "Global Positioning System; Signals, Measurements, and Performance," Lincoln, Massachusetts, Ganga-Jamuna Press, 2001.

[29] Halsell, C. A., "Orbit Determination of the Global Positioning Satellite System Using Inter-Satellite Range Measurements," Masters Thesis, University of Texas at Austin, December 1984.

[30] Sobel, D., "Longitude: The True Story of a Lone Genius Who Solved the Greatest Scientific Problem of His Time," Walker Publishing Company, 1995.

[31] Logsdon, T., "The Navstar Global Positioning System," Van Nostrand Reinhold, New York, New York, 1992.

[32] Northern Lights Software Associates, www.nlsa.com.

[33] ARINC Research Corporation, "ICD-200C: Navstar GPS Space Segment / Navigation User Interfaces," Technical Report, United States Air Force, 1993.

[34] Parkinson, B.W. and Spilker, J.J., "Global Positioning System: Theory and Applications, Volume 1," American Institute of Aeronautics and Astronautics, Inc., Washington D.C., 1996.

[35] Arsenault, T. "Navstar GPS Constellation Status," Department of Geodesy and Geomatics Engineering, University of New Bruswick, gge.unb.ca/homepage.php3, Aug 2004.

[36] Crossbow Technology Inc., www.xbow.com/Support/Support_ pdf_files/NAV420AppNote.pdf, January 2006.

[37] Raquet, J., "EENG533: Navigation Using GPS," AFIT, Spring 2005.

[38] Trimble Corporate, www.trimble.com/gps/how2.html, 2006.

[39] Ashby, N., "Relativity in the Global Positioning System," www.livingreviews.org/lrr-2003-1, Max-Planck-Gesellschaft, 2003.

[40] Ashby, N., "Relativity in the Global Positioning System," Living Reviews in Relativity, Vol. 6, Max Planck Institute for Gravitational Physics, Germany, January 2003.

[41] Raquet, J., "EENG633: Advanced GPS Theory and Applications," AFIT, Summer 2005.

[42] Raquet, J. and Warren, D., "Broadcast vs. Precise Ephemerides: A Historical Perspective," GPS Solutions, 2003.

[43] Beckman, Celano, Warriner, Francis, Gifford, and Howe, "Two-Way Time Transfer to Airborne Platforms Using Commercial Satellite Modems," Timing Solutions Corporation.

[44] OnStar by GM, www.onstar.com, 2006.

[45] Cloud Cap Technologies, www.cloudcaptech.com/whatsnew.htm, 2006.

[46] Goodman, S., Precision Agriculture, www.ghcc.msfc.nasa.gov/precisionag, NASA, October 1999.

Vita

Lieutenant Kendra Cook graduated with honors from Boston University with a B.S. in Aerospace Engineering and a minor in French Studies in May 2004. She commissioned through Air Force ROTC Detachment 355 and was assigned to the Air Force Institute of Technology where she is obtaining a M.S. degree in Astronautical Engineering. Upon graduation she will be assigned to the National Air and Space Intelligence Center (NASIC) at Wright-Patterson AFB, OH while finishing the requirements for a M.S. in Computer Engineering.

REPORT DOCUMENTATION PAGE

Form Approved
OMB No. 074-0188

1. REPORT DATE *(DD-MM-YYYY)*	2. REPORT TYPE	3. DATES COVERED *(From – To)*
23-03-2006	Master's Thesis	March 2005 – March 2006

4. TITLE AND SUBTITLE

CHARACTERIZING THE IMPACT OF PRECISION TIME AND RANGE MEASUREMENTS FROM TWO-WAY TIME TRANSFER SYSTEMS ON NETWORK DIFFERENTIAL GPS POSITION SOLUTIONS

5a. CONTRACT NUMBER

5b. GRANT NUMBER

5c. PROGRAM ELEMENT NUMBER

6. AUTHOR(S)

Cook, Kendra L. B., 2D LT, USAF

5d. PROJECT NUMBER

5e. TASK NUMBER

5f. WORK UNIT NUMBER

7. PERFORMING ORGANIZATION NAMES(S) AND ADDRESS(S)

Air Force Institute of Technology
Graduate School of Engineering and Management (AFIT/EN)
2950 Hobson Way, Building 640
WPAFB OH 45433-8865

8. PERFORMING ORGANIZATION REPORT NUMBER

AFIT/GA/ENG/06-02

9. SPONSORING/MONITORING AGENCY NAME(S) AND ADDRESS(ES)

N/A

10. SPONSOR/MONITOR'S ACRONYM(S)

11. SPONSOR/MONITOR'S REPORT NUMBER(S)

12. DISTRIBUTION/AVAILABILITY STATEMENT

APPROVED FOR PUBLIC RELEASE; DISTRIBUTION UNLIMITED.

13. SUPPLEMENTARY NOTES

14. ABSTRACT

Many GPS applications require precise relative positioning of a network of vehicles (such as aircraft, tanks, troops, etc). Although GPS has become commonplace in today's society, there are still limitations affecting the system. Recent advances in dynamic Two-Way Time Transfer (TWTT) have potentially provided a means to improve precise relative positioning accuracy over differential GPS (DGPS)-only approaches. TWTT is a technique in which signals are simultaneously exchanged between users. This research investigates the impact of using Two-Way Time Transfer (TWTT) time measurements to augment differential GPS systems to improve the relative positioning solutions of vehicle networks. Incorporating the TWTT time meas. into the DGPS solution improves the 3-D relative positioning accuracy by up to 44% with pseudorange measurements and 35% with phase measurements. Normally, the TWTT meas. are used in a manner that cancels out the impact of the vehicle position in order to obtain a precise relative time measurement. The research also implements an innovative approach to using TWTT meas. to obtain a precise measurement of the vehicle position in addition to the time measurement. The results show that 3-D relative positioning solutions can be improved by up to 48% when using pseudorange measurements augmented with TWTT time and range meas., and up to 40% when using phase meas. augmented with TWTT time and range meas.

15. SUBJECT TERMS

Global Positioning System, Two-Way Time Transfer

16. SECURITY CLASSIFICATION OF:			17. LIMITATION OF ABSTRACT	18. NUMBER OF PAGES	19a. NAME OF RESPONSIBLE PERSON
a. REPORT	b. ABSTRACT	c. THIS PAGE			John F. Raquet
U	U	U	UU	128	19b. TELEPHONE NUMBER *(Include area code)* (937) 255-6565, x4580 (emailname@afit.edu)